

## **6. THE "AVERAGE SEISMIC COEFFICIENT" FOR STEEP SLOPES**

The frequency domain analysis of the effect of topography on ground motions presented in this section yields an insight into the factors controlling the seismic response of steep slopes. In this chapter, previous studies directed toward the seismic stability analysis of slopes are reviewed. In addition, two landmark studies of the use of average seismic coefficients for stability analyses are presented in detail: Seed and Martin (1966) and Makdisi and Seed (1978). Then, based on the concepts presented in these studies, a methodology for determining average seismic coefficient profiles for steep slopes is developed.

### **6.1 STUDIES OF SLOPE RESPONSE**

To date, most of the research effort in seismic slope stability has been directed toward the assessment of the stability of earth dams. These are obviously critical structures that warrant such studies, and the procedures and concepts developed for dams may often be extended to banks or bluffs. However, there are also significant differences between the response of bluffs and dams and, therefore, it is important to first review studies undertaken specifically for slopes or bluffs.

One of the first studies to specifically consider the seismic response of earth banks was conducted by Idriss and Seed (1967). This study, prompted by the extensive landslides generated during the 1964 Alaskan Earthquake, used the finite element method to conduct a parametric study on the response of 2H:1V clay slopes

(~27 degrees) on clay foundations. This work was later continued to include slopes as steep as 45 degrees (Idriss, 1968). The authors used triangular visco-elastic elements to model the slopes on rigid foundations. The 1940 El Centro N/S and vertical seismograms were used as the input motions, with the acceleration values scaled by 0.5, giving a peak base horizontal acceleration of 0.16g and peak base vertical acceleration of 0.13g. When considering horizontal motions, the authors found that magnitude of the peak surface acceleration was in all cases greater at the crest of the slope than at points lower on the slope. However, when comparing the peak surface acceleration at the crest to that at some distance behind the crest, they found that while in some cases the acceleration at the crest was much greater, in other cases that there was little difference between the response at the crest and that at some distance behind the crest. Vertical motions generated by the horizontal component of the base motion were greatest near the crest of the slope; however, the vertical component of the base motion had little effect on the horizontal shear stresses within the embankment. From the data presented, it is apparent that the natural period of the soil column either behind the crest or in front of the toe, was responsible for much more amplification of the input motion than the slope geometry itself.

Kovacs et al. (1971) performed laboratory shaking table experiments on clay banks, in part to further validate the use of the finite element method in this type of analysis. The physical model was 10 feet long, 0.25 to 0.5 feet thick, and 1.25 feet wide, and constructed with montmorillonite-kaolinite clay. The model was 0.25 feet high, had 4H:1V slopes (14 degrees), and was excited using sinusoidal motions of

varying frequency. Frequencies were selected to maximize the free field response either in front or behind the slope. The laboratory model were compared to the results of finite element analyses similar to those used by Idriss and Seed (1967). Kovacs et al. concluded that the thickness of the soil deposit was the predominant factor in determining the site response. They also concluded that there was a good agreement between the physical model and the numerical model when laboratory measurements of soil modulus and damping were used in the finite element analyses.

## **6.2 STUDIES OF EMBANKMENT DAM RESPONSE**

Newmark (1963) proposed the concept that the stability of an earth dam should be assessed in terms of earthquake-induced deformations, rather than the minimum factor of safety. Subsequently, Newmark (1965) presented a procedure in which deformations were modeled using the analogy of a block on an inclined surface.

Seed and Goodman (1964) used the sliding block analogy to develop a procedure to estimate the yield acceleration of slopes in cohesionless material, i.e. the acceleration at which slippage, and thus deformations occur. They found a considerable difference between the yield acceleration and the acceleration at which noticeable deformation occurred for short duration accelerations. Goodman and Seed (1966) also performed shake table tests on sand embankments in an effort to predict earthquake-induced deformations. They found good agreement between the laboratory tests and their analytical procedure. Their study showed that accelerations

were amplified from the base to the crest of the embankment by as much as 100 percent.

Seed (1965) extended Newmark's deformation concept and developed a method of assessing the seismic stability of earth dams based on deformations. Seed's method incorporated the time history of forces and the laboratory cyclic soil properties for the first time. For the purposes of this analysis, pore pressures were assumed not to dissipate during the earthquake.

Bustamante (1965) conducted shaking table tests on cohesionless embankments with side slopes as steep as 42 degrees, and proposed a wedge method of stability analysis to model the deformations observed in the shaking table tests. Within a stated 10 to 20 percent accuracy, horizontal accelerations were observed not to vary along the height of the embankment.

Seed and Martin (1966) applied the one-dimensional shear slice method, first proposed by Mononobe et al. (1936), to calculate average seismic coefficients for use in the stability analyses of earth dams. This method simulates the dam as a series of thin horizontal slices. Seed and Martin assumed that: (1) that dam is infinitely long and rests on a rigid foundation, (2) the dam is composed of a homogeneous, visco-elastic material, (3) the width to height ratio is large enough so that bending can be neglected and deformations are only due to shear, (4) the shear stress on any horizontal plane is uniform, and (5) the effect of stored water is negligible. Using this procedure to calculate acceleration time histories throughout the height of the dam, they were able to develop equivalent seismic force series that, in effect, represented the forces acting on the dam during the earthquake. Based on this

analysis, an average seismic coefficient was developed that represented the effect of the earthquake on the dam. The results of this study are discussed in greater detail later.

Ambraseys and Sarma (1967) used a similar approach, also using the shear slice method, to develop average seismic coefficients for earth dams. Sarma (1975) then developed a simplified procedure to estimate earthquake-induced deformations of earth dams using an extension of Newmark's sliding block analogy. Incorporating seismically induced pore-pressures in the analysis, Sarma concluded that factors of safety between 0.9 and 1.0 produced only small deformations. This procedure also allowed for the estimation of deformations when the factor of safety was below 1.0, using a triangular pulse to estimate the earthquake loading.

Finally, Makdisi and Seed (1978), making use of the earlier advances, developed a simple and rational procedure to estimate embankment deformations during earthquakes. This procedure has become a standard of practice for calculating embankment deformations. The procedure is based on Newmark's deformation concept and utilizes the average seismic coefficient, as proposed by Seed and Martin (1966), and a yield acceleration which can be calculated by any number of methods. As part of the study, they developed a supplementary procedure to estimate the peak acceleration at the crest of the embankment. Makdisi and Seed state that the procedure is applicable only to compacted cohesive or dense cohesionless embankments that experience little reduction in strength due to seismic loading. The simplicity of this procedure is very attractive, and its application to the current study of the seismic response of steep slopes is discussed below.

### 6.3 THE SEED AND MARTIN (1966) APPROACH

Seed and Martin (1966) discuss at length the concept of a seismic coefficient and its use in earth dam design. They conclude that there are three common meanings of the term "seismic coefficient" in the pseudo-static analysis of embankments:

(1) The product of the seismic coefficient and the weight of the potential sliding mass represents the maximum inertia force developed on the sliding mass during the earthquake. Seed and Martin concluded that this is an extremely conservative assumption because it applies a transient force (i.e., the earthquake) as a static force and, in effect, means that any permanent deformation is equated with failure of the embankment, regardless of period of time during which the force is applied.

(2) The "seismic coefficient" designates a force acting on the embankment that would generate the same deformations as a given earthquake loading. This results in a force somewhat less than the maximum inertial force, as discussed in (1) above, but Seed and Martin concluded that characterization of such force was nearly impossible at that time.

(3) The "seismic coefficient" designates a force that would result in a more conservative design of the embankment section than would otherwise result. However, this approach often does not result in a more conservative design, since the selected magnitude of seismic coefficient is often such that no modifications are necessary to an embankment designed for static loading.

Seed and Martin (1966) then propose the use of an average seismic coefficient that represents an equivalent seismic force series on the embankment. The method was developed for long triangular embankments composed of homogeneous, visco-elastic material with 20 percent damping. The method uses the shear slice method first proposed by Mononobe et al. (1936) and assumes that the response is controlled by uniform shearing between horizontal slices of the embankment. This assumption is reasonable for sliding masses extending to the centerline of the embankment, but may be 25 to 30 percent conservative for sliding masses extending only halfway to the centerline of the embankment. The basis of the method can be illustrated by the free, undamped vibration of a dam. From the forces acting on a thin slice of the dam, as shown in Figure 6.1, it can be shown that

$$\frac{\partial^2 u}{\partial t^2} = \frac{G}{\rho} \left[ \frac{\partial^2 u}{\partial y^2} + \frac{1}{y} \frac{\partial u}{\partial y} \right] \quad (6.1)$$

where  $u$  is the horizontal displacement at depth  $y$ ,  $t$  is time,  $\rho$  is density, and  $G$  is the shear modulus. The solution of Equation 6.1, with the boundary conditions  $u(y = h, t) = 0$ , and  $\partial u / \partial y (y = 0, t) = 0$ , is

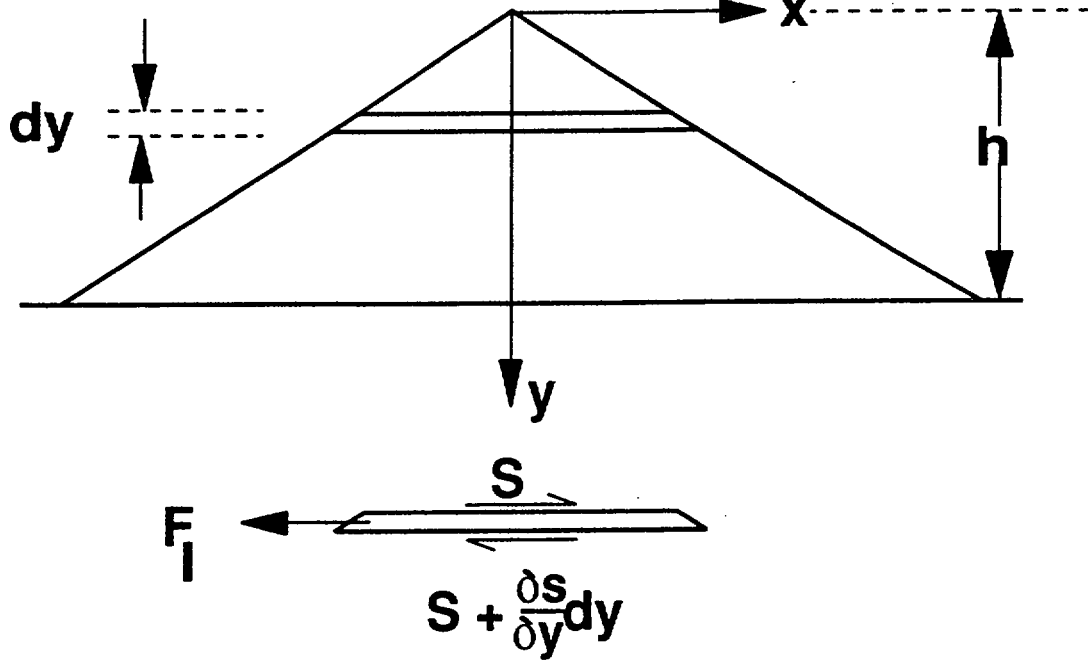
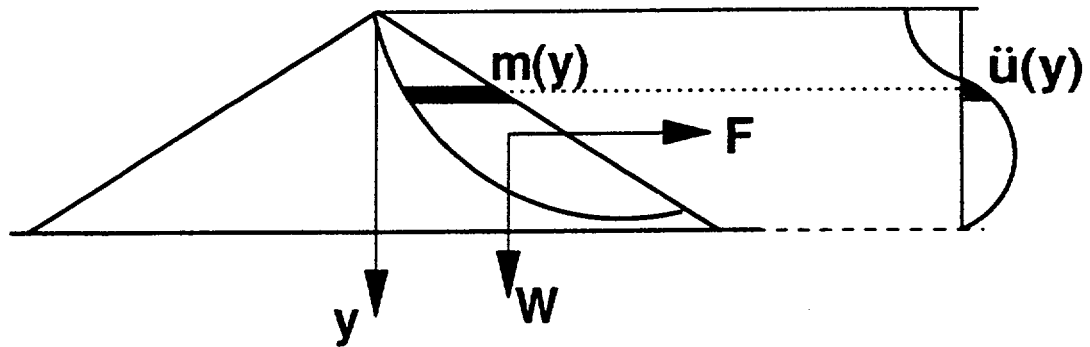


Figure 6.1: The one-dimensional shear slice method.



$$F = \sum m(y) \cdot \ddot{u}(y)$$

$$k_{av} = F/W$$

Figure 6.2: The forces acting on a potential sliding mass (after Seed and Martin, 1966).

$$u(y,t) = \sum_{n=1}^{\infty} [A_n \sin \omega_n t + B_n \cos \omega_n t] J_0(\beta_n \frac{y}{h}) \quad (6.2)$$

where  $h$  is the dam height,  $n$  is the number of the mode,  $\beta_n$  is the zero value of the frequency equation  $J_0(\omega(\rho/G)^{1/2}h) = 0$  having a fixed value for each mode, and  $J_0(\beta_n y/h)$  is the mode shape for the  $n^{\text{th}}$  mode corresponding to the natural frequency  $\omega_n$ , where  $\omega_n = \beta_n y/h(\rho/G)^{1/2}$  radians per second,  $J_0$  is the Bessel function of the first kind and order zero, and  $A_n$  and  $B_n$  are constants determined from initial conditions.

If this same dam is subjected to a random horizontal ground motion,  $\ddot{u}_g$ , then Equation 6.1 becomes

$$\frac{\partial^2 u}{\partial t^2} - \frac{G}{\rho} \left[ \frac{\partial^2 u}{\partial y^2} + \frac{1}{y} \frac{\partial u}{\partial t} \right] = -\frac{\partial^2 u_g}{\partial t^2} \quad (6.3)$$

The general form of the solution for this equation, incorporating viscous damping, is

$$u(y,t) = \sum_{n=1}^{\infty} \frac{2J_0(\beta_n \frac{y}{h})}{\omega_{dn} \beta_n J_0(\beta_n)} \int_0^t \ddot{u}_g^{-\lambda_n \omega_n(t-\tau)} \sin[\omega_{dn}(t-\tau)] d\tau \quad (6.4)$$

where  $\omega_{dn}$  is the damped natural frequency in the  $n^{\text{th}}$  mode,  $\tau$  is time, and  $\lambda$  is the fraction of critical damping.

The absolute acceleration of the dam,  $\ddot{u}_a$ , is the sum of the free vibration acceleration and the random motion at the base of the dam,

$$\ddot{u}_a(y,t) = \ddot{u}(y,t) + \ddot{u}_g(t) \quad (6.5)$$

Seed and Martin (1966) used equations 6.4 and 6.5 to show that the acceleration at any level in the dam,  $y$ , at any time,  $t$ , can be determined by

$$\ddot{u}_a(y,t) = \sum_{n=1}^{\infty} 2\omega_n \frac{1}{\beta_n J_1(\beta_n)} J_0\left(\beta_n \frac{y}{h}\right) \int_0^t \ddot{u}_g^{-\lambda_n \omega_n(t-\tau)} \sin[\omega_{dn}(t-\tau)] d\tau \quad (6.6)$$

They then used a form of Equation 6.6 to calculate the acceleration profile through a dam at various times, and then developed the concept of an "average seismic coefficient". The force acting on the sliding mass, as shown in Figure 6.2, is the sum of forces for each slice, i.e.,

$$F = \sum m(y) \ddot{u}_a(y) \quad (6.7)$$

where  $m$  = the mass of the individual slice, and  $\ddot{u}_a$  = the absolute acceleration of that slice at a given time. The force can also be expressed in terms of an average seismic coefficient,  $k_{av}$ , as

$$F = k_{av} W \quad (6.8)$$

and the average seismic coefficient can be expressed as

$$k_{av} = \frac{F}{W} = \frac{1}{W} \sum m(y) \ddot{u}_a(y) \quad (6.9)$$

Thus  $k_{av}$  is, in effect, a weighted average which accounts for the distribution of acceleration within the sliding mass.

Seed and Martin (1966) greatly simplified the calculation by assuming the sliding mass to be wedge shaped as shown in Figure 6.3, and by utilizing the assumptions of the shear slice method. By calculating the shear force at the base of the wedge and dividing the mass of the wedge, the average seismic coefficient can be computed at any depth and time without the necessity of performing the summation

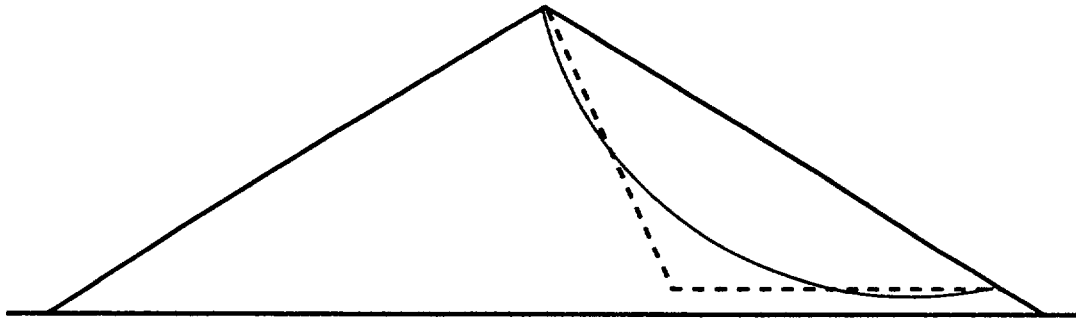


Figure 6.3: Assumed shape of potential sliding mass in Seed and Martin (1966).

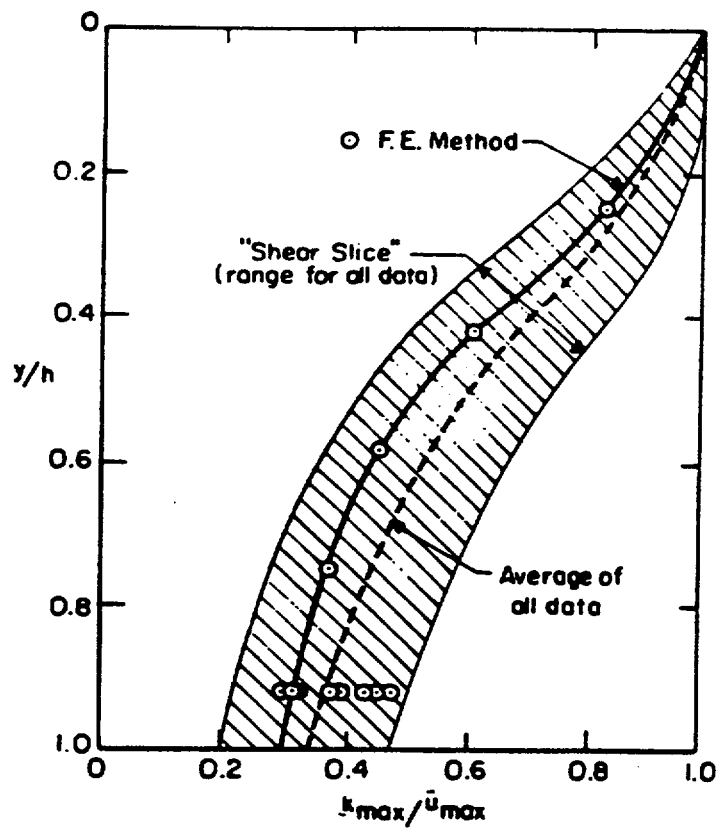


Figure 6.4: Relationship between  $k_{max}/\ddot{u}_{max}$  and depth of sliding mass (from Makdisi and Seed, 1978).

as shown in Equation 6.9. Also, by geometrical similarity, and by the assumptions in the shear slice method, the average seismic coefficient can be shown to be independent of the base width of the wedge and the inclination of the failure surface. As a result, this method is even more attractive due to its simplicity.

However, since the intent was to quantify the force that could be used in deformation analyses, simply selecting the maximum average seismic coefficient was already deemed over-conservative due to the short duration of the peak load. Therefore Seed and Martin (1966) proposed the concept of an "equivalent seismic force series". This involves judgement in selecting the average amplitude of significant force cycles, as well as period and duration, from the time history of the average seismic coefficient for a given depth of the dam. From the data presented in their study, the "equivalent maximum seismic coefficient" from the equivalent seismic force series was on the average 65 to 70 percent (range 50 to 85 percent) of the peak average seismic coefficient for any height in the dam.

Seed and Martin (1966) concluded that the height and composition of the dam played a significant role in calculating the seismic coefficient, and that the response is primarily due to the fundamental period of the dam. Though they believed that their procedure was a reasonable approach for the calculation of the dynamic force generated in a dam by an earthquake, they also stressed the limitations. The analyses assumed uniform shear along any horizontal slice through the dam, and preliminary analyses indicated that this assumption could be 25 to 30 percent conservative for failure surfaces extending only half way to the dam centerline. Also, the procedure

does not incorporate vertical motion, or energy absorption due to plasticity or inelasticity.

#### **6.4 THE MAKDISI AND SEED (1978) METHOD**

Makdisi and Seed (1978) used the concept of the average seismic coefficient and yield acceleration to develop a simplified procedure for estimating earthquake-induced deformations in dams and embankments. In their procedure, the yield acceleration is first calculated using a limit equilibrium analysis. The yield acceleration is, in this case, defined as that average horizontal acceleration that produces an inertia force such that the factor of safety against sliding goes to unity.

The earthquake-induced acceleration is then determined for the embankment. Makdisi and Seed (1978) analyzed several dams using an equivalent-linear finite element computer program. Using the results of these analyses, in combination with data developed by Ambraseys and Sarma (1967) and Seed and Martin (1966), they were able to develop a relationship between the maximum crest acceleration of the dam,  $\ddot{u}_{\max}$ , and the maximum average acceleration of the potential sliding mass,  $k_{\max}$ , as a function of the depth of the sliding mass. This relationship is shown in Figure 6.4. For design purposes, using the upper bound of the data would result in values 10- to 30-percent higher than the average value shown in Figure 6.4. Thus, only the peak crest acceleration of the dam or embankment has to be computed in order to get a reasonable estimate of the maximum average acceleration that would be experienced for a sliding mass at any depth in the embankment. The peak crest

acceleration can be computed using a finite element analysis or using a simplified procedure based on the shear slice method (Makdisi and Seed, 1977).

The permanent deformations are computed by assuming that all motions occur in the horizontal plane. Then, for all instances when the earthquake-induced acceleration exceeds the yield acceleration, the permanent deformations are calculated using numerical integration. Makdisi and Seed (1978) considered directions of sliding other than horizontal, but found that the direction made little difference in the computed deformations. They also found a distinct pattern in the magnitude of the computed deformations, and were able to normalize the deformations with the first natural period of the embankment as a function of the ratio of the yield acceleration and maximum average induced acceleration for various earthquake magnitudes. The simplified procedure allows the estimation of earthquake-induced deformations of dams by calculating the peak crest acceleration, the first natural period of the dam, and the yield acceleration.

A main assumption in this method is that the embankment material behaves elastically up to yield, but then *exhibits perfectly plastic behavior above yield* (writer's emphasis). The method generally applies to embankments constructed of compacted cohesive soil, or those constructed of dry or dense cohesionless soil, which loose little strength due to cyclic loading.

## 6.5 APPLICATION OF $k_{av}$ TO STEEP SLOPES

The simple and rational approach taken by Makdisi and Seed (1978) is very attractive; however, there are several assumptions in the procedure that do not apply to steep slopes in weakly cemented sand. Most importantly, the brittle nature of weakly cemented sand in the vicinity of the slope (Sitar, 1990) does not lend itself to a deformation based analysis and, therefore, a factor of safety based analysis rather than a deformation based analysis is more appropriate.

The intent of the work presented in the following sections is to develop a procedure for the analysis of the seismic response and stability of steep natural slopes. This procedure has to account for the semi-infinite extent of the soil mass behind the crest, which is characteristic of many natural slopes. It also has to account for a steep, relatively shallow, planar failure surface. In this context, a simple procedure which would allow the estimation of the crest acceleration based on a simple one-dimensional analysis is needed, since the simplified methods used for the analysis of dams (e.g. Makdisi and Seed, 1977) are not appropriate for semi-infinite geometries where the shear stress along any given horizontal plane is not uniform.

### 6.5.1 Distribution of Weight in the Potential Sliding Mass

Seed and Martin (1966) used Equation 6.9 to define the average seismic coefficient,  $k_{av}$ . They were able to avoid the summation procedure by assuming that the total inertia force induced by the earthquake was represented by the shear force

at the horizontal base of the failure wedge. In the case of steep slopes, however, the failure surface looks more like that shown in Figures 2.10 and 2.11.

If, in Equation 6.9, the unit weight is assumed to be constant within the failure wedge, and the absolute acceleration of an individual slice is given in terms of the acceleration of gravity, then the average seismic coefficient can be calculated as

$$k_{av} = \sum \frac{m(y)}{M} \ddot{u}_a(y) \quad (6.10)$$

where  $M$  is the total mass of the wedge. This is essentially a "weighted" average.

For the wedge shown in Figure 6.5, weight must be given for each slice in order to develop the "weighted" average seismic coefficient from the summation in Equation 6.10. As demonstrated below, conveniently, the weighting of an individual slice is independent of the slope angle and the angle of the failure surface. Consider the geometry of the potential sliding wedges shown in Figure 6.5. Assuming a unit width, the corresponding volumes are given by:

$$ABD = 0.5(x_1)^2 \tan S_1$$

$$ACE = 0.5(x_2)^2 \tan S_1$$

$$BCED = 0.5((x_2)^2 - (x_1)^2)$$

$$ABF = 0.5(x_1)^2 \tan (S_1 + S_2)$$

$$ACG = 0.5(x_2)^2 \tan (S_1 + S_2)$$

$$DEGF = ACG - ABF - BCED$$

$$AEG = ACE - ACE$$

The weighting,  $\Delta M_i$ , given to a horizontal slice (e.g. DEGF) is then given by



$$\Delta M_i = \frac{DEGF}{AEG} = \frac{0.5 \tan(S_1 + S_2)(x_2^2 - x_1^2) - 0.5 \tan S_1(x_2^2 - x_1^2)}{0.5 \tan(S_1 + S_2)(x_2^2) - 0.5 \tan S_1(x_2^2)} \quad (6.11)$$

$$\Delta M_i = \frac{x_2^2 - x_1^2}{x_2^2} \quad (6.12)$$

From Equation 6.12, it can be seen that the weighting factor,  $\Delta M_i$ , is independent of the slope angle,  $S_1$ , and the angle of the failure plane,  $S_2$ . This simple result based on the similarity of the triangles simplifies the calculation of the average seismic coefficient for varying slope geometries, if an acceleration value can be determined for each slice.

### 6.5.2 Selection of an Acceleration Profile

When using GROUND2D, it is convenient to compute the acceleration that occurs at face of the slope for each slice, rather than trying to obtain the average value along the slice. Not only is it convenient, but it also simplifies the procedure, since the response calculation is then independent of the length of the slice. While not appropriate for deep-seated failure surfaces in embankment dams, this appears to be a reasonable, though somewhat conservative, assumption for the analysis of steep slopes.

GROUND2D was used to calculate the acceleration time histories for various elevations at the slope face and at H/4 behind the face for a 100-ft vertical slope. The input motion used in the analysis was UCSC0, recorded at the University of

California at Santa Cruz during the 1989 Loma Prieta Earthquake. The shear wave velocity profile used is shown in Figure 6.6; damping averaged about 5 percent. Poisson's ratio and the unit weight of the material were assumed to be 0.3 and 120 pcf, respectively.

The two acceleration profiles calculated were then used to compute the average seismic coefficient time history at each position. From each  $k_{av}$  time history, the maximum average seismic coefficient,  $k_{max}$ , was selected. The profiles of  $k_{max}$  at each location are presented in Figures 6.7. A comparison of the profiles shows that the  $k_{max}$  values calculated at H/4 behind the face are approximately 15 percent lower than those at the slope face. This is an upper bound difference, since the average acceleration within an individual slice would be somewhere between these two values. Note that the failure surface is inclined from a point behind the crest (in this case H/4) to the slope face, as shown in Figures 2.10 and 2.11. Moreover, H/4 is an extreme value for the typically shallow failures observed in actual earthquakes. For these reasons, the selection of the acceleration at the slope face for use in calculating  $k_{av}$  appears to be a reasonable and conservative assumption.

### **6.5.3 Evaluation of Crest Acceleration**

Since most practitioners do not have the time or the means to perform a two-dimensional dynamic finite element analysis for most slope response problems, it is desirable to develop a simplified procedure to estimate the acceleration at the crest of the steep slope. Makdisi and Seed (1977) proposed a simplified method based on

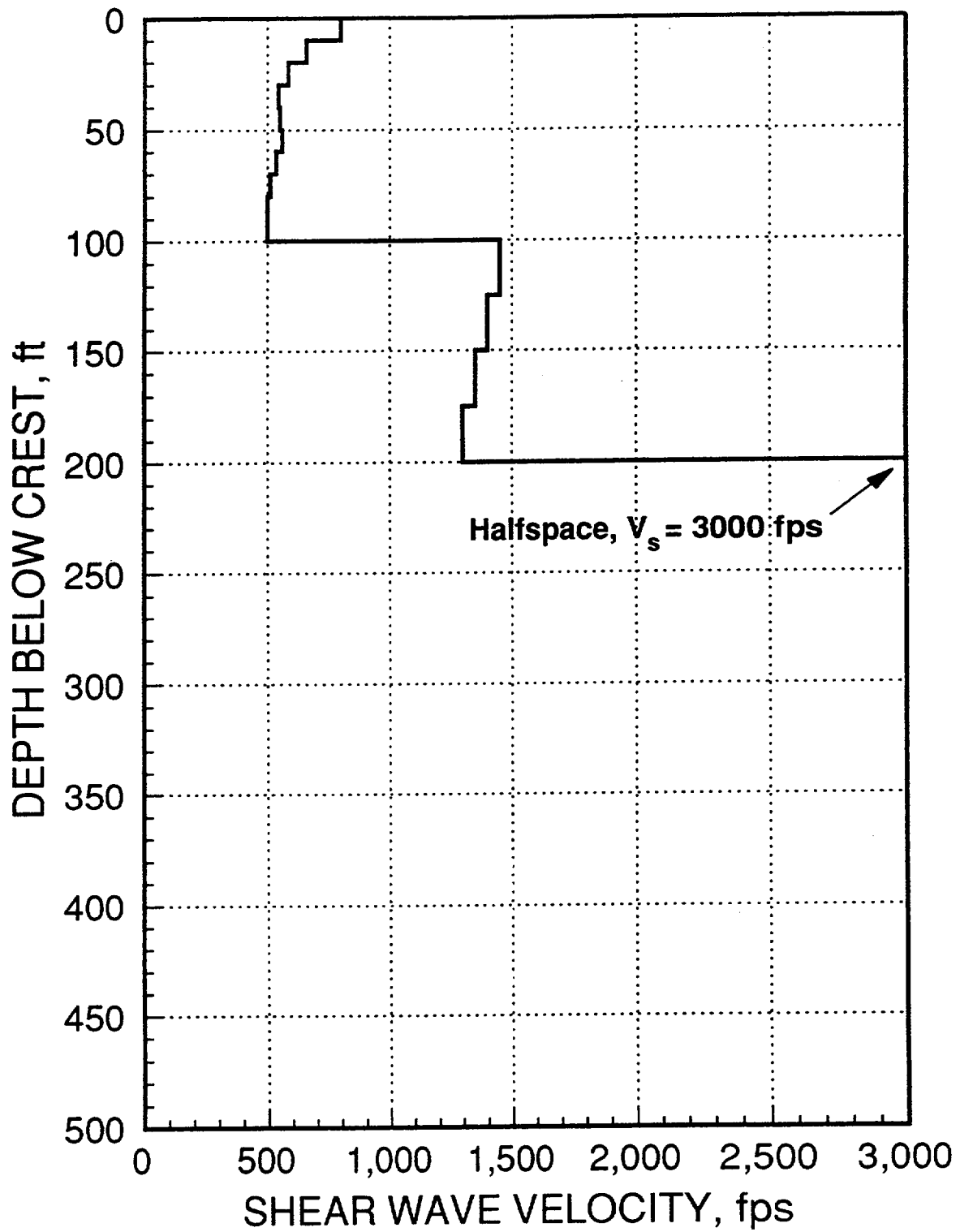


Figure 6.6: Shear wave velocity profile used for comparison of  $k_{max}$  profiles.

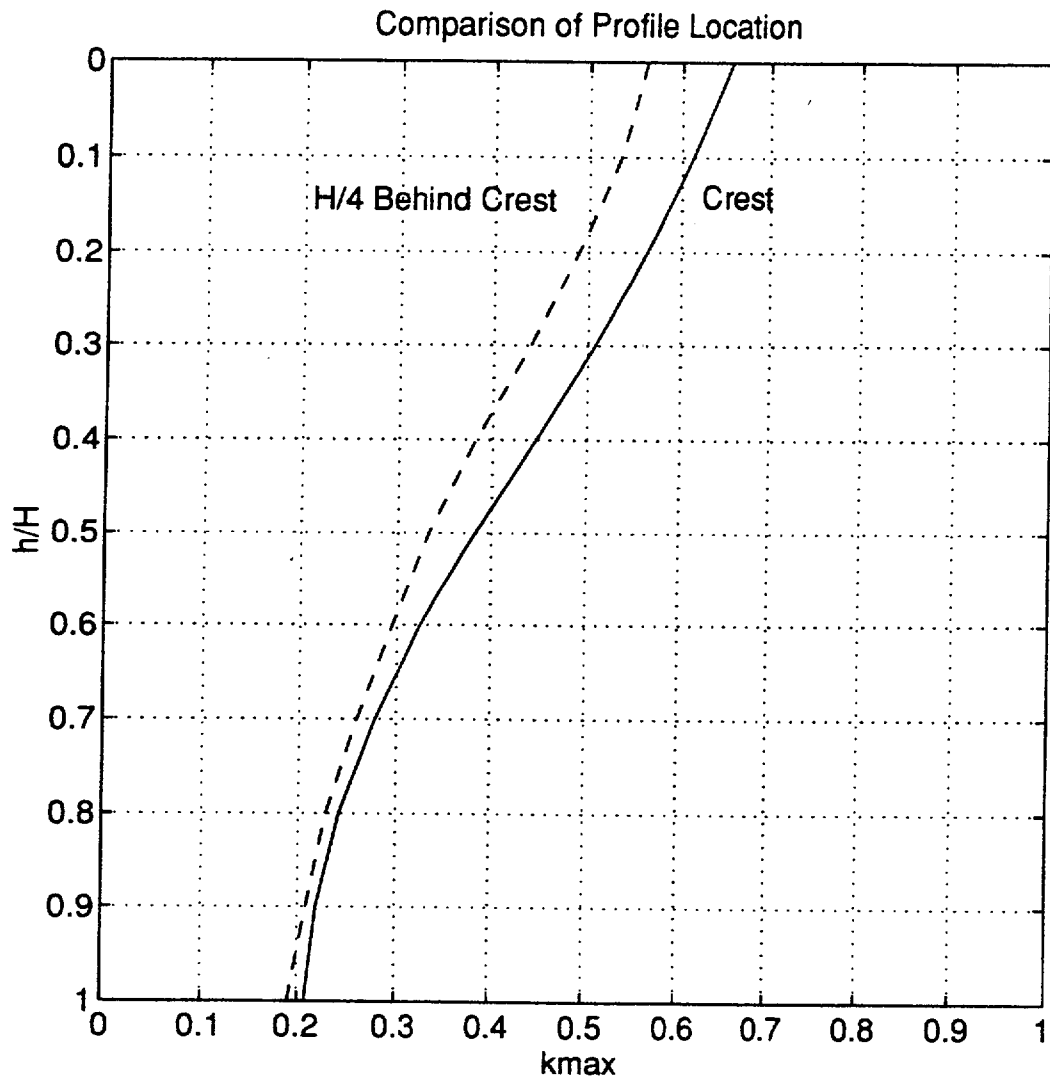


Figure 6.7: Comparison of  $k_{max}$  profiles at slope crest and H/4 behind slope crest.

the shear slice theory to estimate the maximum crest acceleration of an embankment. Though developed for dry or very dense sand or clayey soil embankments of finite width, it is of interest to compare it to the results obtained from a hyperelement analysis of a steep slope.

For the comparison, a 100-ft vertical slope composed of cemented sand was selected, with an initial shear wave velocity of 1000 fps and a unit weight of 120 pcf. The cemented sand rests on a rock foundation with  $V_s = 3000$  fps. Two seismograms were used: the El Centro N/S seismogram recorded in the 1940 El Centro Earthquake and the UCSC0 record, recorded at the University of California at Santa Cruz during the 1989 Loma Prieta Earthquake. The shear modulus reduction and damping curves for the cemented sand are shown in Figures 6.8a and 6.8b, respectively. The response spectra for the source motions are shown in Figures 6.9a (El Centro N/S) and 6.9b (UCSC0).

The Seed and Makdisi (1977) procedure assumes a one-dimensional structure resting on a rigid base. In their procedure, the first step is to assume an initial value of  $G/G_{\max}$  so that the initial  $G$ , shear strain ( $\gamma_{ave}$ ), and damping ( $\lambda$ ) can be determined from the modulus reduction and damping curves. The shear modulus is related to the shear wave velocity by  $G = \rho V^2$ . The next step is to calculate the first 3 natural frequencies of the dam using the shear slice method using the equation

$$\omega_n = \frac{\beta_n V_s}{H} \quad (6.13)$$

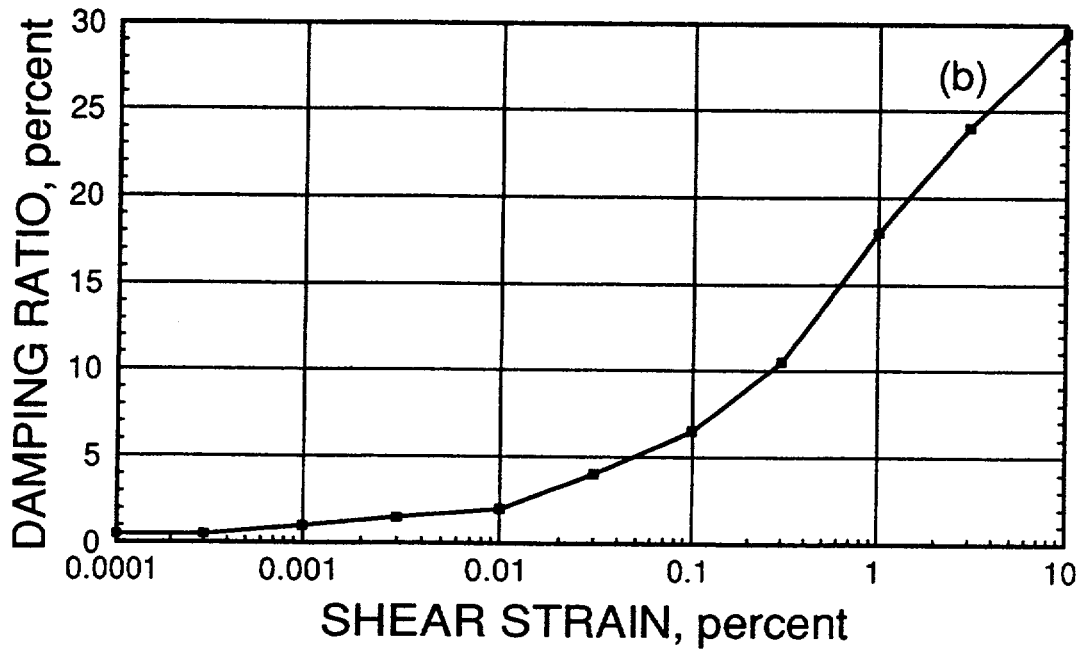
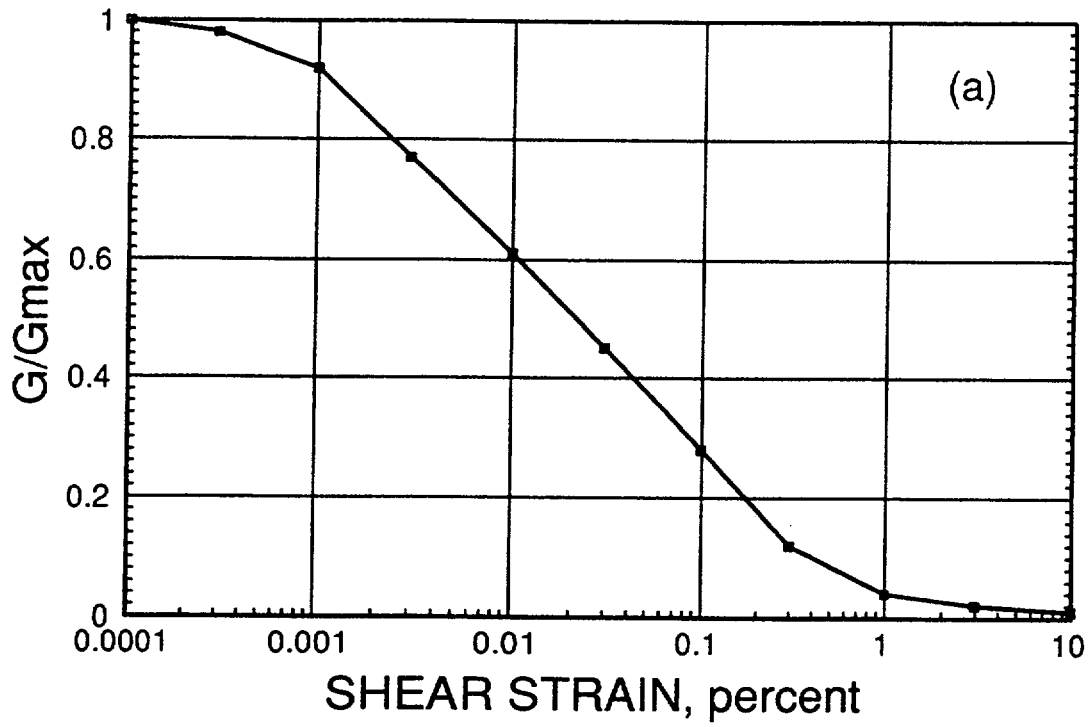


Figure 6.8: Shear modulus reduction (a) and damping (b) curves for weakly cemented sand (after Wang, 1986).

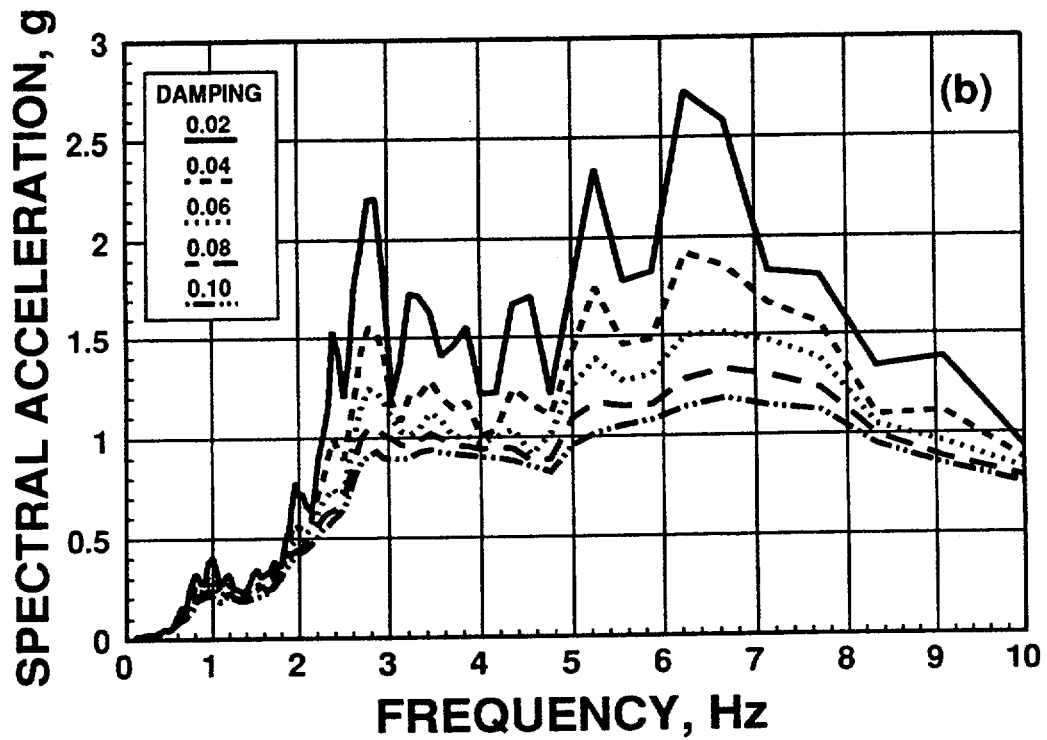
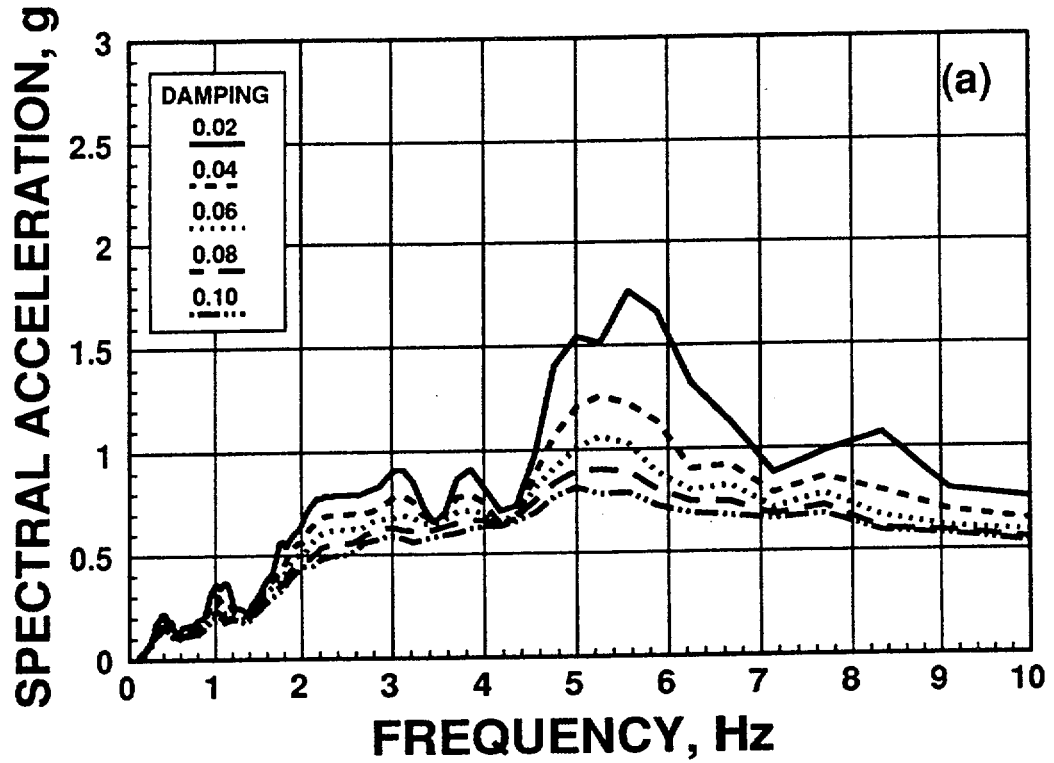


Figure 6.9: Acceleration response spectra for El Centro NIS seismogram (a) and UCSC0 seismogram (b).

where  $\omega_n$  = the natural frequency of the  $n^{\text{th}}$  mode,  $\beta_n$  are derived from Equation 6.4 and always have the following values:  $\beta_1 = 2.4$ ,  $\beta_2 = 5.52$ , and  $\beta_3 = 8.65$ . The maximum crest acceleration for each mode is then calculated using

$$\ddot{u}_{n_{\max}} = \phi_n S_{an} \quad (6.14)$$

where  $S_{an}$  is the spectral acceleration of the  $n^{\text{th}}$  mode and  $\phi_n$  is the mode participation factor of the  $n^{\text{th}}$  mode. The values for the first three modes are always  $\phi_1 = 1.6$ ,  $\phi_2 = 1.06$ , and  $\phi_3 = 0.86$ . Once the maximum crest acceleration for each of the first 3 modes is determined, then the maximum crest acceleration is approximated by taking the square root of the sum of the squares of the crest acceleration of the first 3 modes. The average equivalent cyclic shear strain is then estimated using the shear slice theory. Assuming the equivalent cyclic shear strain is approximately 0.65 of the maximum average shear strain, Makdisi and Seed (1977) were able to simplify this calculation to

$$(\gamma_{ave})_{eq} = (0.65)(0.3) \frac{H}{V_s^2} S_{a1} \quad (6.15)$$

where 0.3 is the average value of the first mode participation factor for the entire height of the dam. Once the average shear strain is calculated, new values of  $G/G_{\max}$  and  $\lambda$  are determined and the second iteration is begun. The authors indicate that the procedure converges in usually 3 iterations. The strain-compatible shear wave

velocity obtained from this procedure was 510 fps, and the damping value obtained was 7 percent.

The same slope was also analyzed using the computer program GROUND2D for SV-waves incident at  $0^\circ$  and  $-30^\circ$ . For this simple geometry, only the left and right transmitting elements were necessary. The same strain-compatible soil properties used in the Makdisi and Seed procedure were also used in GROUND2D.

The results of these analyses are compared in Table 6.1. The results show that the estimated amplification of the input motion is much greater using the Makdisi and Seed procedure than obtained using the 2-D GHE method for the vertical slope. This is to be expected, since the assumptions in the one-dimensional shear slice theory do not fit the case of steep slope in a semi-infinite domain. In addition, a considerable amount of vertical acceleration is calculated at the crest of the steep slope in GHE method, actually greater than the horizontal acceleration, which cannot be quantified using the 1-D procedure. Though the 1-D procedure cannot evaluate inclined waves, there is little difference observed between the vertical and inclined wave case using the GHE method.

Input Motion	GHE Method				Makdisi and Seed
	Horizontal $a_{max}$		Vertical $a_{max}$		Horizontal $a_{max}$
	F= $0^\circ$	F= $-30^\circ$	F= $0^\circ$	F= $-30^\circ$	F= $0^\circ$
EL Centro N/S	0.49	0.48	0.68	0.54	1.24
UCSC0	0.70	0.58	0.73	0.75	1.72

## 6.6 CONCLUSIONS

An approach similar to that used by Seed and Martin (1966) and Makdisi and Seed (1977, 1978) can be used to develop average seismic coefficients for steep slopes, as long as the conditions particular to steep slopes are met. In this study, the average seismic coefficient is calculated using a weighted average summation procedure within the potential failure wedge, rather than using the shear slice method, because of the steepness of the failure surface and the semi-infinite extent of the material behind the crest. For convenience, the accelerations used in the analysis herein are those computed at the slope face, which appears to be a reasonable and conservative assumption. Finally, the peak crest acceleration is computed using two-dimensional seismic site response analysis, because the simplified procedure based on the shear slice method (Makdisi and Seed, 1977), originally developed for embankment dam response, tends to over-estimate the peak acceleration for the cases considered herein.



## 7. THE SEISMIC RESPONSE OF STEEP SLOPES

In the previous chapter, the concept of the average seismic coefficient for steep slopes was discussed. It is now possible to consider realistic slope geometries, material properties, and actual seismograms in order to quantify the effect of topography for slope stability purposes. In this chapter, the results of analyses are presented in the time domain for several realistic site models. Crest amplification and average seismic coefficients for steep slopes are developed, and the effects of incident wave directivity and inclination are considered. Finally, recommendations for incorporating the results of this study in stability analyses are presented.

### 7.1 PROTOTYPE SITE CHARACTERIZATION

The analyses were based on two prototype sites. One is located at Seacliff State Beach, just south of Santa Cruz, California on Monterey Bay; the other is located in the Westlake area of Daly City, California (Figure 7.1). Both sites encompass steep coastal bluffs in weakly cemented sands and are known to have experienced slope failures during seismic events.

A boring was drilled at each site to determine the site-specific stratigraphy and to gather samples for possible testing. Shear wave velocity profiles were also obtained. A gamma log was also performed at the Daly City site to help evaluate the stratigraphy.

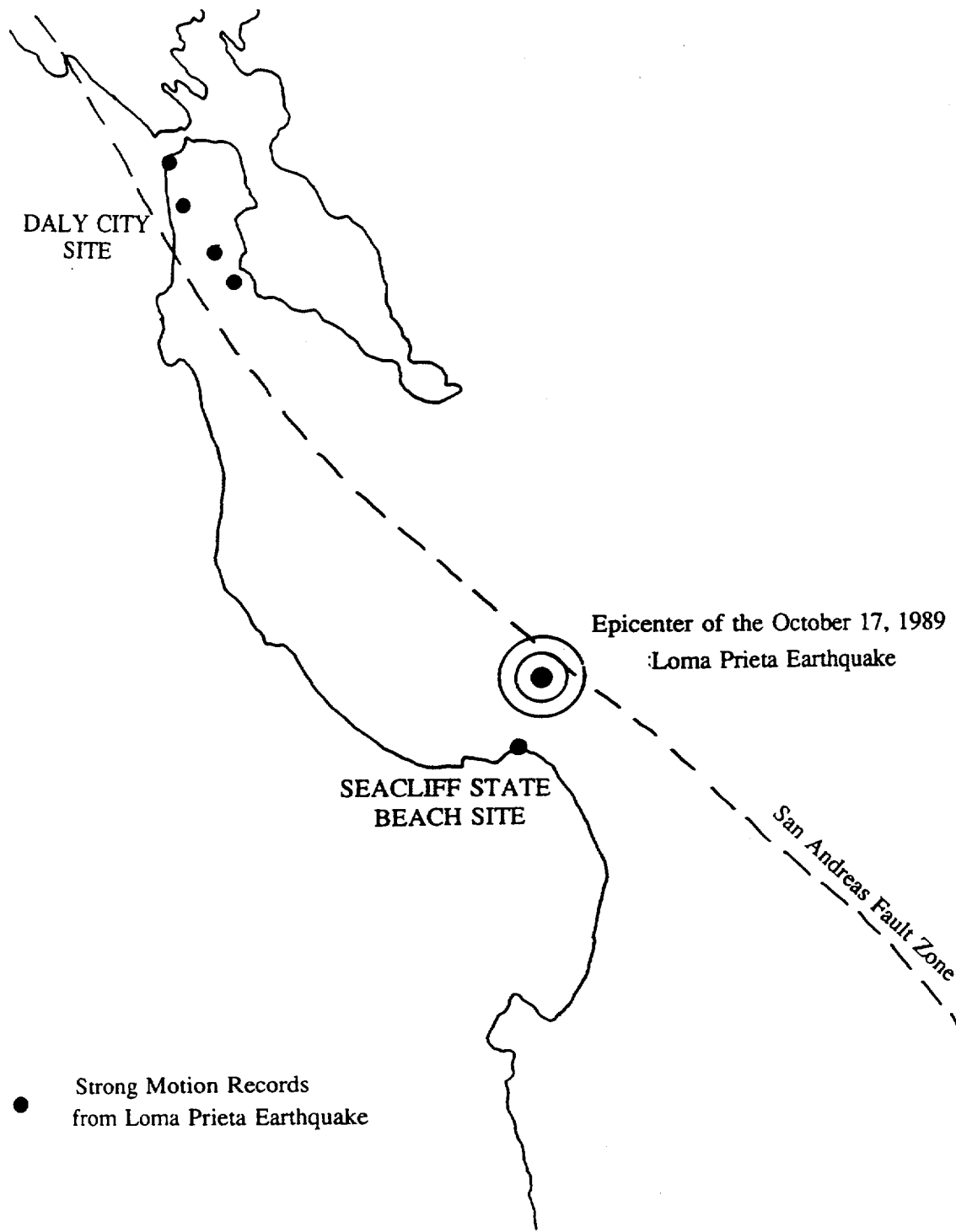


Figure 7.1: Location map for prototype sites.

A general description of each prototype site and the results of the field exploration are presented herein. A description of the soil boring procedure, the boring logs, and the gamma log are presented in Appendix A. The shear wave velocity data and a description of the procedures used to perform the shear wave velocity testing are presented in Appendix B.

### **7.1.1 Seacliff State Beach Site**

The Seacliff State Beach site is located just south of Santa Cruz, California. The coastal bluffs at the site are nearly vertical and about 30 m high. The terrain behind the crest of the slopes is flat and level for several hundred meters. Plant and Griggs (1990) identify two geologic units at the site. The top 5 meters of the bluffs are Quaternary marine terrace deposits consisting of predominately poorly-consolidated sand. They are underlain by a moderately indurated and weakly jointed sandstone member of the Pliocene epoch Purisima formation.

The Seacliff State Beach site was selected due to its relatively simple geology and its record of observed failures during seismic events. Plant and Griggs provide a detailed description of slope failures at this site following the 1989 Loma Prieta earthquake and indicate that two types of failures occurred. Translation failures originating along joints or weathering surfaces occurred in the top 12 meters of the bluffs. These failures were vertical in the Quaternary sediments and tended to flatten out in the Purisima formation. Tension cracks were observed extending 1 to 6 m behind the slope crests. The other type of failure was block sliding and toppling

observed to occur over undercut bases. Failures of coastal bluffs were also observed in this general area during the 1906 San Francisco earthquake (Lawson, 1908).

The results of the boring and shear wave velocity testing at the Seacliff site were generally in agreement with the observations by Plant and Griggs. The samples recovered from the boring indicated a surficial layer of sandy silt to a depth of 11 ft (3.1 m), with an increasing sand content with depth. This material is the Quaternary period sand referred to by Plant and Griggs. It is underlain by a poorly-graded, uniform, fine sand to the terminal depth of the boring at 100 ft (33 m). Based on borehole samples, cementation increases with depth, and the unit is a part of the Purisima formation. The boring log for the Seacliff site is presented in Appendix A.

The results of the shear wave velocity ( $V_S$ ) testing for the site are presented in Figures 7.2 and 7.3. The raw data for the  $V_S$  testing are presented in Appendix B. Figure 7.2 shows the shear wave travel time plotted against depth; the average and interval shear wave velocities are presented in Figure 7.3. The  $V_S$  measured at the site generally increases with depth and ranges from 850 to about 2200 ft/sec. In the upper Quaternary material, the  $V_S$  is 850 ft/sec. In the Pliocene material, the  $V_S$  ranges from 1000 to more than 2200 ft/sec, and averages approximately 1900 ft/sec.

### **7.1.2 Daly City Site**

The Daly City site is located in the Westlake area of Daly City, California. Here, the coastal bluffs are moderately steep, with slopes between 40 to 55 degrees, and attain heights in excess of 150 meters. The bluffs face to the west. The terrain

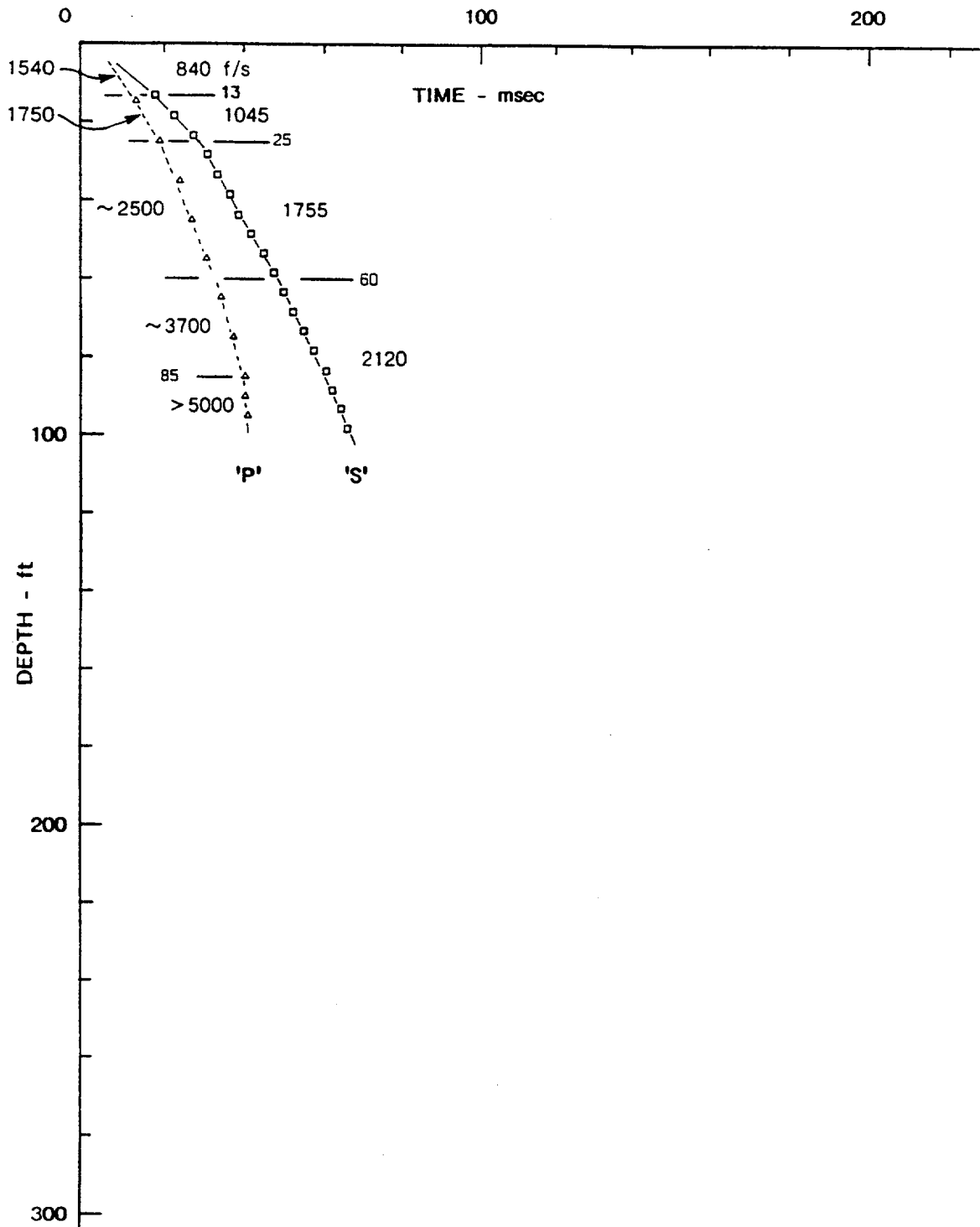


Figure 7.2: Downhole travel times of compression and shear waves signals, together with corresponding velocities, for Seacliff State Beach site.

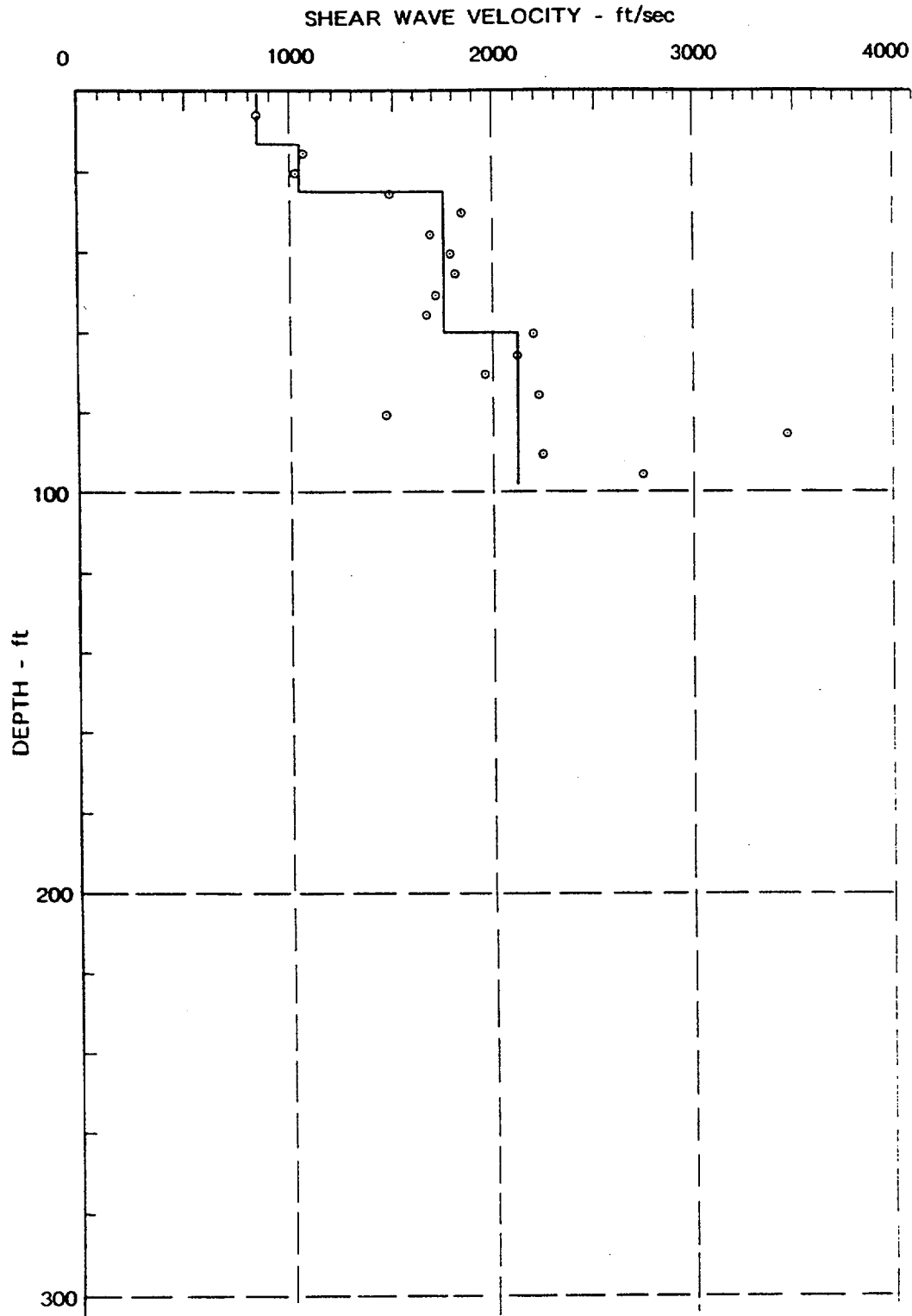


Figure 7.3: Average and interval shear wave velocities for Seacliff State Beach site.

behind the crest of the bluffs is relatively flat, sloping approximately 5 degrees to the north.

Bonilla (1959) indicates that the bluffs in Daly City are almost entirely composed of the Merced formation. In this area, the Merced formation predominantly consists of uncemented sand, with up to a third of the formation composed of silt and clay size particles, and may be over a kilometer thick at this location. The bedding strikes approximately N40W, and dips 30 to 70 degrees to the northeast. The Colma formation overlies the Merced in the Daly City area, but is not found within 500 m of the bluffs evaluated in this study.

Though the geology of this site is more complex than the Seacliff site, it was selected as a prototype site because of its geometry, and because of its long history of failures during seismic events. Failures were documented along these bluffs in the 1906 and 1957 San Francisco earthquakes by Youd and Hoose (1978), and the 1989 Loma Prieta earthquake (Sitar, 1991).

The field exploration at the Daly City site confirms the complex geology, and generally agrees with the description by Bonilla (1959). Samples from the boring indicate that the site is underlain by alternating layers of weakly cemented and uncemented, poorly-graded sand and claystone of the Merced formation to the terminal depth of the boring of 330 ft. The sand is essentially uncemented and uniformly graded, and the layer thicknesses ranges from 10 to over 50 ft. The clay is very stiff to hard, often slickensided, and occurs in layers up to 70 ft thick. The boring logs are presented in Appendix A. Strata breaks indicated by the gamma log generally agree with the those in the boring log. More importantly, review of the

gamma log indicates that the material below a depth of 250 ft is relatively uniform and coarse grained. This indicates that the material between depths of 250 and 330 ft is a sand, as indicated by sample SH-10 (taken with a pitcher-barrel), rather than a sandy silt, as indicated by drill cutting samples B-9 and B-10.

The results of the shear wave velocity testing for the site are presented in Figures 7.4 and 7.5. Figure 7.4 shows the shear wave travel time plotted against depth; the average and interval shear wave velocities are presented in Figure 7.5. The raw data for the shear wave velocity testing is presented in Appendix B. The shear wave velocity at the site generally increases with depth from 700 to about 2400 ft/sec.

## **7.2 SITE SPECIFIC ANALYSES**

Site specific analyses were performed to determine the effect of topography on the seismic response of actual sites. The slopes analyzed include typical sections from the two prototype sites, Seacliff State Beach and Daly City, as well as an idealized site with cross-section similar to slopes that failed in the Northridge Earthquake (Pacific Palisades) and the Petrolia Earthquake (Centerville Beach). The analyses used 3 different seismograms from earthquakes recorded in California: the 1940 El Centro N/S record, the 1989 Loma Prieta UCSC0 record, and the 1992 Landers JOS90 record. These seismograms are shown in Figure 7.6. The acceleration response spectra for these outcrop motions are shown in Figures 6.11a, 6.11b, and 7.7. The intent was to evaluate the relationships between crest amplification and average seismic coefficient based on a variety of realistic conditions.

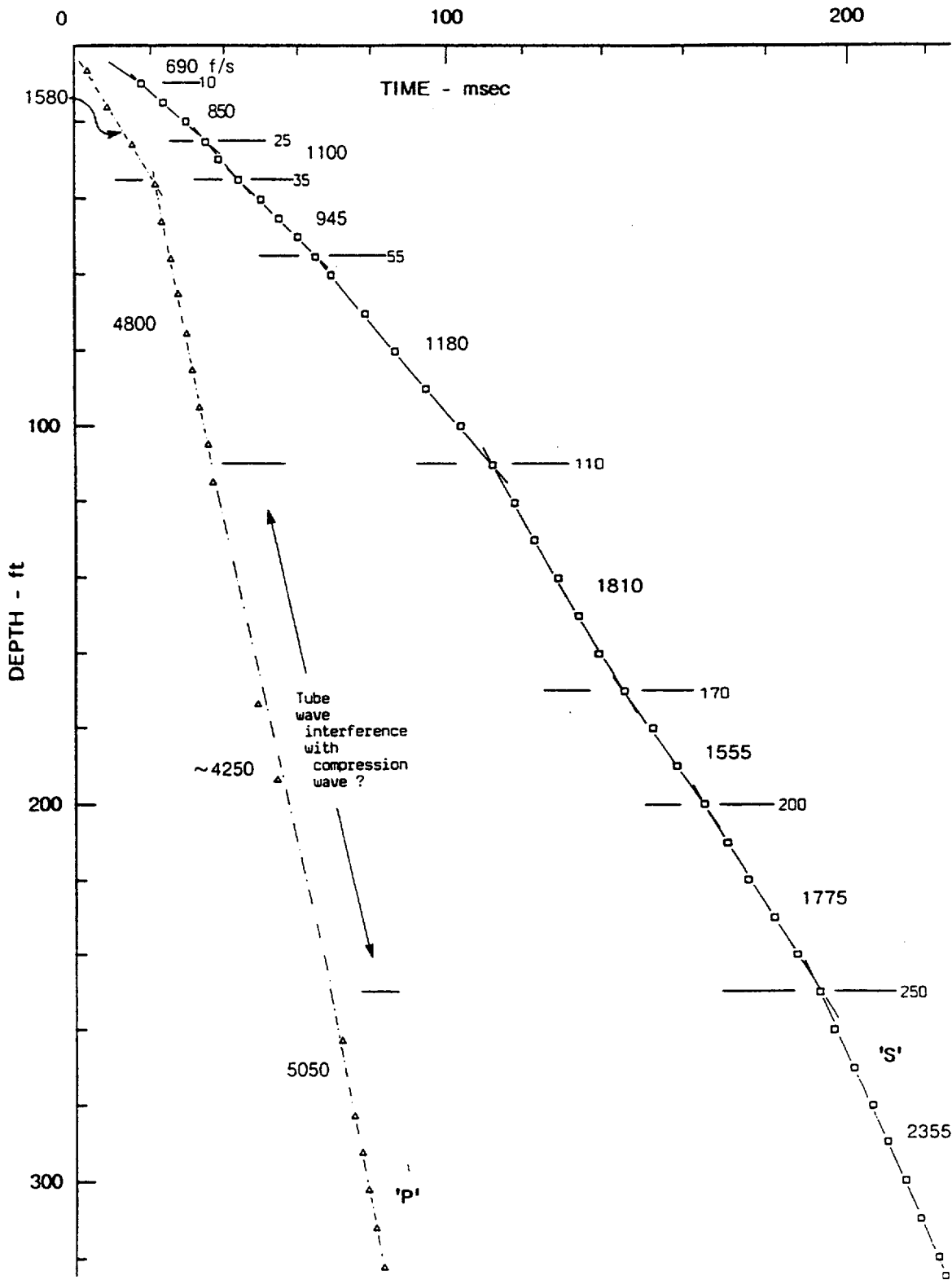


Figure 7.4: Downhole travel times of compression and shear waves signals, together with corresponding velocities, for Daly City site.

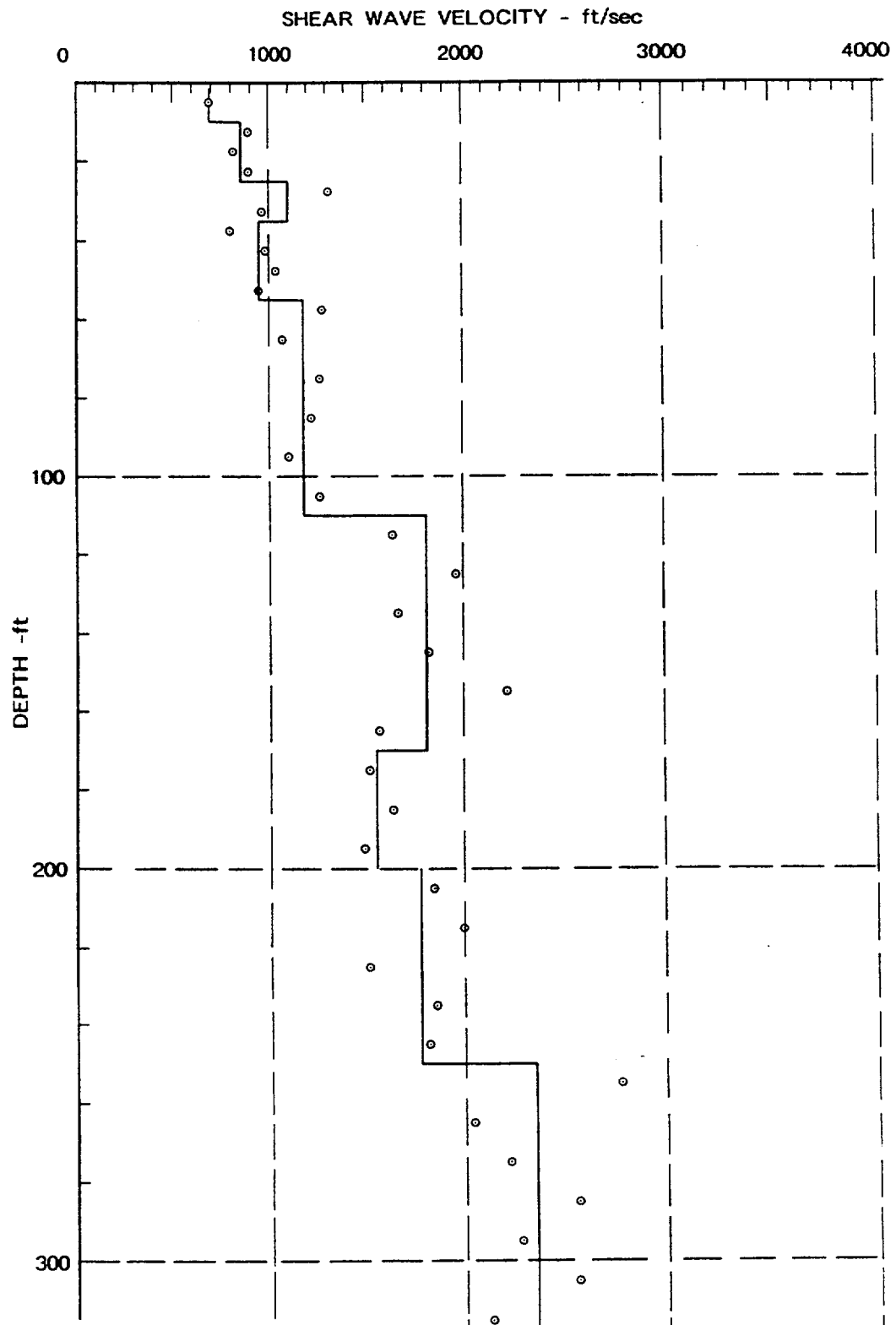


Figure 7.5: Average and interval shear wave velocities for Daly City site.

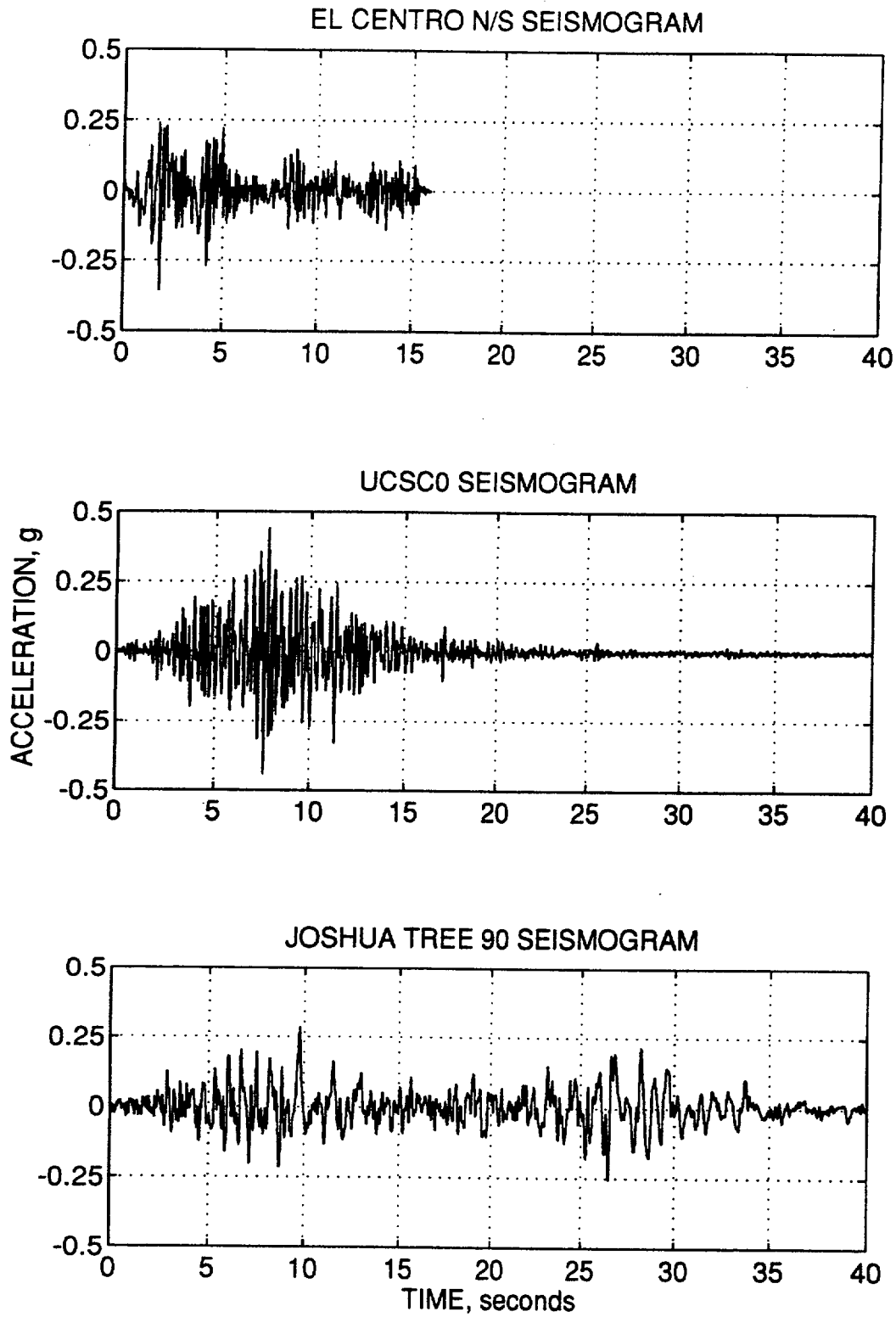


Figure 7.6: Seismograms used in analysis.

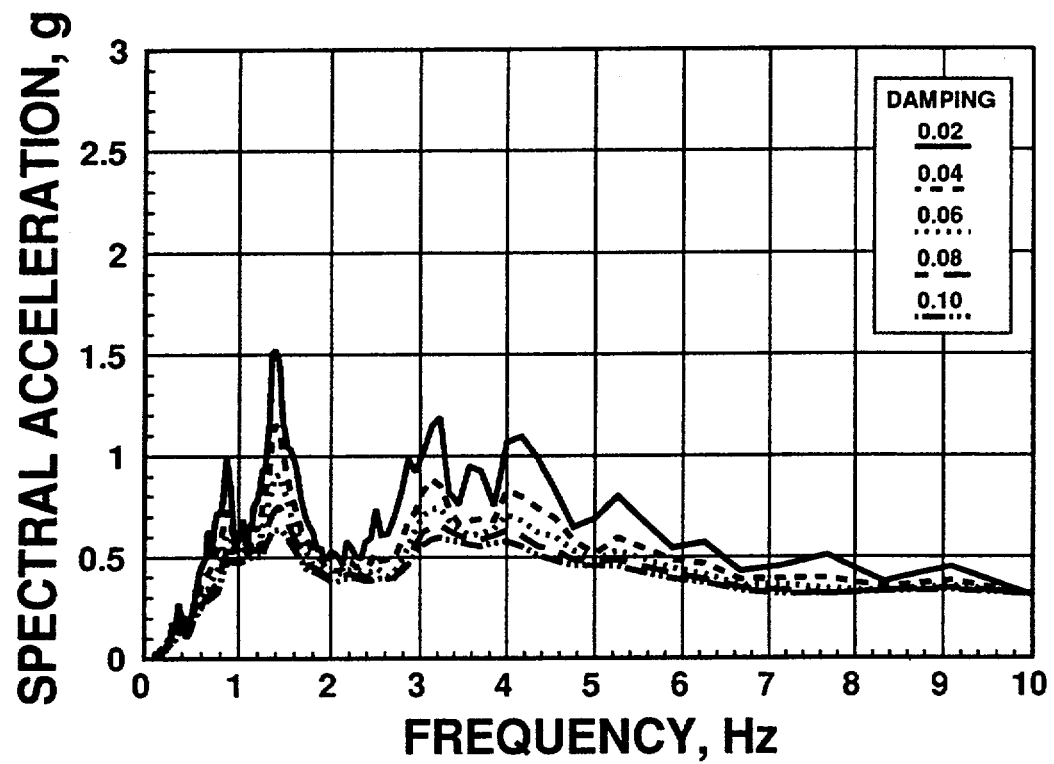


Figure 7.7: Acceleration response spectra for JOS90 seismogram.

### 7.2.1 Seismograms Used in Analysis

The El Centro N/S ( $M_W = 6.9$ ) seismogram from the May 18, 1940, El Centro, California, Earthquake was selected primarily because of its historical use in slope and embankment response studies (e.g. Seed and Martin, 1968). The peak acceleration in the record is 0.32g and the predominant frequencies are between 5 Hz and 6 Hz.

UCSC0 was recorded at the University of California at Santa Cruz campus during the October 17, 1989 Loma Prieta Earthquake ( $M_S = 7.1$ ). The peak recorded acceleration at this station was 0.42g. The predominant frequencies for this outcrop motion occur at 3 Hz and between 5 and 7 Hz. This record was selected because it likely has a frequency content representative of the motion experienced by the Seacliff State Beach prototype site.

The JOS90 record is from the June 28, 1992, Landers, California, Earthquake ( $M_S = 7.5$ ). This record was selected primarily because it contained low frequency motion that was not observed in the other two records. The seismogram was recorded at the Joshua Tree Fire Station approximately 14 kilometers from the epicenter. It has a peak acceleration of 0.28g, and predominant frequencies near 1 Hz and between 3 and 4 Hz.

### 7.2.2 Slope Models

The properties and slope geometries of two of the models were based on the prototype sites at Seacliff State Beach and Daly City, as already stated. In addition, a third model was developed based on an idealized representation of a combination of slopes at the Pacific Palisades, which failed during the 1994 Northridge earthquake and a slope at Centerville Beach which failed during the 1992 Petrolia earthquake.

Each model consisted of a left and a right transmitting element, with each element divided into layers that are at most  $\lambda/10$  thick. This dimension was based on the iterated shear wave velocity within the layer and the highest frequency of motion under consideration. The frequencies considered in the analyses were between 0.1 and 10 Hz, which is in the general range of engineering interest and contains the dominant frequencies of the seismograms used in the analyses.

The first model, SEACLIFF, is a 90-ft high, 75-degree slope which is representative of the specific conditions occurring at the Seacliff State Beach site. In order to determine the effect of the top boundary of the visco-elastic halfspace, three different depths of this boundary were analyzed: 90-ft, 135-ft, and 220-ft below the crest of the slope. The iterated shear wave velocity profile used in the analysis is presented in Figure 7.8. The "iterated" soil properties are the strain-compatible soil properties obtained from one-dimensional equivalent-linear site response analysis using the computer program SHAKE (Schnabel et al., 1972) and the UCSC0 record as the input motion. The iterated soil properties obtained using the other two earthquake records were very similar to those from the UCSC0 record, and, in order

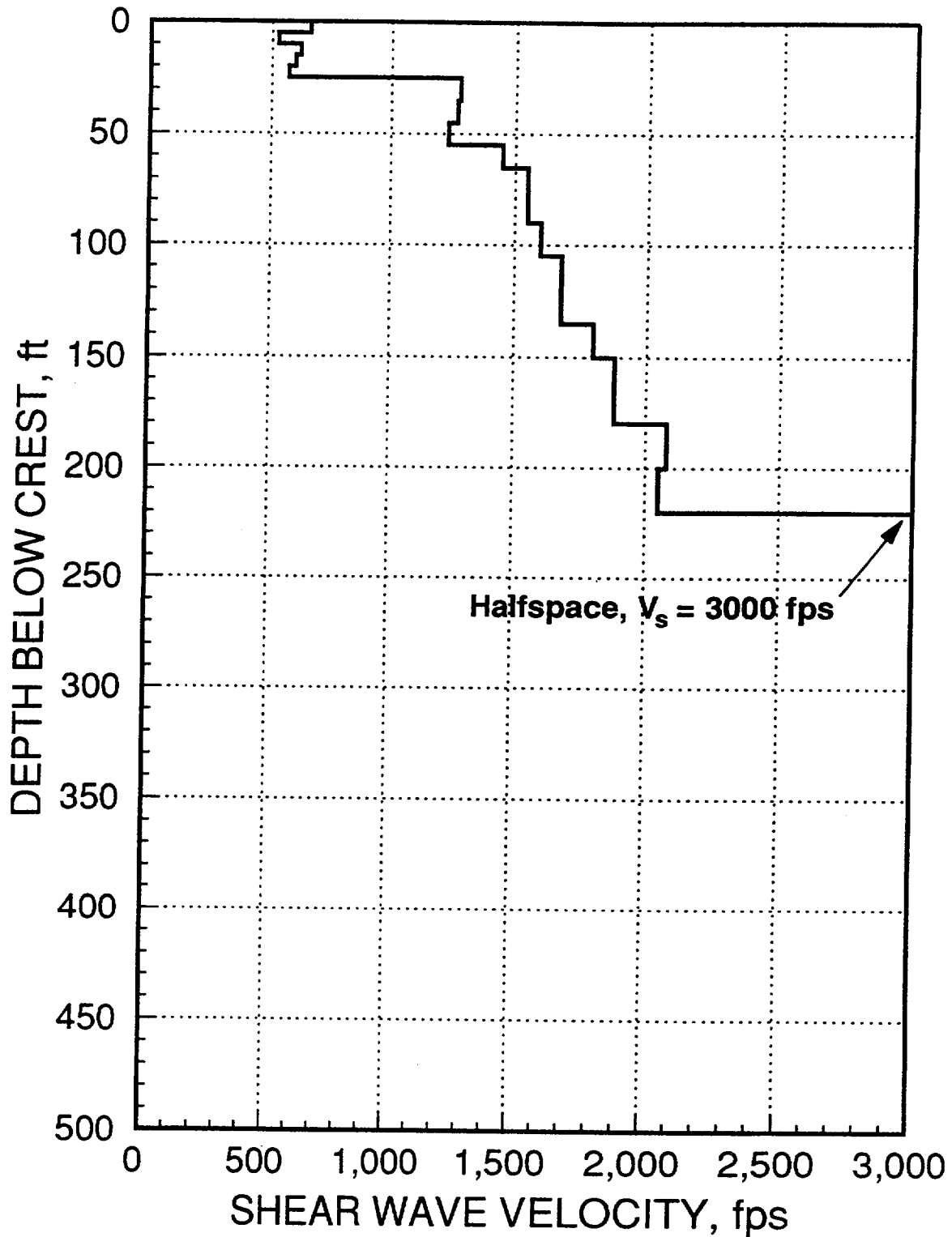


Figure 7.8: Shear wave velocity profile used in analysis of Seacliff model.

to make a direct comparison between the different frequency contents of the earthquakes, the same iterated profile was used in each analysis. The iterated damping values in all models ranged from about 3 to 6 percent. Damping in the halfspace was assumed to be 0.5 percent.

The second model, DALY CITY, is representative of the conditions at the Daly City prototype site, and consists of a 380-ft high, 45-degree slope. The shear wave velocity profile used is presented in Figure 7.9. The visco-elastic halfspace boundary was located 440-ft beneath the crest of the slope. The depth of this boundary was limited by the number of degrees-of-freedom allowed by GROUND2D for each element.

The final model, PACIFIC PALISADES, is based on a composite, idealized geometry of slopes that failed in the Pacific Palisades during the January 17, 1994, Northridge Earthquake, and at Centerville Beach during the April 24 and 25, 1992, Petrolia Earthquakes. This model consists of a 200-ft high, 60-degree slope with a visco-elastic halfspace boundary located 300 feet below the crest of the slope. Since there is no site specific data available for these sites, the soil properties used in the analyses are based on the properties determined at the two other sites, which are believed to be typical for cemented sands. These properties are shown in Figure 7.10. Though site specific properties would have been desirable, the analyses at least allow for a reasonable comparison of the response of a slope with geometry intermediate between the two prototype sites.

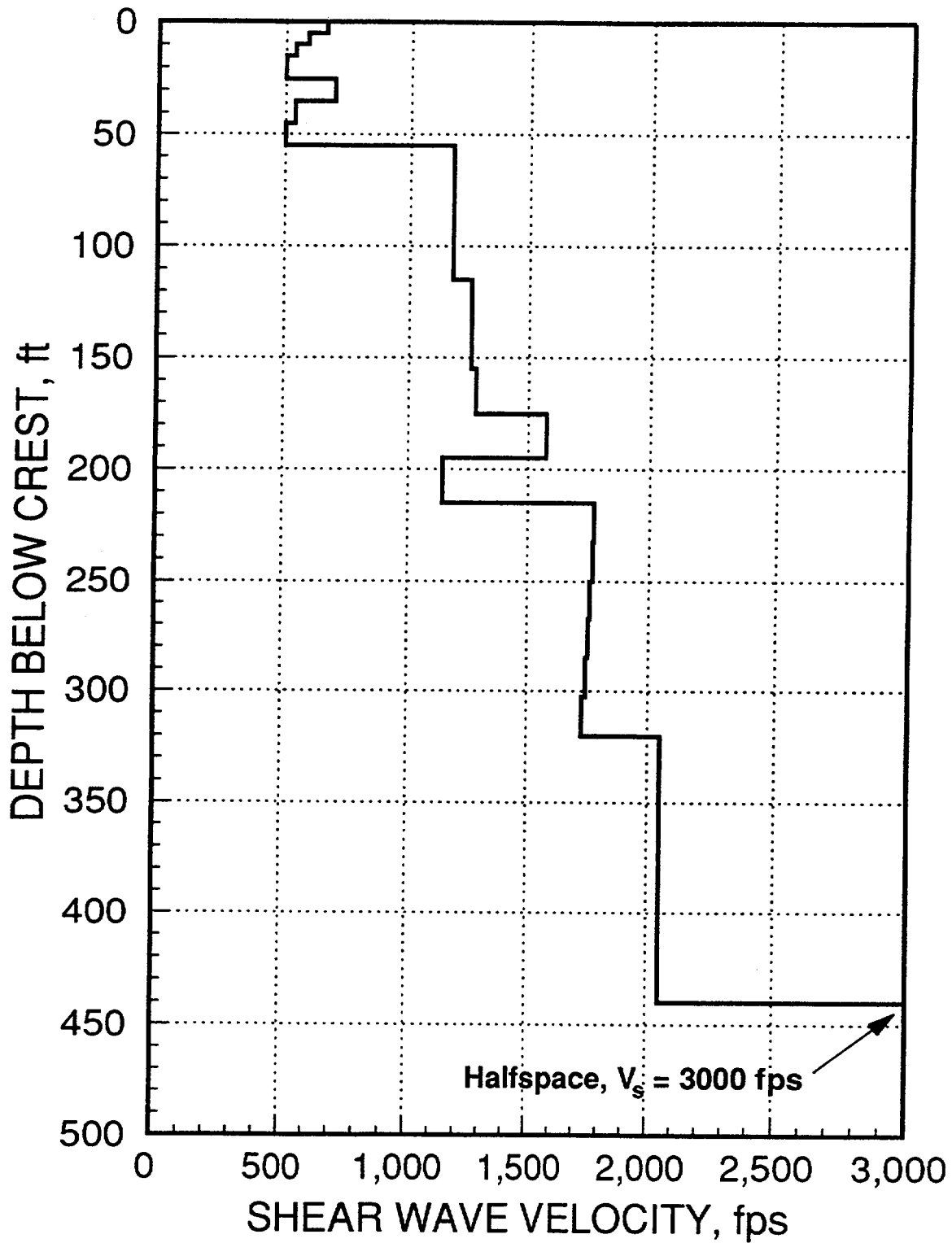


Figure 7.9: Shear wave velocity profile used in analysis of Daly City model.

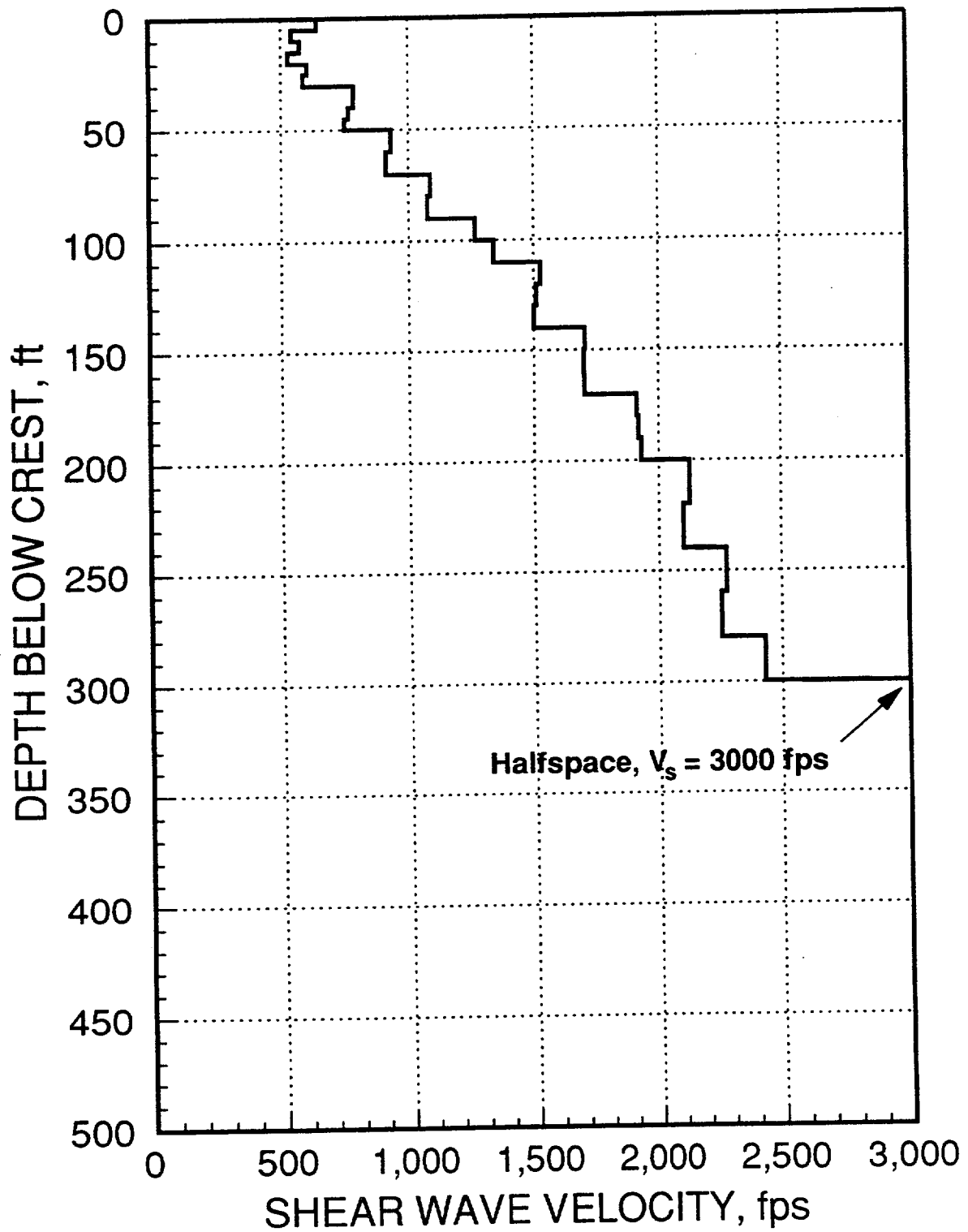


Figure 7.10: Shear wave velocity profile used in analysis of Pacific Palisades model.

## 7.3 RESULTS

In each analysis, acceleration time histories were computed along the face of the slope and in the free field behind the crest and in front of the toe. The free field response is taken as the one-dimensional response of the transmitting element under consideration. Based on the acceleration time histories, average seismic coefficient time histories were calculated using the weighted average procedure shown in Equation 6.10. From the time histories, the maximum average seismic coefficients were determined as a function of depth. In addition, the amplification of the motion at the crest of the slope was determined from the acceleration time histories computed.

### 7.3.1 Slope Crest Amplification

The comparison of the maximum acceleration computed at the crest of the slope and in the free field is presented in Table 7.1. The table shows the following: the ratio of  $Z/H$ , the input motion, the slope height, the slope angle, the topographic frequency ( $\omega_t = 0.2\lambda/H$ ), as discussed in Chapter 5, the natural frequency of the soil profile behind the crest of the slope ( $\omega_n = (V_s)_{\text{average}}/4H$ ), and the dominant frequencies of the earthquake motion ( $\omega_{\text{eq}}$ ) which were selected, with judgement, from the response spectra of each input motion. The site response is characterized by maximum acceleration at various locations as follows:  $a_{\text{fft}}$ , the maximum free field acceleration in front of the toe;  $a_{\text{ffc}}$ , the maximum free field acceleration behind the

Table 7.1: Summary of Results for 2-D Site Response Analysis

Z/H	SITE MODEL	Input Motion	H (ft)	S (deg.)	$\omega_l$ (Hz)	$\omega_n$ (Hz)	$\omega_{eq}$ (Hz)	$a_{fft}$ (g)	$a_{ffc}$ (g)	$a_{max}$ (g)	$A_t$ (%)	$A_s$ (%)	$A_a$ (%)
1.5	Pacific Palisades	ECNS	200	60	1.26	1.32	5-6	0.43	0.74	1.24	67	72	188
	Pacific Palisades	UCSC0	200	60	1.26	1.32	3,5-7	0.57	0.83	1.46	76	46	156
	Pacific Palisades	JOS90	200	60	1.26	1.32	1,3-4	0.27	0.52	0.79	52	92	192
1.16	Daly City	ECNS	380	45	0.75	0.85	5-6	0.44	0.60	0.87	45	36	98
	Daly City	UCSC0	380	45	0.75	0.85	3,5-7	0.57	0.72	1.02	41	26	79
	Daly City	JOS90	380	45	0.75	0.85	1,3-4	0.28	0.48	0.75	56	71	168
2.44	Seacliff	ECNS	90	75	2.46	1.76	5-6	0.51	0.78	1.13	45	53	122
	Seacliff	UCSC0	90	75	2.46	1.76	3, 5-7	0.64	0.86	1.33	55	34	108
	Seacliff	JOS90	90	75	2.46	1.76	1,3-4	0.30	0.45	0.65	44	50	117
1.5	Seacliff	ECNS	90	75	2.46	2.39	5-6	0.48	0.84	1.21	44	75	152
	Seacliff	UCSC0	90	75	2.46	2.39	3, 5-7	0.66	1.04	1.55	49	58	135
	Seacliff	JOS90	90	75	2.46	2.39	1,3-4	0.29	0.45	0.65	44	55	124
1.0	Seacliff	ECNS	90	75	2.46	3.07	5-6	0.32	0.81	1.15	42	153	259
	Seacliff	UCSC0	90	75	2.46	3.07	3, 5-7	0.42	1.12	1.57	40	167	274
	Seacliff	JOS90	90	75	2.46	3.07	1,3-4	0.27	0.51	0.75	47	89	178

crest; and  $a_{\max}$  the maximum crest acceleration (see Figure 7.11). In addition, three measures of amplifications are computed: "topographic amplification", i.e. the amplification of the free field motion at the crest; "site amplification", i.e. the amplification due to the natural frequencies of the site; and "apparent amplification", i.e. the apparent amplification of the motion between the base and the crest.

Mathematically, these parameters are obtained as follows:

$$\text{Topographic Amplification, } A_t = \frac{a_{\max} - a_{ffc}}{a_{ffc}} \quad (7.1)$$

$$\text{Site Amplification, } A_s = \frac{a_{ffc} - a_{ff}}{a_{ff}} \quad (7.2)$$

$$\text{Apparent Amplification, } A_a = \frac{a_{\max} - a_{ff}}{a_{ff}} \quad (7.3)$$

Consequently,

$$A_a = (1+A_t)(1+A_s)$$

Thus, the apparent amplification is completely described by the site amplification and the topographic amplification. The apparent amplification is the parameter commonly noted in field studies of topographic effects following earthquakes, and it does not take into account site amplification due to the natural frequencies of the soil

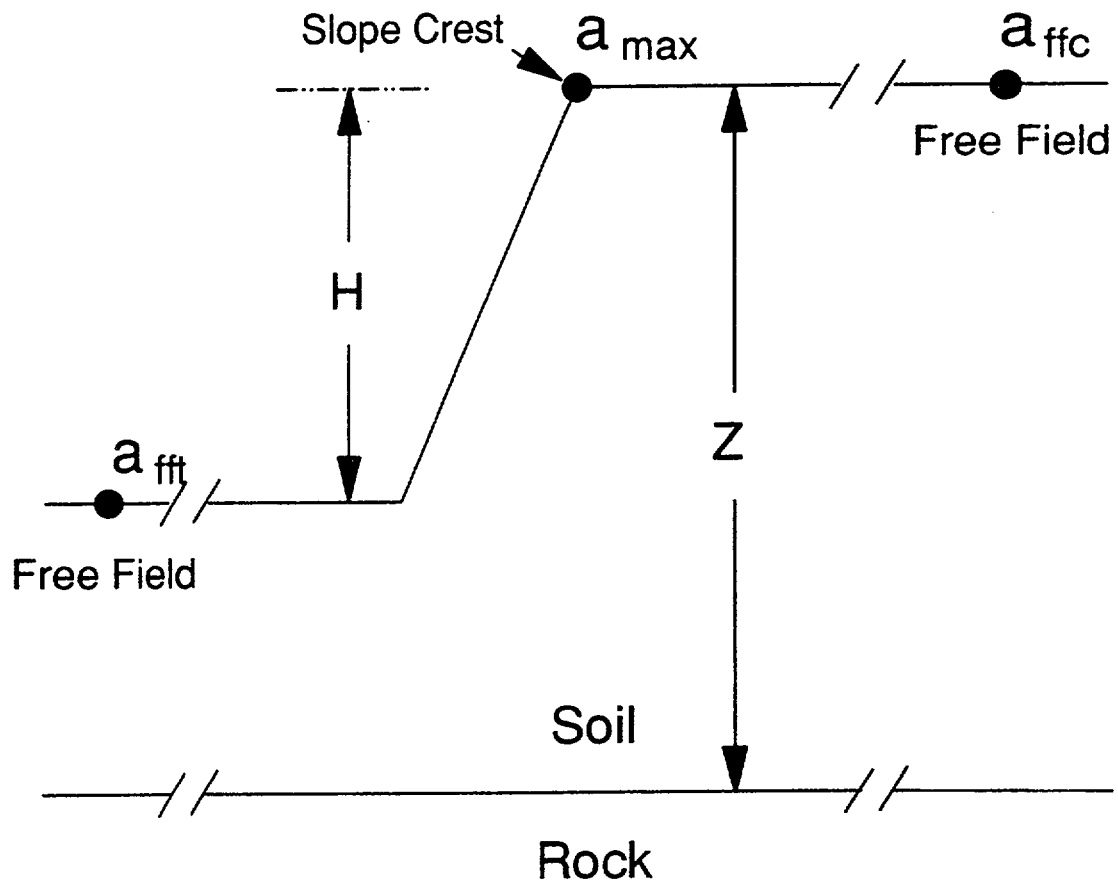


Figure 7.11: Acceleration locations calculated in study.

column. In this study, the topographic and site amplification are treated separately in an attempt to determine the contribution of the different factors. It must be noted that the "site amplification" used herein is *not* the same as the site amplification normally used in geotechnical engineering (i.e. amplification over outcrop motion).

The results of the analyses in Table 7.1 are grouped by the  $Z/H$  ratio for each slope model. Overall, the analyses show that the average topographic amplification is on the order of 50 percent, compared with the average site amplification of 72 percent and an average apparent amplification 157 percent (i.e., over 3 times the base motion). Perhaps more interesting is the range of values for the different measures of amplification: 40 to 76 percent for topographic amplification, as compared to between 26 to 167 for site amplification. In general, the site amplification has a greater effect than the topographic amplification, and the topographic amplification has less variability than the site amplification for the models studied.

A comparison of the data for each site and input motion shows that the greatest apparent amplification occurs along with the greatest site amplification. The converse is also true: the least apparent amplification occurs along with the least site amplification. This further shows the primary dependence of the acceleration at the crest of the slope on the site amplification. The individual sets of results are reviewed in more detail below in order to evaluate the dependency of slope response on the frequency content of the earthquake.

**Pacific Palisades Model.** The Pacific Palisades model shows that the greatest  $A_s$  occurs when the predominant frequency of the earthquake, in this case JOS90, matches the natural frequency of the site, as would be expected. It is more difficult to determine the effect of the frequency content of the earthquake on  $A_t$ . The highest values of  $A_t$  occur for the earthquakes with the highest predominant frequency, and not when  $\omega_{eq} \approx \omega_t$ . The results illustrate the importance of higher frequencies on topographic amplification, as was indicated in the parametric study in the preceding chapter.

**Daly City Model.** The Daly City model analyses show that both peak values of  $A_t$  and  $A_s$  occur for JOS90, when  $\omega_{eq} \approx \omega_t \approx \omega_s$ , which would coincide with the first spike in the response spectra shown in Figure 6.20. The values of  $A_t$  and  $A_s$  for the other two earthquake records are lower, markedly so for  $A_s$ .

**Seacliff Models.** The Seacliff model was used to analyze the influence of the boundary of the halfspace below the crest of the slope. The position of the halfspace boundary relative to the slope crest is represented by the ratio  $Z/H$ , where  $Z$  is the depth to the boundary below the slope crest and  $H$  is the height of the slope (see Figure 7.11). The results show that  $A_s$  increases dramatically, from an average of 46 to an average of 136 percent, as  $Z/H$  decreases and the soil column get shorter and the natural frequency of the deposit matches more closely the predominant frequencies of the input seismograms. However, though  $A_t$  tends to decrease slightly with  $Z/H$ , there does not seem to be a simple relationship between  $A_t$  and  $\omega_t$ .

**Summary.** In general, the results of the analyses of acceleration distribution in the models show that the site amplification due to the soil column is more important than topographic amplification. The effect of site amplification is readily estimated using existing methods and it does vary predictably with the frequency content of the earthquake. Topographic amplification also varies with the frequency content of the earthquake, however, a simple relationship to between frequency content and response is not evident from this study. In general, topographic amplification,  $A_t$ , appears to be affected by a broad band of frequencies and the magnitude of  $A_t$  is generally on the order of 50 percent in the cases considered here.

### 7.3.2 Maximum Average Seismic Coefficients

Time histories of average seismic coefficient,  $k_{av}$ , were developed from the 3 input seismograms for each of the 5 site models as a function of the depth of the toe of the failure wedge. From each time history, the maximum average seismic coefficient,  $k_{max}$ , was selected, and a profile of  $k_{max}$  for each model was developed. Similar to the procedure used in Makdisi and Seed (1978), the  $k_{max}$  profiles were normalized by the maximum crest acceleration of the model  $a_{max}$ . Profiles of  $k_{max}/a_{max}$  versus normalized depth,  $h/H$ , are presented in Figures 7.12 through 7.16, for each site model. The results are also summarized in Figure 7.17, along with the range of values from Makdisi and Seed (1978).

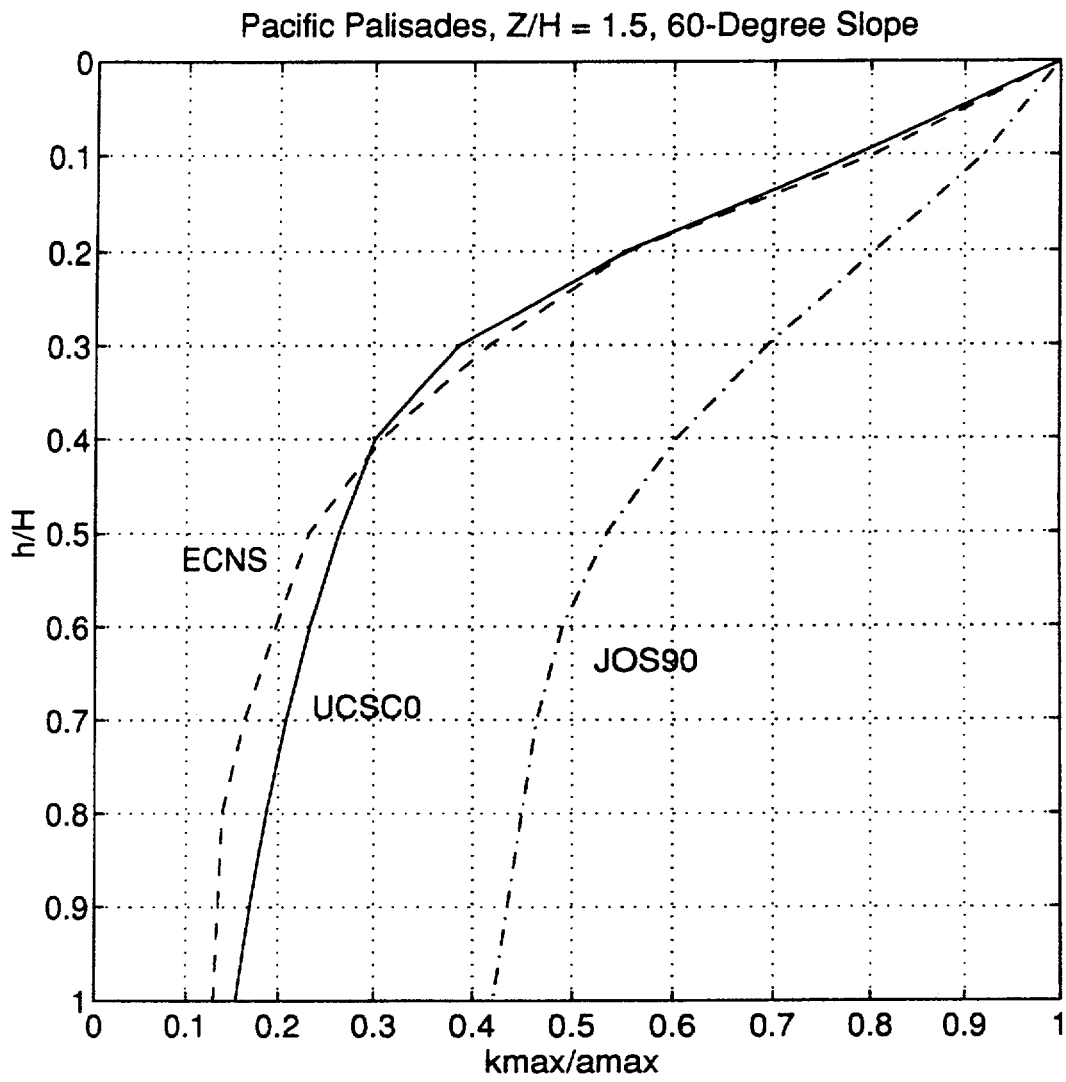


Figure 7.12: Normalized maximum seismic coefficient profile for Pacific Palisades model,  $Z/H = 1.5$ .

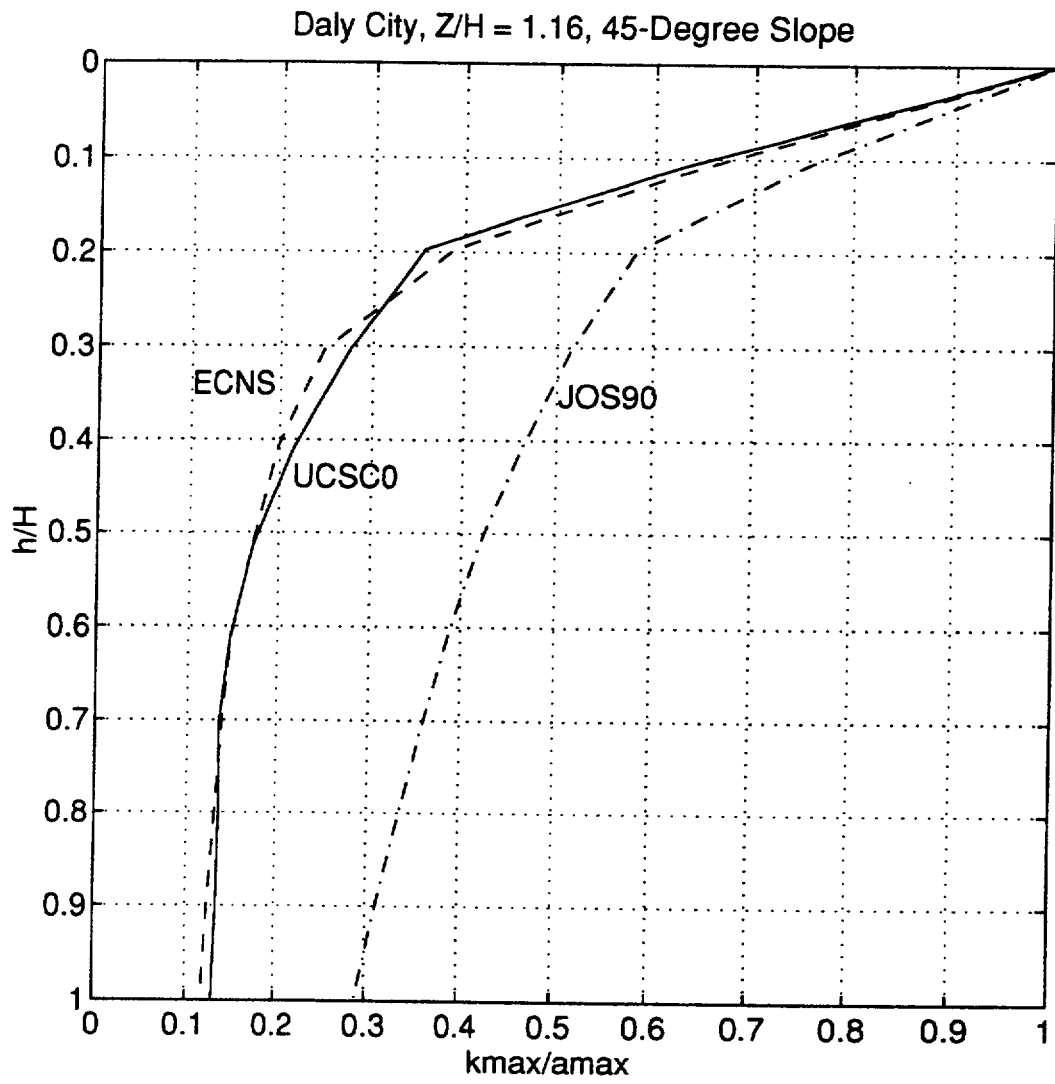


Figure 7.13: Normalized maximum seismic coefficient profile for Daly City model,  $Z/H = 1.16$ .

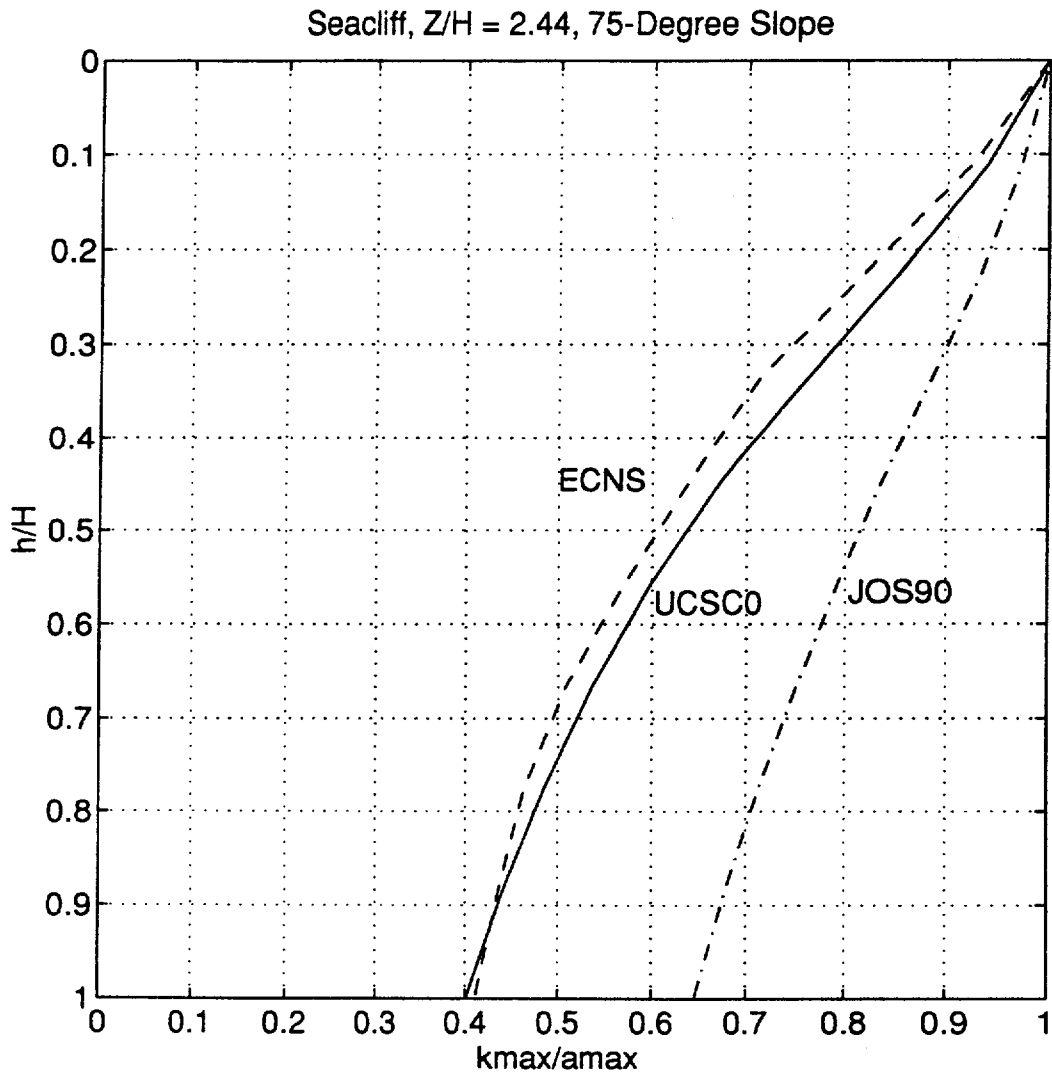


Figure 7.14: Normalized maximum seismic coefficient profile for Seacliff model,  $Z/H = 2.44$ .

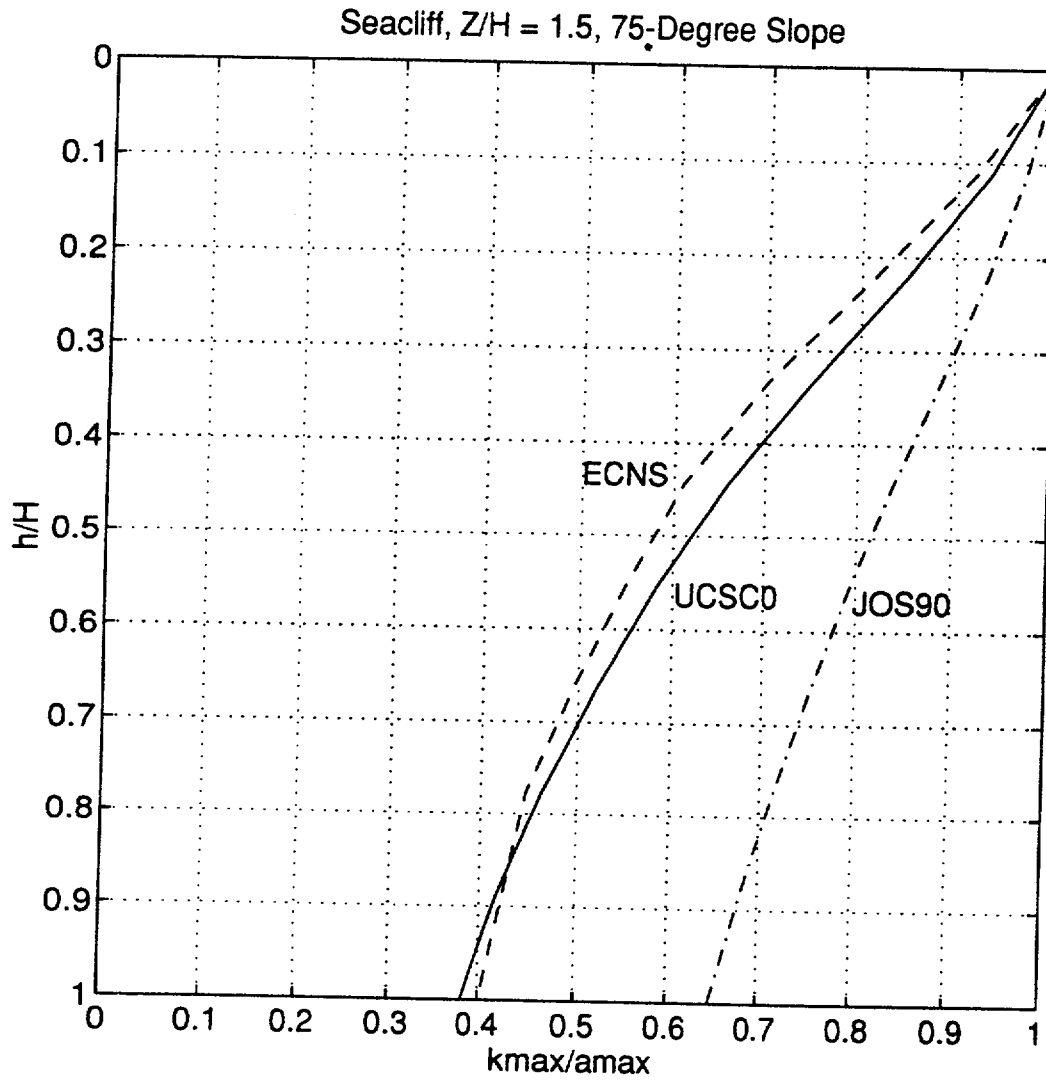


Figure 7.15: Normalized maximum seismic coefficient profile for Seacliff model,  $Z/H = 1.5$ .

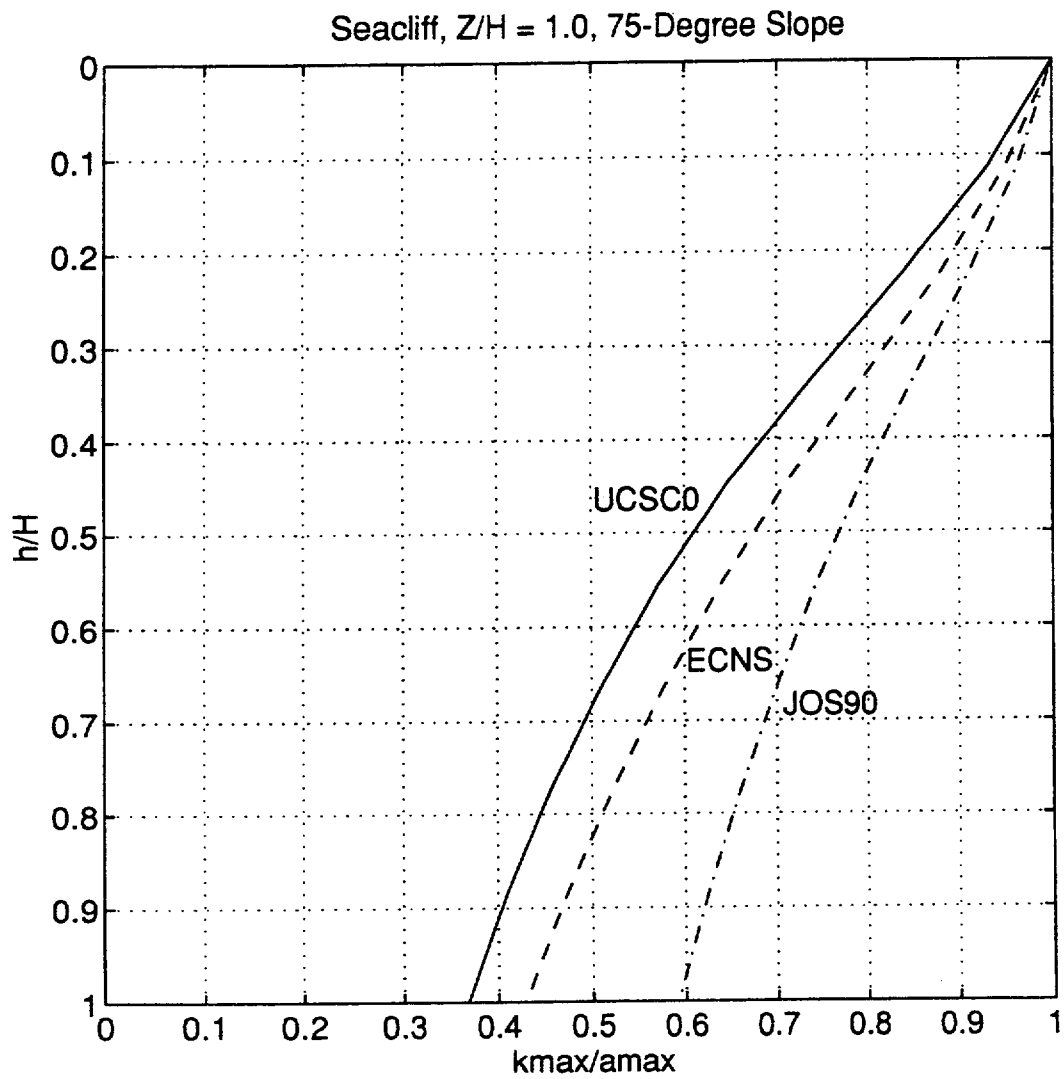


Figure 7.16: Normalized maximum seismic coefficient profile for Seacliff model,  $Z/H = 1.00$ .

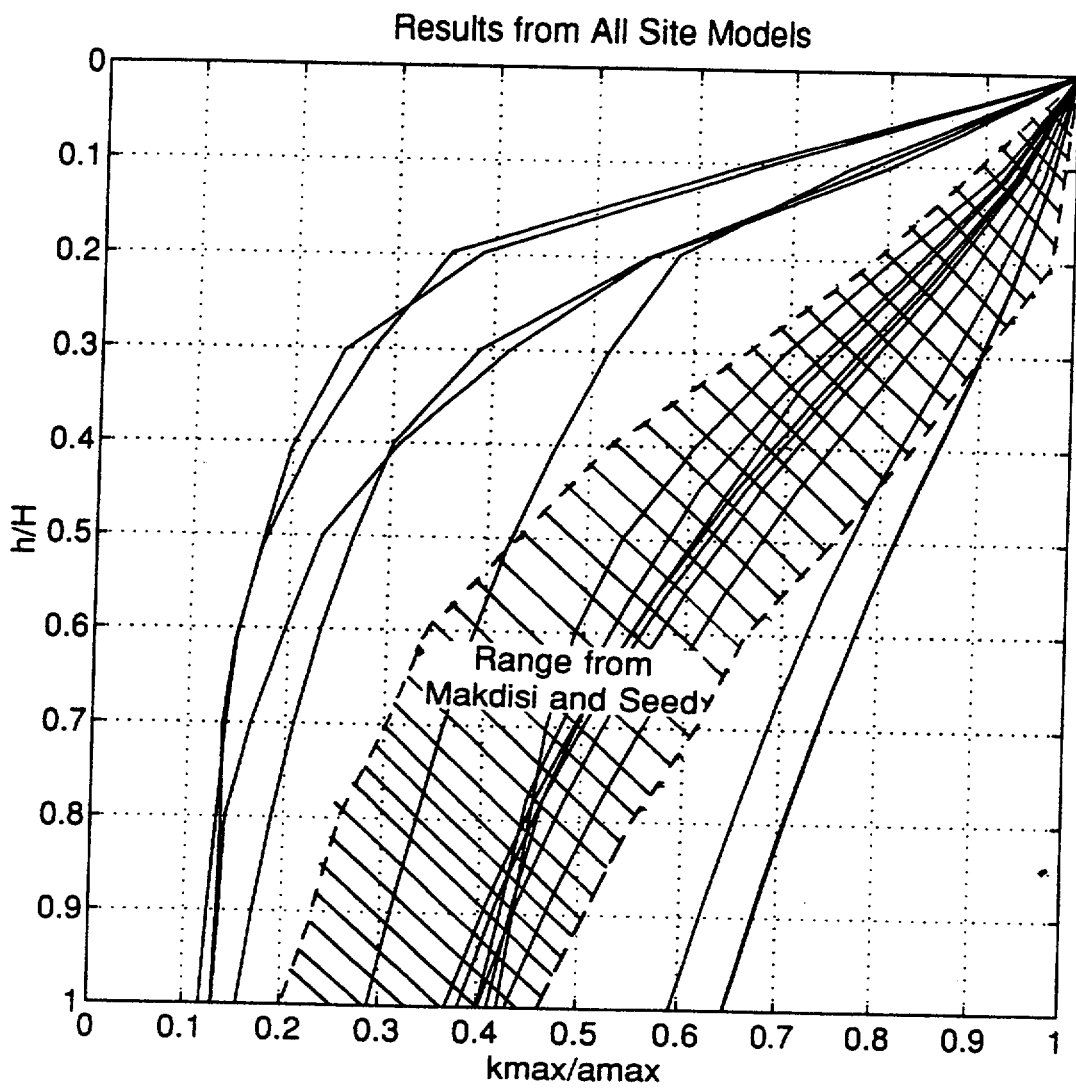


Figure 7.17: Summary plot of all results compared to Makdisi and Seed (1978).

An overall review of the results reveals a wider range values than presented by Makdisi and Seed (1978), exceeding both the upper and lower bounds. The upper bound of this data is the Seacliff Model with the JOS90 motion, while the lower bound is Daly City Cliff Model with the UCSC0 motion. For each site model, the shape of the profiles are similar, with the upper bound created by the JOS90 input motion in each case. The results from the UCSC0 and ECNS input motions are very similar within each set, the lower bound being formed by one or the other, or a combination of the two, depending on the model set.

A comparison between profiles of  $k_{\max}/a_{\max}$  for different sites, but the same input motion shows that the  $k_{\max}/a_{\max}$  profile tends to increase (i.e. shift to the right) with increasing slope angle. This is consistent for all input motions. A comparison between the Seacliff models of the  $k_{\max}/a_{\max}$  profile using the same input motion, but varying H/Z, shows a similarity of results, indicating that the  $k_{\max}/a_{\max}$  profile is somewhat independent of the depth to the halfspace boundary.

These results also indicate that the  $k_{\max}/a_{\max}$  profile is dependent on the frequency content of the earthquake, as exhibited by the comparison within sets, and the slope angle, as exhibited by the comparison between sets. The contrast between the profile shapes for the 75- and 45-degree slopes can be explained by focussing of the motion at the crest of the slope, and attenuation of the motion along the face of the flatter slope. This effect would result in the reduction of  $k_{\max}/a_{\max}$  as the failure surface extends down the slope. In addition, points along the flatter slopes may be more out of phase with the crest motion than points along the steeper slopes.

## 7.4 INFLUENCE OF INCLINED WAVES

Results of analyses of inclined incident waves in a stepped halfspace (Chapter 5) indicate that there is a potential for increased amplification of inclined SV-waves traveling into a steep slope. Consequently, it is of interest to analyze the time-domain response of a slope model subjected to inclined SV-waves. The model used in this analysis is the Seacliff model with the slope angle of  $75^\circ$ , height of 90 feet, and a  $Z/H$  ratio of 1.0. The model is subjected to the suite of 3 seismograms inclined at angles of  $10^\circ$ ,  $20^\circ$ , and  $30^\circ$  into the slope (negative angles, as defined earlier).

The results of these analyses are presented in Table 7.2 for the horizontal response and Table 7.3 for the vertical response. The comparison of the inclined wave analysis results in Table 7.2 with the results of analyses with vertically propagation waves shows two important outcomes: (1) In all cases the topographic amplification,  $A_t$ , and the apparent amplification,  $A_a$ , are greater for the inclined case than for the case of a vertically propagating wave. In addition, the site amplification,  $A_s$ , is always less for the inclined case than for the vertical case; and (2) The value of acceleration at the crest of the slope,  $a_{max}$ , increases slightly for the  $10^\circ$  case as compared to the case of the vertically propagating wave; and for waves inclined at  $20^\circ$  and  $30^\circ$ , the crest acceleration actually decreases. This apparent contradiction can be explained by the wave splitting at material interfaces, and by increased damping due to an increased travel path for inclined waves. The increased topographic amplification due to inclined waves, up to twice the vertical case, is offset

by reduced site amplification. This result indicates that inclined waves may not be critical to the stability of the slope, at least for the material properties and incident angles analyzed in this study.

*Table 7.2: Summary of Horizontal Results for Inclined Wave Analysis of Seacliff Model with Z/H = 1.0*

Incident Wave Inclination (deg)	Input Motion	$\omega_t$ (Hz)	$\omega_n$ (Hz)	$\omega_{eq}$ (Hz)	$a_{fft}$ (g)	$a_{ffc}$ (g)	$a_{max}$ (g)	$A_t$ (%)	$A_s$ (%)	$A_a$ (%)
0	ECNS	2.46	3.07	5-6	0.32	0.81	1.15	42	153	259
	UCSC0	2.46	3.07	3, 5-7	0.42	1.12	1.57	40	167	274
	JOS90	2.46	3.07	1,3-4	0.27	0.51	0.75	47	89	178
10	ECNS	2.46	3.07	5-6	0.31	0.78	1.20	54	152	287
	UCSC0	2.46	3.07	3, 5-7	0.41	1.08	1.69	56	163	312
	JOS90	2.46	3.07	1,3-4	0.26	0.49	0.77	57	88	196
20	ECNS	2.46	3.07	5-6	0.27	0.62	1.08	74	130	300
	UCSC0	2.46	3.07	3, 5-7	0.36	0.79	1.49	89	119	314
	JOS90	2.46	3.07	1,3-4	0.22	0.33	0.64	94	50	191
30	ECNS	2.46	3.07	5-6	0.26	0.60	1.07	78	131	312
	UCSC0	2.46	3.07	3, 5-7	0.34	0.74	1.44	94	118	324
	JOS90	2.46	3.07	1,3-4	0.22	0.32	0.64	100	45	190

*Table 7.3: Summary of Vertical Response Results for Inclined Wave Analysis of Seacliff Model with Z/H = 1.0*

Incident Wave Inclination (deg)	Input Motion	$\omega_t$ (Hz)	$\omega_n$ (Hz)	$\omega_{eq}$ (Hz)	$a_{v,fft}$ (g)	$a_{v,ffc}$ (g)	$a_{v,max}$ (g)	$a_{max}/a_{v,max}$ (ratio)
0	ECNS	2.46	3.07	5-6	0	0	0.57	0.50
	UCSC0	2.46	3.07	3,5-7	0	0	0.86	0.55
	JOS90	2.46	3.07	1,3-4	0	0	0.26	0.35
10	ECNS	2.46	3.07	5-6	0.07	0.10	0.52	0.43
	UCSC0	2.46	3.07	3,5-7	0.09	0.14	0.70	0.41
	JOS90	2.46	3.07	1,3-4	0.05	0.06	0.23	0.30
20	ECNS	2.46	3.07	5-6	0.17	0.25	0.42	0.39
	UCSC0	2.46	3.07	3,5-7	0.21	0.32	0.67	0.45
	JOS90	2.46	3.07	1,3-4	0.14	0.15	0.24	0.38
30	ECNS	2.46	3.07	5-6	0.18	0.29	0.35	0.33
	UCSC0	2.46	3.07	3,5-7	0.24	0.37	0.57	0.40
	JOS90	2.46	3.07	1,3-4	0.15	0.16	0.23	0.36

The vertical response of the model due to inclined SV-waves are summarized in Table 7.3, along with the results for the case of a vertically propagating wave. The results show that the maximum vertical acceleration,  $a_{v,max}$ , is typically 30 to 50 percent of the maximum horizontal acceleration,  $a_{max}$ , which is lower than the cases studied by Sitar and Clough (1983), in which the peak vertical response was nearly equal to the peak horizontal response. Also, the ratio between the vertical and horizontal response varies with the wave inclination as well as with the specific input

motion. The results also show that even though vertical accelerations occur in the free field due to wave splitting, as shown by  $a_{v,fft}$  and  $a_{v,ffc}$ , the vertical response at the crest is still greatest for the case of the vertically propagating wave for all earthquakes considered. Thus, as with the horizontal response, the vertical response results show that the inclined wave may not be as critical to the stability of the slope as the vertically propagating wave.

## 7.5 CONCLUSIONS

Case studies of the seismic response of steep slopes were performed. The response was quantified in terms of the amplification of the peak free field acceleration at the crest of the slope, and in terms of the profile of the maximum average seismic coefficient,  $k_{max}$ , normalized by the peak crest acceleration,  $a_{max}$ .

The results of the analyses indicate that the amplification due to the natural frequency of the site dominates the response, as was also observed by Idriss and Seed (1967), and that this effect varies greatly, depending on the relationship between the natural frequency and the predominant frequency of the input motion. The amplification due to topography, on the other hand, shows less variability. The topographic amplification ranges between 40 and 76 percent of the free field motion behind the crest, and is on the order on 50 percent when the predominant frequency of the earthquake is near the natural frequency of the site. This also corresponds to the peak overall response of the crest. This amount of topographic amplification agrees with results previous equivalent linear finite element studies of steep slopes

(Sitar and Clough, 1983). Their data show a 70 percent amplification at the crest when the predominant frequency of the earthquake is near the topographic frequency ( $\omega_{eq} \approx 4.5$  Hz,  $\omega_t \approx 4$  Hz, and  $\omega_s \approx 2.5$  Hz), and a 40 percent amplification at the crest when the predominant frequency of the earthquake is closer to the natural frequency of the site ( $\omega_{eq} \approx 4.5$  Hz,  $\omega_t \approx 2.6$  Hz, and  $\omega_s \approx 3.2$  Hz). Therefore, a reasonable estimate of the acceleration at the crest of the slope could be made by increasing the estimated free field motion behind the crest by about 50 percent, although in some cases, this simple adjustment could be somewhat unconservative. A conservative approach would be to select an input motion for the free field analysis that has a predominant frequency near the natural frequency of the profile behind the crest ( $\omega_{eq} = \omega_s$ ). In such a case, increasing the computed free field motion by 50 percent would be amply conservative.

The  $k_{max}/a_{max}$  profiles presented herein are of the same general shape, but cover a broader range, than the profiles developed by Makdisi and Seed (1978). Moreover, the  $k_{max}/a_{max}$  profiles vary with the frequency content of the earthquake and the slope angle. The ratio of  $k_{max}/a_{max}$  increases with slope angle, with the steepest slopes forming an upper bound. Thus, when selecting a value of  $k_{max}/a_{max}$  for a particular slope, it would seem appropriate to use the upper bound values for steep slopes (greater than 60 degrees); and average values for moderately steep slopes (less than 60 degrees).

The results of the analyses of inclined incident waves show that, even though the topographic amplification is greater for inclined waves, the magnitude of the acceleration at the crest (both horizontal and vertical) is greatest for the case of

vertically propagating waves. The ratio between the peak vertical and horizontal response in the time domain ranges from 0.3 to 0.5, and was observed to vary with incident angle and input motion.

## **7.6 IMPLICATIONS FOR STABILITY ANALYSES OF STEEP SLOPES**

Though the study presented herein was carried out specifically for steep slopes in weakly cemented sands, the procedures used in the seismic response portion of the study are equally applicable to steep slopes in other materials. Therefore, based on the relationships between the peak acceleration at the crest and the maximum seismic coefficient, a procedure for incorporating the results of this study into the stability analysis of steep slopes can be suggested, as follows:

(1) The initial step should be a one-dimensional seismic site response analysis in the free field behind the crest of the slope (e.g. using SHAKE) using an input motion appropriate for the site under consideration. When considering topographic effects, ample conservatism can be obtained by selecting an input motion with a predominant frequency close to the natural frequency of the site.

(2) To account for the effect of topography, the maximum ground surface acceleration obtained by the 1-D analysis should be increased by 50 percent to estimate the maximum acceleration at the crest of the slope.

(3) Normalized values of  $k_{\max}$  at various depths can be selected from the relationships presented in this study. Upper bound values should be used for steepest slopes, while average values should be used for shallower slopes. The values of  $k_{\max}$  should be multiplied by 0.65 (Seed and Martin, 1967) to get the  $k_{av}$  value to use for analysis.

(4) For steepest slopes,  $k_{av}$  can be used to estimate average tensile stress on failure plane and perform limit equilibrium analysis. For shallower slopes,  $k_{av}$  can be used in typical pseudo-static limit equilibrium analysis. For slopes in weakly cemented sands, static strengths can be used to estimate the dynamic strength of materials, based on results reported by Wang (1986) and Sitar (1990).



## REFERENCES

- Acar, Y. B., and El-Tahir, E. A. (1986). "Low Strain Dynamic Properties of Artificially Cemented Sand," *J. Geotech. Engrg.*, ASCE, 112(11) 1001-1015
- Acar, Y. B., Hilal, H., and Tumay, M. T., (1988). "FEM Analysis of Elastic Stress Distributions in Embankments," *J. Geotech. Engrg.*, ASCE, 114(6) 711-718.
- Bard, P-Y. (1982). "Diffracted Waves and Displacement Field over Two-Dimensional Elevated Topographies," *Geophys. J. R. Astro. Soc.*, 71(3) 731-760.
- Barlow, N. (1933). *Charles Darwin's Diary of the Voyage of H.M.S. Beagle*; Nora Barlow, editor, Cambridge University Press.
- Bonilla, M. G. (1959). "Geologic Observation in the Epicentral Area of the San Francisco Earthquake of March 22, 1957," *Special Report 57*, G. B. Oakenshott editor, California Division of Mines, 25-37.
- Boore, D. M. (1972). "A Note on the Effect of Simple Topography on Seismic SH Waves," *Bulle. Seis. Soc. Am.*, 62(1) 275-284.
- Bouchon, M. (1973). "Effect of Topography on Surface Motion," *Bulle. Seis. Soc. Am.*, 63(3) 615-632.
- Boughton, N. O. (1970). "Elastic Analysis for Behavior of Rockfill," *J. Soil Mech. and Found. Div.*, 96(SM5) 1715-1733.
- Bustamante, J. T. (1965). "Dynamic Behavior of Noncohesive Embankment Models," *Proceedings, 3rd World Conference on Earthquake Engineering*, New Zealand, III(IV:596-IV:612).
- Carrillo, A., and Garcia, E. (1985). "A Study on Stability of Natural Cliffs with Seismic Effects," *Proceedings, Eleventh I.C.S.M.F.E.*, San Francisco. Vol. 4, 1937-1941.
- Celebi, M. (1987). "Topographic and Geological Amplification Determined from Strong-Motion and Aftershock Records of the 3 March 1985 Chile Earthquake," *Bulle. Seis. Soc. Am.*, 77(4) 1147-1167.
- Celebi, M. (1991). "Topographic and Geological Amplification: Case Studies and Engineering Implications," *Structural Safety*, 10 (1991) 199-217.
- Chen, J. (1980) "Analysis of Local Variations in Free Field Seismic Ground Motion," thesis presented to University of California at Berkeley, Berkeley, California in partial satisfaction of the requirements for the degree of Doctor of Philosophy.

- Clough, G. W., Sitar, N., Bachus, R. C., and Rad, N. S. (1981). "Cemented Sands under Static Loads," *J. Geotech. Engrg.*, ASCE, 107(6) 799-817
- Clough, G. W., Iwabuchi, J. N., Rad, N. S. (1989). "Influence of Cementation on Liquefaction of Sands," *J. Geotech. Engrg.*, ASCE, 115(8) 1102-1117.
- Clough, R. W. and Woodward, R. (1967). "Analysis of Embankment Stresses and Deformations," *J. Soil Mech. and Found. Div.*, ASCE, 93 (4) 529-549.
- Dakoulas, P. (1993). "Earth Dam-Canyon Interaction Effects for Obliquely Incident SH Waves." *J. Geotech. Engrg.*, ASCE, 119(11) 1696-1716.
- Davis, L. L., and West, L. R. (1973). "Observed Effects of Topography on Ground Motion," *Bulle. Seis. Soc. Am.*, 63(1) 283-298.
- Deng, N. (1991). "Two-Dimensional Site Response Analyses", thesis presented to University of California at Berkeley, Berkeley, California in partial satisfaction of the requirements for the degree of Doctor of Philosophy.
- Deng, N., Ashford, S. A., and Lysmer, J. (in press). *GROUND2D: A Two-Dimensional Seismic Site Response Analysis Program*, Earthquake Engineering Research Center Report, College of Engineering, University of California, Berkeley.
- Dobrin, M. B. (1976). *Introduction to Geophysical Prospecting, 3rd ed.*, McGraw-Hill Book Co., New York.
- Duncan, J. M., and Goodman, R. E. (1968). "Finite Element Analysis of Slopes in Jointed Rock." *Report No. TE-68-1*, College of Engineering, Univ. of California, Berkeley, Calif.
- E.P.R.I. (Electric Power Research Institute) (1991). *Proceedings: NSF/EPRI Workshop on Dynamic Soil Properties and Site Characteristics*, Report No. EPRI NP-7337, VI.
- Farquharson, F. B., and Hennes, R. G. (1940). "Gelatin Models for Photoelastic Analysis of Stress in Earth Masses," *Civil Engrg.*, 10(4) 211-214.
- Frydman, S., (1980). "Liquefaction Study of Cemented Sands," *J. Geotech. Engrg.*, ASCE, 105(3) 419-436.
- Gazetas, G., and Dakoulas, P. (1992). "Seismic Analysis and Design of Rockfill Dams: State-of-the-Art," *Soil Dynamics and Earthquake Engineering*, 11(1992) 27-61.
- Geli, L., Bard, P-Y., and Jullien, B. (1988). "The Effect of Topography on Earthquake Ground Motion: A Review and New Results," *Bulle. Seis. Soc. Amer.*, 78(1) 42-63.

Goodman, R. E., and Seed, H. B. (1966). "Earthquake Induced Displacements in Sand Embankments," *J. Soil Mech. and Found. Div.*, ASCE, 92(SM2) 125-146.

Griffiths, D. V. and Prevost, J. H. (1988). "Two- and Three-Dimensional Dynamic Finite Element Analyses of the Long Valley Dam," *Geotechnique*, 38(3) 367-388.

Harp, E. L., Wilson, R. C., Wieczorak, G. F., and Keefer, D. K. (1978). "Landslides from the February 4, 1976 Guatemala Earthquake: Implications for Seismic Hazard Reduction in the Guatemala City Area," *Proceedings of the Second Int. Conf. on Microzonation for Safer Construction-Research and Application*, San Francisco, 353-366.

Haruyama, M. (1973). "Geological, Physical, and Mechanical Properties of Shirasu and it's Engineering Classification," *Soils and Foundations*, JSSFE, 13(3) 45-60.

Idriss, I. M. and Seed, H. B. (1967). "Response of Earthbanks During Earthquakes," *J. Soil Mech. and Found. Div.*, ASCE, 93(SM3) 61-82.

Idriss, I. M. (1968). "Finite Element Analysis for the Seismic Response of Earth Banks," *J. Soil Mech. and Found. Div.*, ASCE, 94(SM3) 617-636.

Knopoff, L., Fredricks, R. W., Gangi, A. F. and Porter, L. D. (1957). "Surface Amplitudes of Reflected Body Waves." *Geophysics*, 22(4) 842-847.

Kovacs, W. D., Seed, H. B., and Idriss, I. M. (1971). "Studies of Seismic Response of Clay Banks," *J. Soil Mech. and Found. Div.*, ASCE, 97(SM2) 441-455.

Kulhawy, F. H. and Duncan, J. M. (1972). "Stresses and Movements in Oroville Dam," *J. Soil Mech. and Found. Div.*, ASCE, 98(SM7) 653-665.

Kuwano, J. and Ishihara, K. (1988). "Analysis of Permanent Deformation of Earth Dams Due to Earthquakes," *Soils and Foundations*, JSSFE, 28(1) 41-55.

La Rochelle, P. (1960). "The Short-Term Stability of Slopes in London Clay," thesis presented to the Univ. of London, at London, England, in partial fulfillment of the requirements of the degree of Doctor of Philosophy.

Lawson, A.C. (1908). *California Earthquake of April 18, 1906*, Publication No. 87, Report to the State Earthquake Investigation Committee, Vol. 1. Carnegie Institute of Washington, Washington D.C.

Lefebvre, G., Duncan, J. M., and Wilson, E. L. (1973). "Three-Dimensional Finite Element Analysis of Dams," ASCE, *J. Soil Mech. and Found. Div.*, 99(SM7) 495-507.

Lysmer, J., Ashford, S. A., and Deng, N. (in press). *Spatial Variations of Ground Motion*, Earthquake Engineering Research Center Report, College of Engineering, University of California, Berkeley.

Makdisi, F. I., and Seed, H. B. (1977). "A Simplified Procedure of Estimating Earthquake-Induced Deformations in Dams and Embankments." *EERC Research Report*, Report No. UCB/EERC-77/19

Makdisi, F. I., and Seed, H.B. (1978). "Simplified Procedure for Estimating Dam and Embankment Earthquake-Induced Deformations," *J. Geotech. Engrg. Div., ASCE*, 104(GT7) 849-867.

May, T. W. (1980). "The Effectiveness of Trenches and Scarps in Reducing Seismic Energy." *Ph.D. Thesis in Engineering*, U.C. Berkeley, Dec. 1980.

Middlebrooks, T. A., Discussion of "Gelatin Models for Photoelastic Analysis of Stress in Earth Masses," by F.B. Farquharson and R.G. Hennes, *Civil Engrg.*, 10(8) 529-530.

Mononobe, N., Takata, A., and Matumura, M. (1936). "Seismic Stability of the Earth Dam," Section and Congress on Large Dams, Washington, 4(1936) 435-442.

Murata, H., and Yamanouchi, T. (1978). "Dilatancy and Failure Mechanism in Undisturbed Shirasu." *Soils and Foundations*, 18(2) 59-67.

Naylor, D. J., Maranha Das Neves, E., and Mattar Jr., D. (1986). "Prediction of Construction Performance of Beliche Dam," *Geotechnique*, 36(3) 359-376.

Naylor, D. J., and Mattar Jr., D. (1988). "Layered Analysis of Embankment Dams," *Numerical Methods in Geomechanics (Innsbruck, 1988)*, Balkema, Rotterdam, 1199-1205.

Newmark, N. M. (1965) "Effects of Earthquakes on Dams and Embankment." *paper presented at the Fifth Rankine Lecture*, I.C.E., London, England, Feb.

O'Rourke, T. D., and Crespo, E. (1988). "Geotechnical Properties of Cemented Volcanic Soil," *J. Geotech. Engrg.*, ASCE, 114(10) 1126-1147.

Plant, N. and Griggs, G.B. (1990). "Coastal Landslides Caused by the October 17, 1989 Earthquake," *California Geology*, 43(4) 75-84.

Reid, H.F. (1910). *The California Earthquake of April 18, 1906: Vol.2 The Mechanics of the Earthquake*, Report of the State Earthquake Commission, Carnegie Institute of Washington, Washington D.C.

- Rogers, A. M., Katz, L. J., and Bennett, T. J. (1974). "Topographic Effects on Ground Motion for Incident P-Waves: A Model Study," *Bulle. Seis. Soc. Am.*, 64(2) 437-456.
- Rogers, F.J. (1908). "Experiments with a Shaking Machine," in *California Earthquake of April 18, 1906*, Publication No. 87, Report to the State Earthquake Investigation Committee, Vol. 1 (A.C. Lawson, ed.) Carnegie Institute of Washington, Washington D.C. pp. 326-335.
- Sanchez-Sesma, F., Herrera, I., and Aviles, J. (1982). "A Boundary Method for Elastic Wave Diffraction: Application to Scattering SH Waves by Surface Irregularities," *Bulle. Seis. Soc. Am.*, 72(2) 473-490.
- Sarma, S. K. (1975). "Seismic Stability of Earth Dams and Embankments," *Geotechnique*, 25(4) 743-761.
- Saxena, S. K. and Lastrico, M. (1978). "Static Properties of Lightly Cemented Sand," *J. Geotech. Engrg. Div.*, ASCE, 104(GT12) 1449-1465
- Schnabel, P. B., Lysmer, J., and Seed, H. B. (1972). "SHAKE," *NISEE/Computer Applications*, EERC, Report No. EERC 72-12.
- Seed, H. B. (1966). "A Method for Earthquake Resistant Design of Earth Dams," *J. Soil Mech. and Found. Div.*, ASCE, 92(SM1) 13-41.
- Seed, H. B. (1964). "Earthquake Stability of Slopes of Cohesionless Soils," *J. of Soil Mech. and Found. Div.*, ASCE, 90(SM6) 43-73.
- Seed, H. B., Lee, K. L., and Idriss, I.M. (1969). "Analysis of Sheffield Dam Failure," *J. Soil Mech. and Found. Div.*, ASCE, 95(SM6) 1453-1490.
- Seed, H. B. and Martin, G. R. (1966) "The Seismic Coefficient in Earth Dam Design." *J. Soil Mech. and Found. Div.*, ASCE, 92(SM3) 25-58.
- Seed, R. B. et al. (1990). *Preliminary Report on the Principal Geotechnical Aspects of the October 17, 1989 Loma Prieta Earthquake*, Report No. UCB/EERC-90/05, Earthquake Engineering Research Center, University of California, Berkeley. April.
- Shakal, A., et al. (1992). *CSMIP Strong-Motion Records from the Petrolia, California Earthquakes of April 25-26, 1992*, Report No. OSMS 92-05, California Strong Motion Instrumentation Program, California Division of Mines and Geology.
- Sills, L. (1978). "Scattering of Horizontally Polarized Shear Waves by Surface Irregularities," *Geophys. J. R. Astro. Soc.*, 54(2) 319-348.

- Sitar, N. (1990). "Seismic Response of Steep Slopes in Weakly Cemented Sands and Gravels," *Proceedings, H. Bolton Seed Memorial Symposium*, Vol. II, 67-82.
- Sitar, N. (1991). "Earthquake-Induced Landslides in Coastal Bluffs and Marine Terrace Deposits," *Special Publication No. 1, Loma Prieta Earthquake*, Assoc. of Eng. Geol., 75-82.
- Sitar, N. and Clough, G. W. (1979). "Behavior of Slopes in Weakly Cemented Soils under Seismic Loading," *Proceedings of the Second U. S. National Conference on Earthquake Engineering*, Stanford, California. 1006-1015.
- Sitar, N. and Clough, G. W. (1983). "Seismic Response of Steep Slopes in Cemented Soils," *J. Geotech. Engrg.*, ASCE, 109(2) 210-227.
- Smith, I. M., and Hobbs, R. (1974). *Geotechnique*, 24(4) 531-559.
- Smith, W. D. (1975). "The Application of Finite Element Analysis to Elastic Body Wave Propagation Problems," *Geophys. J. R. Astro. Soc.*, 42(2) 747-768.
- Taylor, D.W. (1948). *Fundamentals of Soil Mechanics*. John Wiley & Sons, New York.
- Taylor, R. L., (1977) "Computer Procedures for Finite Element Analysis," Chapter 24 of *The Finite Element Method* by O. C. Zienkiewicz, Third Edition, McGraw Hill, London.
- Timoshenko, S. P., and Goodier, J. N. (1970) *Theory of Elasticity, Third Ed.*, McGraw-Hill Book Company, New York.
- Vrymoed, J. (1981). "Dynamic FEM Model of Oroville Dam," *J. Geotech. Engrg. Div., ASCE*, 107(GT8) 1057-1077.
- Wang, Y. D. (1986). "Investigation of Constitutive Relations for Weakly Cemented Sands," Ph.D. Dissertation, Department of Civil Engineering, Univ. of Calif., Berkeley. 293 p.
- Yamanouchi, T. (1977). "Tensile Stresses in Unsupported Slopes of a Pumice Soil," *Proceedings, Ninth I.C.S.M.F.E.*, Tokyo, Vol. 3 418-419.
- Yamanouchi, T., and Murata, H. (1973). "Brittle Failure of Volcanic Ash Soil 'Shirasu'," *Proceedings, Eighth I.C.S.M.F.E.*, Moscow. 495-500.
- Youd, T. L., and Hoose, S. H. (1978). "Historic Ground Failures in Northern California Triggered by Earthquakes," *Geological Survey Professional Paper 993*, U.S. Government Printing Office, Washington.

Zahradnik, J., and Urban, L. (1984). "Effect of a Simple Mountain Range on Underground Seismic Motion," *Geophys. J. R. Astro. Soc.*, 79(1) 167-183.

Zienkiewicz, O. C., Valliappan, S., and King, I. P. (1968) *Geotechnique*, 18(1) 56-66.



## APPENDIX A. SOIL BORINGS

A single boring was drilled at each prototype site using the rotary wash method. A 5-inch diameter pilot hole was first drilled in order to obtain samples. Samples were generally collected at 5- to 20-foot intervals to a depth of 100 feet. For the deeper Daly City borehole, samples were only obtained at changes in stratigraphy below 100 feet. For the most part, relatively undisturbed 3-inch diameter samples were obtained using a Pitcher barrel sampler. On a few occasions, the Standard Penetration Test was performed, and disturbed, driven samples were obtained. The main purpose of the sampling was the evaluation of site stratigraphy.

Once sampling was completed, the boring was reamed out to 8-inches. The drilling fluid was then thinned out and 4-inch diameter Schedule 40 P.V.C. pipe was installed to the bottom of the boring. The pipe was the bell and spigot type and was capped on the bottom. In order to lower the pipe through the drilled fluid, the pipe was filled with clean water. The annulus between the pipe and the boring was then tremie grouted with a portland cement and bentonite grout. The grout mix was approximately 4 sacks (376 pounds) of Type I-II Portland Cement and 1/4 to 1/3 sack (16 pounds) of high-yield bentonite per 55-gallons of water. At the Daly City site, the grout was placed over a two-day period to prevent excessive shrinkage of the grout. Once the grout was placed, the top of the pipe was capped to await future testing and possible installation of strong motion instrumentation.

The boring logs for each of the two boreholes are presented in the following pages, along with the gamma log from the Daly City site.

PROJECT NUMBER S-22614	BORING NUMBER SC-1	SHEET / OF /
<b>SOIL BORING LOG</b>		

PROJECT USGS Research Project LOCATION Seacliff State Beach  
 ELEVATION 95 ft. DRILLING CONTRACTOR Pitcher Drilling Co., Palo Alto, CA  
 DRILLING METHOD AND EQUIPMENT Rotary Wash, Failing 1500 Rig  
 WATER LEVELS Not Measured START 6/10/92 FINISH 6/11/92 LOGGER Scott Ashford

DEPTH BELOW SURFACE (FT)	SAMPLE			STANDARD PENETRATION TEST RESULTS 6"-6" (N)	SOIL DESCRIPTION SOIL NAME, USCS GROUP SYMBOL, COLOR, MOISTURE CONTENT, RELATIVE DENSITY OR CONSISTENCY, SOIL STRUCTURE, MINERALOGY	COMMENTS DEPTH OF CASING, DRILLING RATE, DRILLING FLUID LOSS, TESTS AND INSTRUMENTATION
	INTERVAL	NUMBER AND TYPE	RECOVERY (FT)			
5						
7.5		P-1	1.5	NA	Sandy Silt (ML), brown, moist	- Silty clay at surface: - Increasing sand with depth.
10						
12.5		SH-2	2.3	NA	Silty Sand (SM), brown, moist, some gravel	- Material change @ 11 ft.
20						
22.5		P-3	2.0	NA	Poorly-graded Sand (SP), brown, moist, uniformly graded, fine.	- Intermittent drill chatter to 24'
25						
40						
42.5		P-4	2.5	NA	Poorly-graded Sand (SP), brown, moist, uniform, fine, weakly-cemented.	- Cemented Sand in cuttings starting at 36 ft.
50						
60						
62.5		P-5	2.5	NA	Poorly-graded Sand (SP), brown, moist, uniform, fine, some silt, weakly-cemented.	
75						
97.5						
100		P-6	1.5	NA	Sand with Silt (SP), brown, moist, uniform fine, some gravel	Bottom of Boring @ 100 ft.
125						

PROJECT NUMBER S-22612	BORING NUMBER DC-1	SHEET 1 OF 3
---------------------------	-----------------------	--------------

**SOIL BORING LOG**

PROJECT USGS Research Project LOCATION Skyline Blvd, Daly City  
 ELEVATION 380 Ft. DRILLING CONTRACTOR Pitcher Drilling Co; Palo Alto, CA  
 DRILLING METHOD AND EQUIPMENT Rotary Wash, Fairing 1500 Rig  
 WATER LEVELS Not Measured START 8/1/92 FINISH 9/4/92 LOGGER Scott Ashford

DEPTH BELOW SURFACE (FT)	SAMPLE			STANDARD PENETRATION TEST RESULTS 6"-6" (N)	SOIL DESCRIPTION SOIL NAME, USCS GROUP SYMBOL, COLOR, MOISTURE CONTENT, RELATIVE DENSITY OR CONSISTENCY, SOIL STRUCTURE, MINERALOGY	COMMENTS DEPTH OF CASING, DRILLING RATE, DRILLING FLUID LOSS, TESTS AND INSTRUMENTATION
	INTERVAL	NUMBER AND TYPE	RECOVERY (FT)			
20					Silty Sand (SM), brown, dry, loose, fine	
22.5					Poorly Graded Sand (SP) yellowish-brown, dry, loose, fine	Slight banding between particles Clumps easily broken between thumb and forefinger.
25		SH-1	1.0	Pitcher	Poorly Graded Sand with Silt (SP), brown, moist, uniform, fine	Moderately hard to break pieces between thumb and forefinger. - clay layer 32' to 33'
40						
41.5		S-2	1.5	11-17-18 (35)	Poorly Graded Sand with Silt (SP) brown, medium dense, some red staining and organic seams, uniform, fine, mica, few clay pockets.	Entire 1.5' held together out of sampler.
50						
54						
56.5		SH-3	2.5	Pitcher	Lean Clay (CL), gray, moist, very stiff, with sand	Entered clay @ 53'
75						
77						
79.5		SH-4	2.5	Pitcher	Fat Clay (CH), gray, moist, hard, slickensided, organic pockets	
100						
102.5		SH-5	2.5	Pitcher	Fat Clay (CH), gray, dry, hard, slickensided	
125						
						- sand layer 117' - 118'
						Entered Sand @ 122'
131						
132.5		SH-6	1.0	Pitcher	Poorly Graded Sand (SP) yellowish-brown, moist, un. form, fine, dense, some silt.	

PROJECT NUMBER S-22612	BORING NUMBER DC-1	SHEET 2 OF 3
---------------------------	-----------------------	--------------

**SOIL BORING LOG**

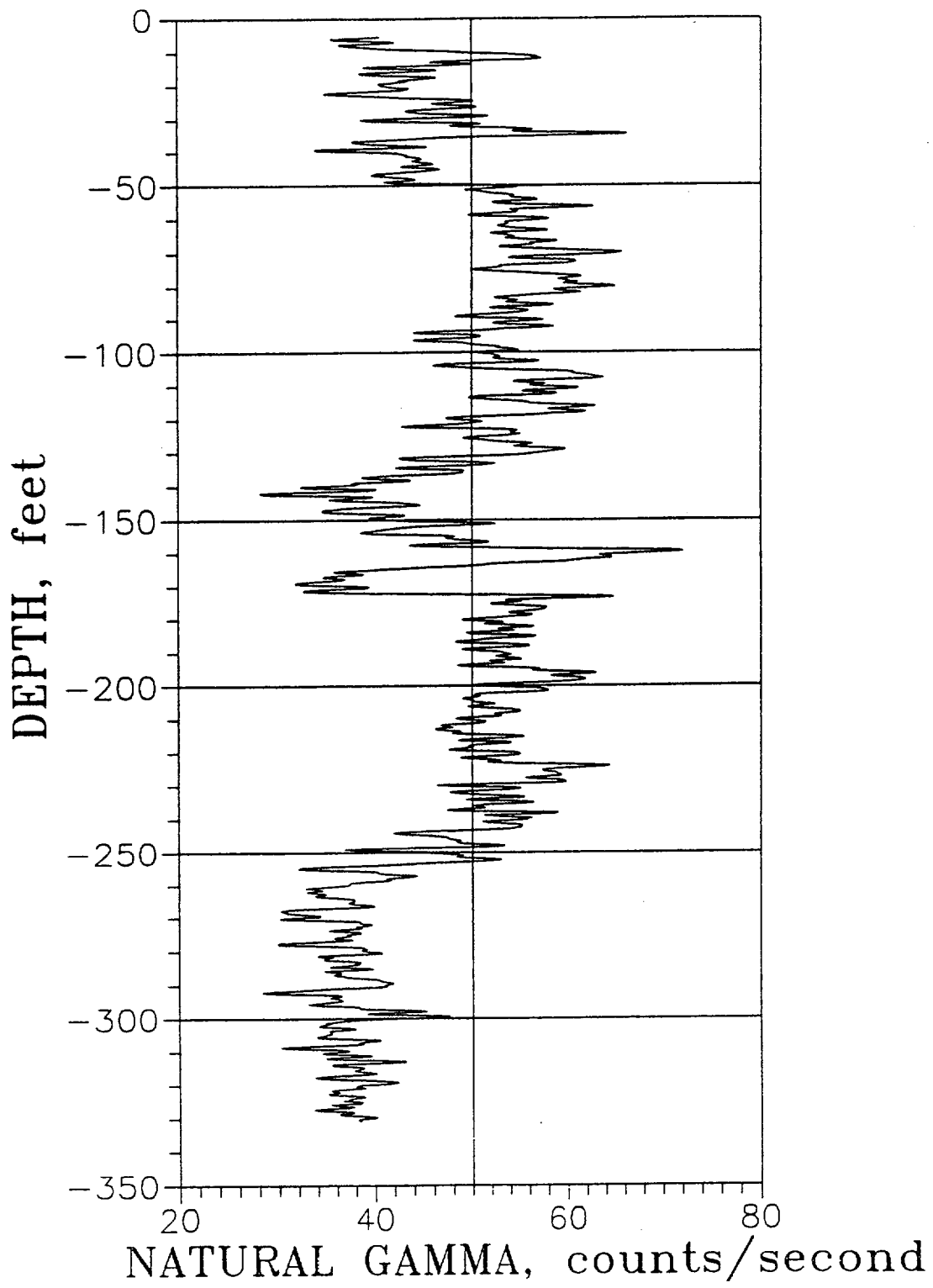
PROJECT USGS Research Project LOCATION Skyline Blvd, Daly City  
 ELEVATION 380 ft. DRILLING CONTRACTOR Pitcher Drilling Co; Palo Alto, CA  
 DRILLING METHOD AND EQUIPMENT Rotary Wash - Failing 1500 R14  
 WATER LEVELS Not measured START 3/1/02 FINISH 3/2/02 LOGGER Scott Ashford

DEPTH BELOW SURFACE (FT)	SAMPLE			STANDARD PENETRATION TEST RESULTS 6"-8"-8" (N)	SOIL DESCRIPTION SOIL NAME, USCS GROUP SYMBOL, COLOR, MOISTURE CONTENT, RELATIVE DENSITY OR CONSISTENCY, SOIL STRUCTURE, MINERALOGY	COMMENTS DEPTH OF CASING, DRILLING RATE, DRILLING FLUID LOSS, TESTS AND INSTRUMENTATION
	INTERVAL	NUMBER AND TYPE	RECOVERY (FT)			
175						Entered Gray Clay Layer @ 170 - still gray clay
200	201 202	SH-7	1.0	Pitcher	Poorly-graded Sand (SP), gray, moist, uniform, fine	Entered Sand @ 193' - becoming silty or clayey @ 203
225						Entered Gray Clay
250	260					
	230	3-8	-	Cuttings	Sandy Silt (ML), bluish-gray	Entered Bluish-gray sandy silt, no change in drilling rate.
275						
	295					
	300	B-9	-	Cutting	Sandy Silt (ML), bluish-gray	- increasing sand content @ 290 - drill chatter,

PROJECT NUMBER S-22612	BORING NUMBER DC-1	SHEET 3 OF 3
<b>SOIL BORING LOG</b>		

PROJECT USGS Research Project LOCATION Skylark Blvd, Daly City  
 ELEVATION 380 Ft DRILLING CONTRACTOR 2+1 Drilling Co, Palo Alto, CA  
 DRILLING METHOD AND EQUIPMENT Rotary Wash - Feeding 1500 Rm  
 WATER LEVELS Not Measured START 3/31/92 FINISH 3/2/92 LOGGER Scott Ashford

DEPTH BELOW SURFACE (FT)	SAMPLE			STANDARD PENETRATION TEST RESULTS 6"-6"-6" (N)	SOIL DESCRIPTION SOIL NAME, USCS GROUP SYMBOL, COLOR, MOISTURE CONTENT, RELATIVE DENSITY OR CONSISTENCY, SOIL STRUCTURE, MINERALOGY	COMMENTS DEPTH OF CASING, DRILLING RATE, DRILLING FLUID LOSS, TESTS AND INSTRUMENTATION
	INTERVAL	NUMBER AND TYPE	RECOVERY (FT)			
325	330 329.5	SH-10	0.5	Pitcher	Poorly-graded Sand (SP), bluish-gray, fine, cemented.	Drilling rate = 2 ft / 7 minutes with rock bit - bluish gray silty sand  BOB @ 331'. Installed 4" SCH-40 PVC Casing, Tremie grouted annulus.
350						



## APPENDIX B. SHEAR WAVE VELOCITY TESTING

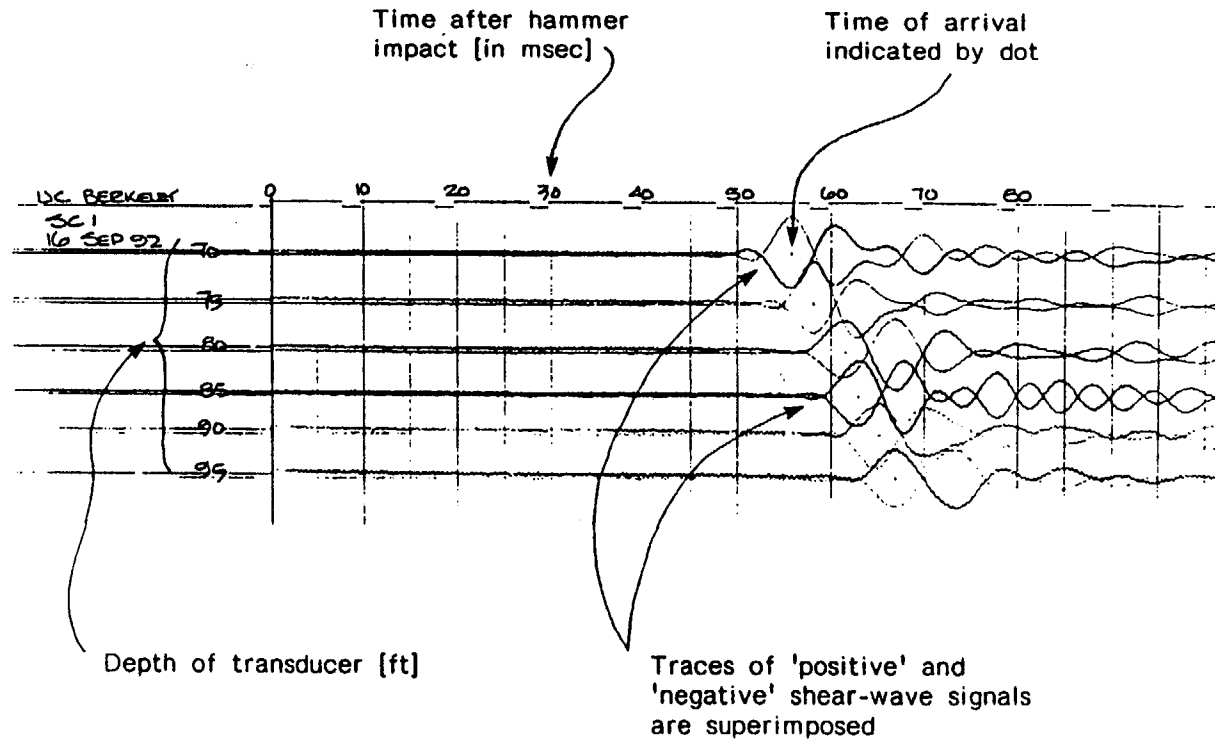
A shear wave velocity ( $V_s$ ) profile was developed at each site in order to provide a quantitative measure of the shear modulus variation as a result of the stratigraphic variability and depth. The downhole method of testing was employed. Bruce Redpath of Redpath Geophysics in Murphys, California, performed the testing. In the downhole method, the travel time of the signal is measured between the source at the ground surface and a receiver in the borehole. The source was a 12-lb hammer striking a horizontal blow to the steel endplate of a 7-foot long, 6-inch by 6-inch wooden plank. A 16-lb hammer was used as the source for the greater depths at the Daly City site. The plank had steel cleats that assisted in transferring the load to the ground surface, and in addition, the plank was held in place by the front wheels of a truck resting on its top. The hammer blow generated a horizontally polarized shear wave that travels through the soil.

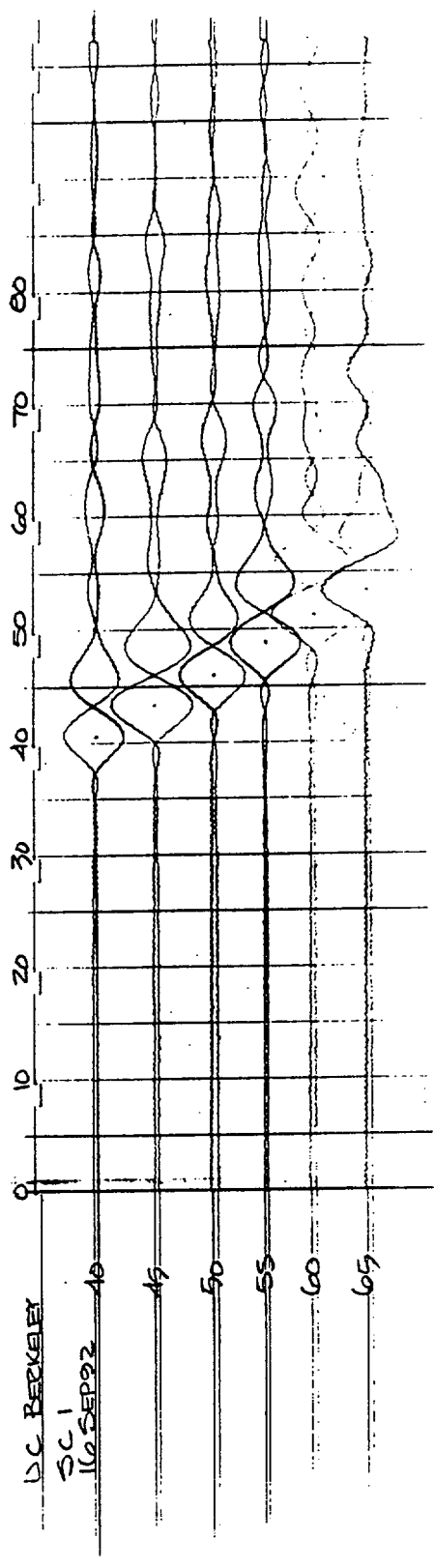
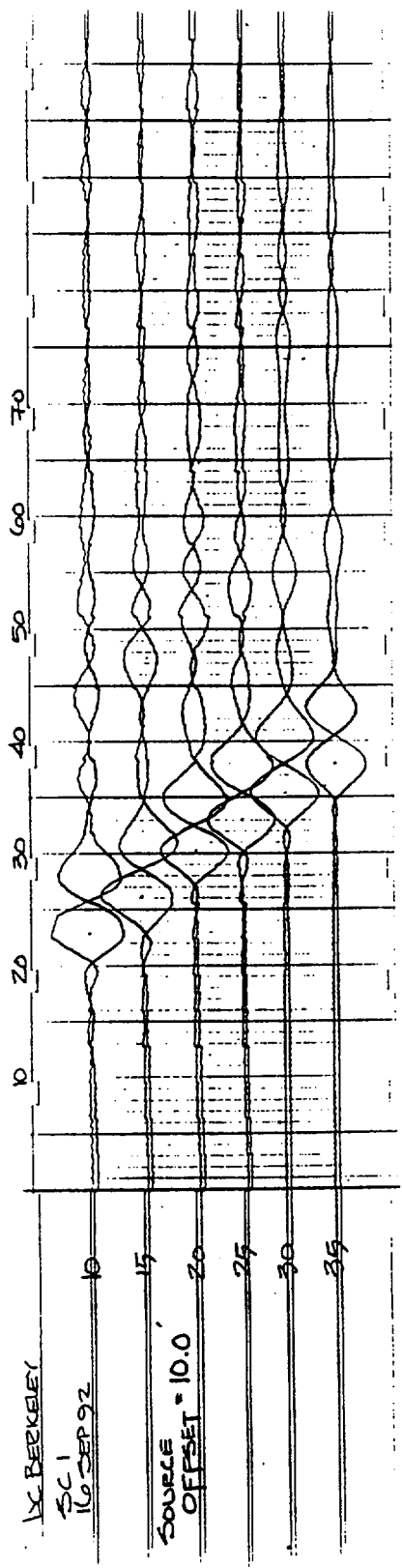
The downhole receiver for the shear wave impulse was a variable-azimuth horizontal geophone. A fluxgate compass was attached to the housing of the geophone allowing the operator to read the azimuth of the geophone housing. This information allowed the operator to line the geophone up with the plank using a gearhead motor attached to the geophone within the housing. Having the geophone always in line with the plank optimized the shear waves signal, thus leading to good quality data. In another attempt to optimize the quality of the data, each end of the plank was struck for each test depth. This resulted in signals of opposite polarity, which were used to check for anomalies in the data and to confirm the velocity at

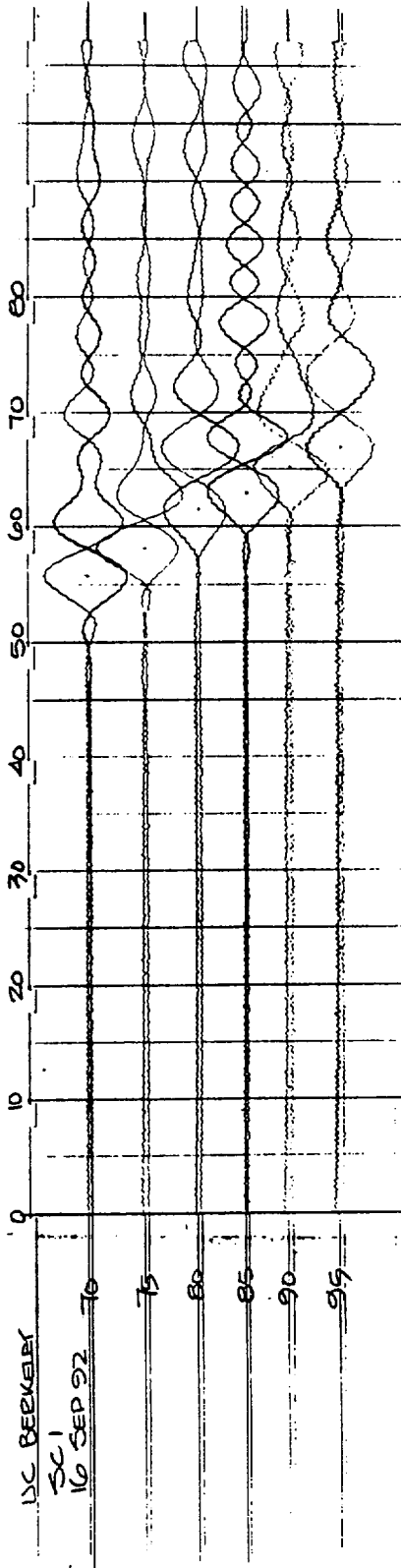
each depth. The geophone housing was held in place at each test depth with a nitrogen filled bladder. Signals were recorded on an OYO/Nimbus ES 1200 12-channel digital seismograph.

At the Seacliff site, the testing was performed on September 16, 1992. The source was located 10 feet from the collar of the borehole, and a 12-lb hammer was used. Tests were performed at 5-foot intervals between depths of 10 and 100 feet, the bottom of the borehole. At the Daly City site, testing was performed on September 17, 1992 using a 16-lb hammer with a source 6.4 feet away from the collar of the borehole. Tests were performed at 5-ft intervals from depths of 10 to 60 feet, and 10-foot intervals thereafter to the terminal depth of the boring at 330 feet.

The shear wave velocity data is presented on the following pages for the Seacliff site (SC-1) and the Daly City site (DC-1).







UC BERKELEY

SC 1

16 SEP 92

70

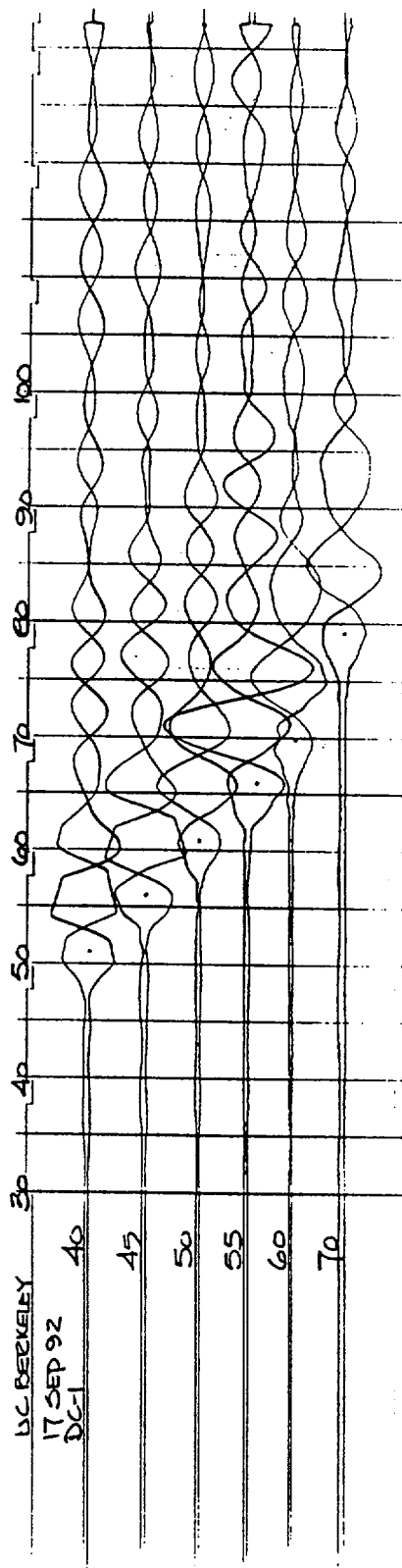
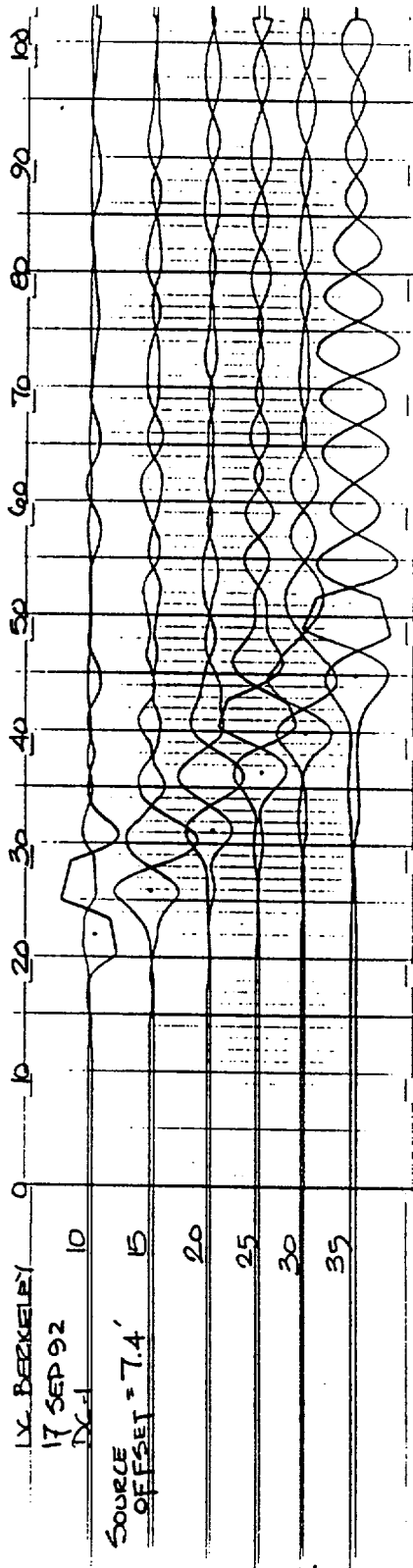
75

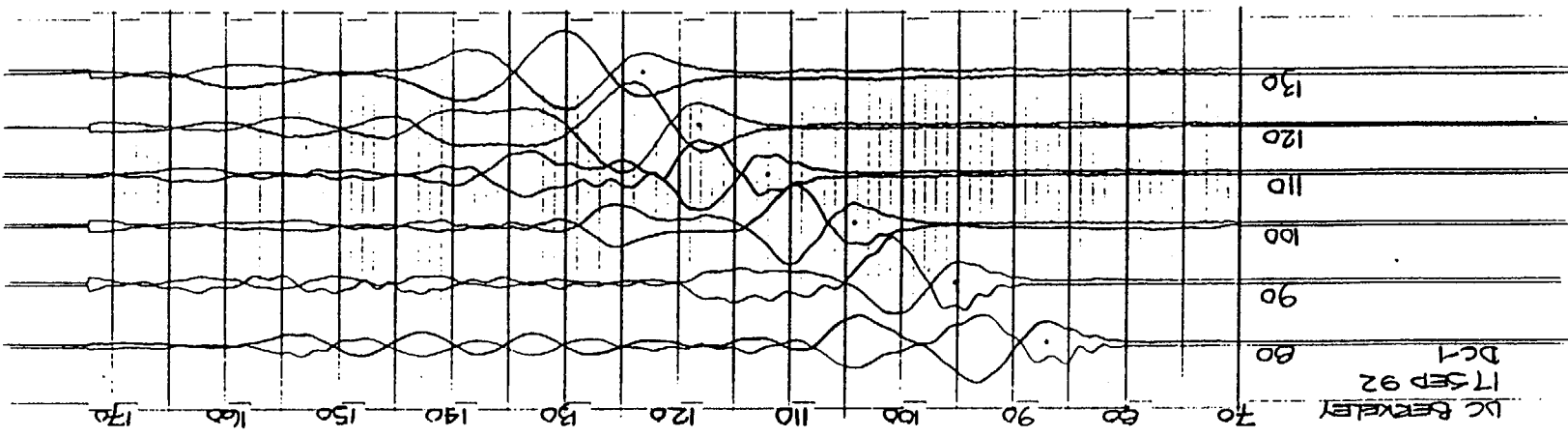
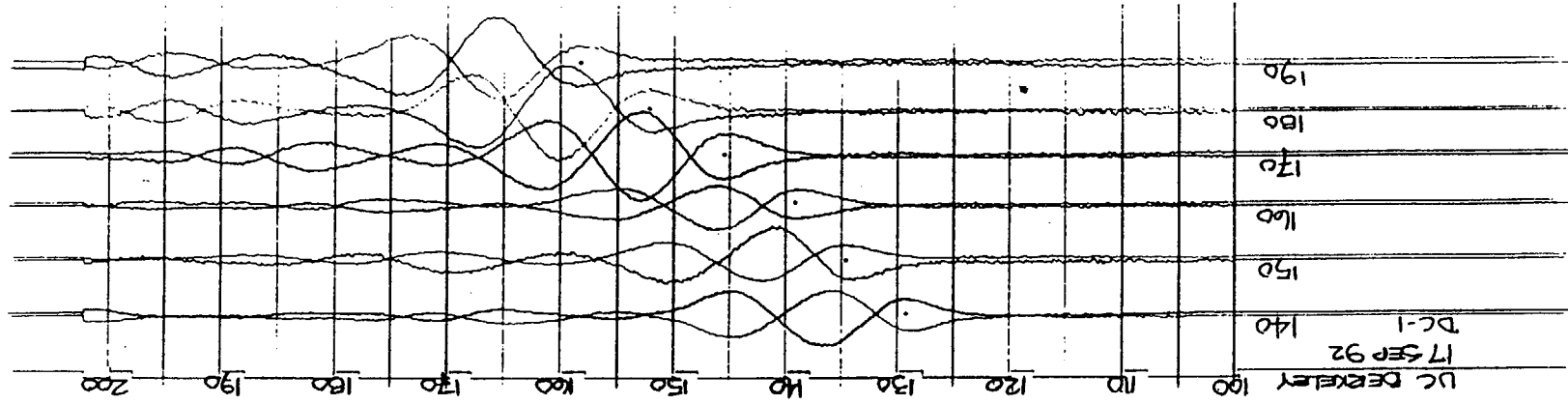
80

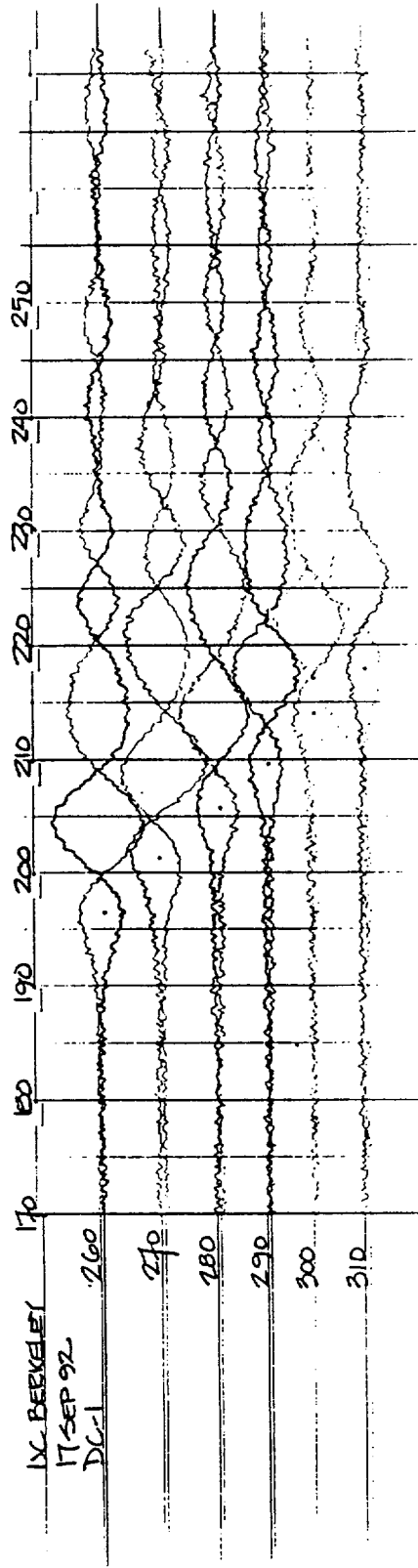
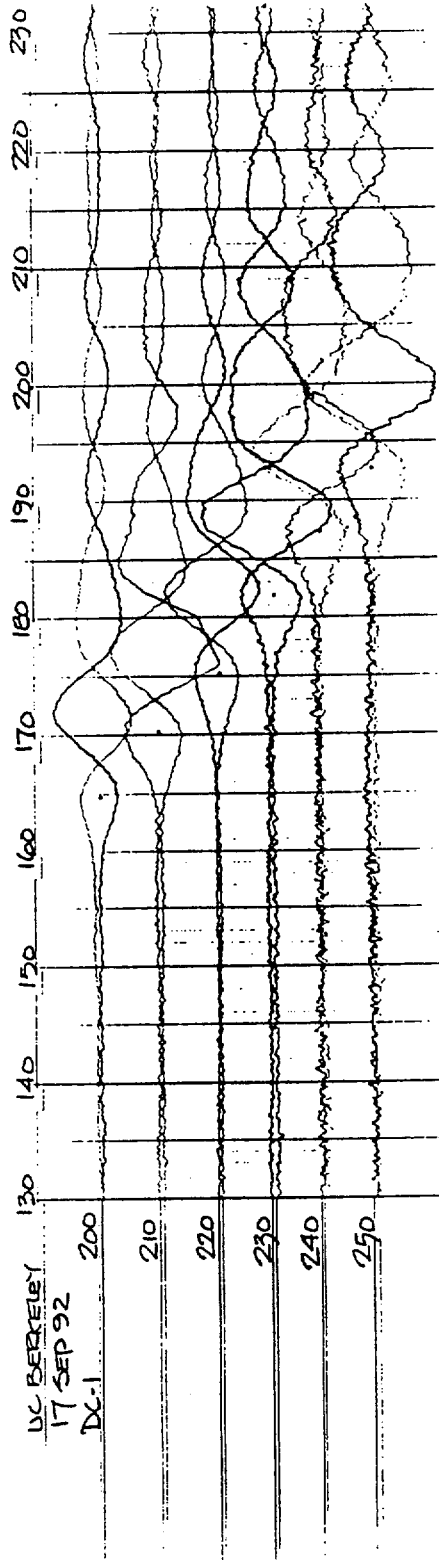
85

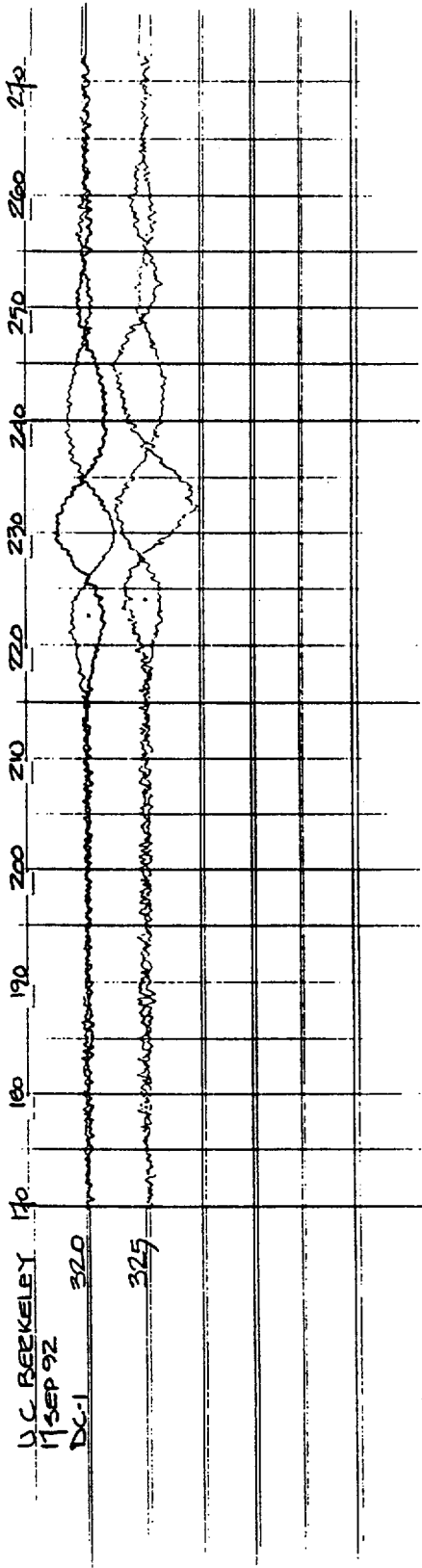
90

95











## EARTHQUAKE ENGINEERING RESEARCH CENTER REPORT SERIES

EERC reports are available from the National Information Service for Earthquake Engineering (NISEE) and from the National Technical Information Service (NTIS). Numbers in parentheses are Accession Numbers assigned by the National Technical Information Service; these are followed by a price code. Contact NTIS, 5285 Port Royal Road, Springfield Virginia, 22161 for more information. Reports without Accession Numbers were not available from NTIS at the time of printing. For a current complete list of EERC reports (from EERC 67-1) and availability information, please contact University of California, EERC, NISEE, 1301 South 46th Street, Richmond, California 94804.

- UCB/EERC-84/01 "Pseudodynamic Test Method for Seismic Performance Evaluation: Theory and Implementation," by Shing, P.-S.B. and Mahin, S.A., January 1984, (PB84 190 644)A08.
- UCB/EERC-84/02 "Dynamic Response Behavior of Kiang Hong Dian Dam," by Clough, R.W., Chang, K.-T., Chen, H.-Q. and Stephen, R.M., April 1984, (PB84 209 402)A08.
- UCB/EERC-84/03 "Refined Modelling of Reinforced Concrete Columns for Seismic Analysis," by Kaba, S.A. and Mahin, S.A., April 1984, (PB84 234 384)A06.
- UCB/EERC-84/04 "A New Floor Response Spectrum Method for Seismic Analysis of Multiply Supported Secondary Systems," by Asfura, A. and Der Kiureghian, A., June 1984, (PB84 239 417)A06.
- UCB/EERC-84/05 "Earthquake Simulation Tests and Associated Studies of a 1/5th-scale Model of a 7-Story R/C Frame-Wall Test Structure," by Bertero, V.V., Aktan, A.E., Charney, F.A. and Sause, R., June 1984, (PB84 239 409)A09.
- UCB/EERC-84/06 "Unassigned," by Unassigned, 1984.
- UCB/EERC-84/07 "Behavior of Interior and Exterior Flat-Plate Connections Subjected to Inelastic Load Reversals," by Zee, H.L. and Moehle, J.P., August 1984, (PB86 117 629/AS)A07.
- UCB/EERC-84/08 "Experimental Study of the Seismic Behavior of a Two-Story Flat-Plate Structure," by Moehle, J.P. and Diebold, J.W., August 1984, (PB86 122 553/AS)A12.
- UCB/EERC-84/09 "Phenomenological Modeling of Steel Braces under Cyclic Loading," by Ikeda, K., Mahin, S.A. and Dermitzakis, S.N., May 1984, (PB86 132 198/AS)A08.
- UCB/EERC-84/10 "Earthquake Analysis and Response of Concrete Gravity Dams," by Fenves, G.L. and Chopra, A.K., August 1984, (PB85 193 902/AS)A11.
- UCB/EERC-84/11 "EAGD-84: A Computer Program for Earthquake Analysis of Concrete Gravity Dams," by Fenves, G.L. and Chopra, A.K., August 1984, (PB85 193 613/AS)A05.
- UCB/EERC-84/12 "A Refined Physical Theory Model for Predicting the Seismic Behavior of Braced Steel Frames," by Ikeda, K. and Mahin, S.A., July 1984, (PB85 191 450/AS)A09.
- UCB/EERC-84/13 "Earthquake Engineering Research at Berkeley - 1984," by EERC, August 1984, (PB85 197 341/AS)A10.
- UCB/EERC-84/14 "Moduli and Damping Factors for Dynamic Analyses of Cohesionless Soils," by Seed, H.B., Wong, R.T., Idriss, I.M. and Tokimatsu, K., September 1984, (PB85 191 468/AS)A04.
- UCB/EERC-84/15 "The Influence of SPT Procedures in Soil Liquefaction Resistance Evaluations," by Seed, H.B., Tokimatsu, K., Harder, L.F. and Chung, R.M., October 1984, (PB85 191 732/AS)A04.
- UCB/EERC-84/16 "Simplified Procedures for the Evaluation of Settlements in Sands Due to Earthquake Shaking," by Tokimatsu, K. and Seed, H.B., October 1984, (PB85 197 887/AS)A03.
- UCB/EERC-84/17 "Evaluation of Energy Absorption Characteristics of Highway Bridges Under Seismic Conditions - Volume I (PB90 262 627)A16 and Volume II (Appendices) (PB90 262 635)A13," by Imbsen, R.A. and Penzien, J., September 1986.
- UCB/EERC-84/18 "Structure-Foundation Interactions under Dynamic Loads," by Liu, W.D. and Penzien, J., November 1984, (PB87 124 889/AS)A11.
- UCB/EERC-84/19 "Seismic Modelling of Deep Foundations," by Chen, C.-H. and Penzien, J., November 1984, (PB87 124 798/AS)A07.
- UCB/EERC-84/20 "Dynamic Response Behavior of Quan Shui Dam," by Clough, R.W., Chang, K.-T., Chen, H.-Q., Stephen, R.M., Ghanaat, Y. and Qi, J.-H., November 1984, (PB86 115177/AS)A07.
- UCB/EERC-85/01 "Simplified Methods of Analysis for Earthquake Resistant Design of Buildings," by Cruz, E.F. and Chopra, A.K., February 1985, (PB86 112299/AS)A12.
- UCB/EERC-85/02 "Estimation of Seismic Wave Coherency and Rupture Velocity using the SMART 1 Strong-Motion Array Recordings," by Abrahamson, N.A., March 1985, (PB86 214 343)A07.
- UCB/EERC-85/03 "Dynamic Properties of a Thirty Story Condominium Tower Building," by Stephen, R.M., Wilson, E.L. and Stander, N., April 1985, (PB86 118965/AS)A06.
- UCB/EERC-85/04 "Development of Substructuring Techniques for On-Line Computer Controlled Seismic Performance Testing," by Dermitzakis, S. and Mahin, S., February 1985, (PB86 132941/AS)A08.
- UCB/EERC-85/05 "A Simple Model for Reinforcing Bar Anchorages under Cyclic Excitations," by Filippou, F.C., March 1985, (PB86 112 919/AS)A05.
- UCB/EERC-85/06 "Racking Behavior of Wood-framed Gypsum Panels under Dynamic Load," by Oliva, M.G., June 1985, (PB90 262 643)A04.

- UCB/EERC-85/07 "Earthquake Analysis and Response of Concrete Arch Dams," by Fok, K.-L. and Chopra, A.K., June 1985, (PB86 139672/AS)A10.
- UCB/EERC-85/08 "Effect of Inelastic Behavior on the Analysis and Design of Earthquake Resistant Structures," by Lin, J.P. and Mahin, S.A., June 1985, (PB86 135340/AS)A08.
- UCB/EERC-85/09 "Earthquake Simulator Testing of a Base-Isolated Bridge Deck," by Kelly, J.M., Buckle, I.G. and Tsai, H.-C., January 1986, (PB87 124 152/AS)A06.
- UCB/EERC-85/10 "Simplified Analysis for Earthquake Resistant Design of Concrete Gravity Dams," by Fenves, G.L. and Chopra, A.K., June 1986, (PB87 124 160/AS)A08.
- UCB/EERC-85/11 "Dynamic Interaction Effects in Arch Dams," by Clough, R.W., Chang, K.-T., Chen, H.-Q. and Ghanaat, Y., October 1985, (PB86 135027/AS)A05.
- UCB/EERC-85/12 "Dynamic Response of Long Valley Dam in the Mammoth Lake Earthquake Series of May 25-27, 1980," by Lai, S. and Seed, H.B., November 1985, (PB86 142304/AS)A05.
- UCB/EERC-85/13 "A Methodology for Computer-Aided Design of Earthquake-Resistant Steel Structures," by Austin, M.A., Pister, K.S. and Mahin, S.A., December 1985, (PB86 159480/AS)A10 .
- UCB/EERC-85/14 "Response of Tension-Leg Platforms to Vertical Seismic Excitations," by Liou, G.-S., Penzien, J. and Yeung, R.W., December 1985, (PB87 124 871/AS)A08.
- UCB/EERC-85/15 "Cyclic Loading Tests of Masonry Single Piers: Volume 4 - Additional Tests with Height to Width Ratio of 1," by Sveinsson, B., McNiven, H.D. and Sucuoglu, H., December 1985, (PB87 165031/AS)A08.
- UCB/EERC-85/16 "An Experimental Program for Studying the Dynamic Response of a Steel Frame with a Variety of Infill Partitions," by Yanev, B. and McNiven, H.D., December 1985, (PB90 262 676)A05.
- UCB/EERC-86/01 "A Study of Seismically Resistant Eccentrically Braced Steel Frame Systems," by Kasai, K. and Popov, E.P., January 1986, (PB87 124 178/AS)A14.
- UCB/EERC-86/02 "Design Problems in Soil Liquefaction," by Seed, H.B., February 1986, (PB87 124 186/AS)A03.
- UCB/EERC-86/03 "Implications of Recent Earthquakes and Research on Earthquake-Resistant Design and Construction of Buildings," by Bertero, V.V., March 1986, (PB87 124 194/AS)A05.
- UCB/EERC-86/04 "The Use of Load Dependent Vectors for Dynamic and Earthquake Analyses," by Leger, P., Wilson, E.L. and Clough, R.W., March 1986, (PB87 124 202/AS)A12.
- UCB/EERC-86/05 "Two Beam-To-Column Web Connections," by Tsai, K.-C. and Popov, E.P., April 1986, (PB87 124 301/AS)A04.
- UCB/EERC-86/06 "Determination of Penetration Resistance for Coarse-Grained Soils using the Becker Hammer Drill," by Harder, L.F. and Seed, H.B., May 1986, (PB87 124 210/AS)A07.
- UCB/EERC-86/07 "A Mathematical Model for Predicting the Nonlinear Response of Unreinforced Masonry Walls to In-Plane Earthquake Excitations," by Mengi, Y. and McNiven, H.D., May 1986, (PB87 124 780/AS)A06.
- UCB/EERC-86/08 "The 19 September 1985 Mexico Earthquake: Building Behavior," by Bertero, V.V., July 1986.
- UCB/EERC-86/09 "EACD-3D: A Computer Program for Three-Dimensional Earthquake Analysis of Concrete Dams," by Fok, K.-L., Hall, J.F. and Chopra, A.K., July 1986, (PB87 124 228/AS)A08.
- UCB/EERC-86/10 "Earthquake Simulation Tests and Associated Studies of a 0.3-Scale Model of a Six-Story Concentrically Braced Steel Structure," by Uang, C.-M. and Bertero, V.V., December 1986, (PB87 163 564/AS)A17.
- UCB/EERC-86/11 "Mechanical Characteristics of Base Isolation Bearings for a Bridge Deck Model Test," by Kelly, J.M., Buckle, I.G. and Koh, C.-G., November 1987, (PB90 262 668)A04.
- UCB/EERC-86/12 "Effects of Axial Load on Elastomeric Isolation Bearings," by Koh, C.-G. and Kelly, J.M., November 1987.
- UCB/EERC-87/01 "The FPS Earthquake Resisting System: Experimental Report," by Zayas, V.A., Low, S.S. and Mahin, S.A., June 1987, (PB88 170 287)A06.
- UCB/EERC-87/02 "Earthquake Simulator Tests and Associated Studies of a 0.3-Scale Model of a Six-Story Eccentrically Braced Steel Structure," by Whittaker, A., Uang, C.-M. and Bertero, V.V., July 1987, (PB88 166 707/AS)A18.
- UCB/EERC-87/03 "A Displacement Control and Uplift Restraint Device for Base-Isolated Structures," by Kelly, J.M., Griffith, M.C. and Aiken, I.D., April 1987, (PB88 169 933)A04.
- UCB/EERC-87/04 "Earthquake Simulator Testing of a Combined Sliding Bearing and Rubber Bearing Isolation System," by Kelly, J.M. and Chalhoub, M.S., December 1990.
- UCB/EERC-87/05 "Three-Dimensional Inelastic Analysis of Reinforced Concrete Frame-Wall Structures," by Moazzami, S. and Bertero, V.V., May 1987, (PB88 169 586/AS)A08.
- UCB/EERC-87/06 "Experiments on Eccentrically Braced Frames with Composite Floors," by Ricles, J. and Popov, E., June 1987, (PB88 173 067/AS)A14.
- UCB/EERC-87/07 "Dynamic Analysis of Seismically Resistant Eccentrically Braced Frames," by Ricles, J. and Popov, E., June 1987, (PB88 173 075/AS)A16.
- UCB/EERC-87/08 "Undrained Cyclic Triaxial Testing of Gravels-The Effect of Membrane Compliance," by Evans, M.D. and Seed, H.B., July 1987, (PB88 173 257)A19.

- UCB/EERC-87/09 "Hybrid Solution Techniques for Generalized Pseudo-Dynamic Testing," by Thewalt, C. and Mahin, S.A., July 1987, (PB 88 179 007)A07.
- UCB/EERC-87/10 "Ultimate Behavior of Butt Welded Splices in Heavy Rolled Steel Sections," by Bruneau, M., Mahin, S.A. and Popov, E.P., September 1987, (PB90 254 285)A07.
- UCB/EERC-87/11 "Residual Strength of Sand from Dam Failures in the Chilean Earthquake of March 3, 1985," by De Alba, P., Seed, H.B., Retamal, E. and Seed, R.B., September 1987, (PB88 174 321/AS)A03.
- UCB/EERC-87/12 "Inelastic Seismic Response of Structures with Mass or Stiffness Eccentricities in Plan," by Bruneau, M. and Mahin, S.A., September 1987, (PB90 262 650/AS)A14.
- UCB/EERC-87/13 "CSTRUCT: An Interactive Computer Environment for the Design and Analysis of Earthquake Resistant Steel Structures," by Austin, M.A., Mahin, S.A. and Pister, K.S., September 1987, (PB88 173 339/AS)A06.
- UCB/EERC-87/14 "Experimental Study of Reinforced Concrete Columns Subjected to Multi-Axial Loading," by Low, S.S. and Moehle, J.P., September 1987, (PB88 174 347/AS)A07.
- UCB/EERC-87/15 "Relationships between Soil Conditions and Earthquake Ground Motions in Mexico City in the Earthquake of Sept. 19, 1985," by Seed, H.B., Romo, M.P., Sun, J., Jaime, A. and Lysmer, J., October 1987, (PB88 178 991)A06.
- UCB/EERC-87/16 "Experimental Study of Seismic Response of R. C. Setback Buildings," by Shahrooz, B.M. and Moehle, J.P., October 1987, (PB88 176 359)A16.
- UCB/EERC-87/17 "The Effect of Slabs on the Flexural Behavior of Beams," by Pantazopoulou, S.J. and Moehle, J.P., October 1987, (PB90 262 700)A07.
- UCB/EERC-87/18 "Design Procedure for R-FBI Bearings," by Mostaghel, N. and Kelly, J.M., November 1987, (PB90 262 718)A04.
- UCB/EERC-87/19 "Analytical Models for Predicting the Lateral Response of R C Shear Walls: Evaluation of their Reliability," by Vulcano, A. and Bertero, V.V., November 1987, (PB88 178 983)A05.
- UCB/EERC-87/20 "Earthquake Response of Torsionally-Coupled Buildings," by Hejal, R. and Chopra, A.K., December 1987.
- UCB/EERC-87/21 "Dynamic Reservoir Interaction with Monticello Dam," by Clough, R.W., Ghanaat, Y. and Qiu, X-F., December 1987, (PB88 179 023)A07.
- UCB/EERC-87/22 "Strength Evaluation of Coarse-Grained Soils," by Siddiqi, F.H., Seed, R.B., Chan, C.K., Seed, H.B. and Pyke, R.M., December 1987, (PB88 179 031)A04.
- UCB/EERC-88/01 "Seismic Behavior of Concentrically Braced Steel Frames," by Khatib, I., Mahin, S.A. and Pister, K.S., January 1988, (PB91 210 898/AS)A11.
- UCB/EERC-88/02 "Experimental Evaluation of Seismic Isolation of Medium-Rise Structures Subject to Uplift," by Griffith, M.C., Kelly, J.M., Coveney, V.A. and Koh, C.G., January 1988, (PB91 217 950/AS)A09.
- UCB/EERC-88/03 "Cyclic Behavior of Steel Double Angle Connections," by Astaneh-Asl, A. and Nader, M.N., January 1988, (PB91 210 872)A05.
- UCB/EERC-88/04 "Re-evaluation of the Slide in the Lower San Fernando Dam in the Earthquake of Feb. 9, 1971," by Seed, H.B., Seed, R.B., Harder, L.F. and Jong, H.-L., April 1988, (PB91 212 456/AS)A07.
- UCB/EERC-88/05 "Experimental Evaluation of Seismic Isolation of a Nine-Story Braced Steel Frame Subject to Uplift," by Griffith, M.C., Kelly, J.M. and Aiken, I.D., May 1988, (PB91 217 968/AS)A07.
- UCB/EERC-88/06 "DRAIN-2DX User Guide," by Allahabadi, R. and Powell, G.H., March 1988, (PB91 212 530)A12.
- UCB/EERC-88/07 "Theoretical and Experimental Studies of Cylindrical Water Tanks in Base-Isolated Structures," by Chalhoub, M.S. and Kelly, J.M., April 1988, (PB91 217 976/AS)A05.
- UCB/EERC-88/08 "Analysis of Near-Source Waves: Separation of Wave Types Using Strong Motion Array Recording," by Darragh, R.B., June 1988, (PB91 212 621)A08.
- UCB/EERC-88/09 "Alternatives to Standard Mode Superposition for Analysis of Non-Classically Damped Systems," by Kusainov, A.A. and Clough, R.W., June 1988, (PB91 217 992/AS)A04.
- UCB/EERC-88/10 "The Landslide at the Port of Nice on October 16, 1979," by Seed, H.B., Seed, R.B., Schlosser, F., Blondeau, F. and Juran, I., June 1988, (PB91 210 914)A05.
- UCB/EERC-88/11 "Liquefaction Potential of Sand Deposits Under Low Levels of Excitation," by Carter, D.P. and Seed, H.B., August 1988, (PB91 210 880)A15.
- UCB/EERC-88/12 "Nonlinear Analysis of Reinforced Concrete Frames Under Cyclic Load Reversals," by Filippou, F.C. and Issa, A., September 1988, (PB91 212 589)A07.
- UCB/EERC-88/13 "Implications of Recorded Earthquake Ground Motions on Seismic Design of Building Structures," by Uang, C.-M. and Bertero, V.V., November 1988, (PB91 212 548)A06.
- UCB/EERC-88/14 "An Experimental Study of the Behavior of Dual Steel Systems," by Whittaker, A.S., Uang, C.-M. and Bertero, V.V., September 1988, (PB91 212 712)A16.
- UCB/EERC-88/15 "Dynamic Moduli and Damping Ratios for Cohesive Soils," by Sun, J.I., Golesorkhi, R. and Seed, H.B., August 1988, (PB91 210 922)A04.
- UCB/EERC-88/16 "Reinforced Concrete Flat Plates Under Lateral Load: An Experimental Study Including Biaxial Effects," by Pan, A. and Moehle, J.P., October 1988, (PB91 210 856)A13.

- UCB/EERC-88/17 "Earthquake Engineering Research at Berkeley - 1988," by EERC, November 1988, (PB91 210 864)A10.
- UCB/EERC-88/18 "Use of Energy as a Design Criterion in Earthquake-Resistant Design," by Uang, C.-M. and Bertero, V.V., November 1988, (PB91 210 906/AS)A04.
- UCB/EERC-88/19 "Steel Beam-Column Joints in Seismic Moment Resisting Frames," by Tsai, K.-C. and Popov, E.P., November 1988, (PB91 217 984/AS)A20.
- UCB/EERC-88/20 "Base Isolation in Japan, 1988," by Kelly, J.M., December 1988, (PB91 212 449)A05.
- UCB/EERC-89/01 "Behavior of Long Links in Eccentrically Braced Frames," by Engelhardt, M.D. and Popov, E.P., January 1989, (PB92 143 056)A18.
- UCB/EERC-89/02 "Earthquake Simulator Testing of Steel Plate Added Damping and Stiffness Elements," by Whittaker, A., Bertero, V.V., Alonso, J. and Thompson, C., January 1989, (PB91 229 252/AS)A10.
- UCB/EERC-89/03 "Implications of Site Effects in the Mexico City Earthquake of Sept. 19, 1985 for Earthquake-Resistant Design Criteria in the San Francisco Bay Area of California," by Seed, H.B. and Sun, J.I., March 1989, (PB91 229 369/AS)A07.
- UCB/EERC-89/04 "Earthquake Analysis and Response of Intake-Outlet Towers," by Goyal, A. and Chopra, A.K., July 1989, (PB91 229 286/AS)A19.
- UCB/EERC-89/05 "The 1985 Chile Earthquake: An Evaluation of Structural Requirements for Bearing Wall Buildings," by Wallace, J.W. and Moehle, J.P., July 1989, (PB91 218 008/AS)A13.
- UCB/EERC-89/06 "Effects of Spatial Variation of Ground Motions on Large Multiply-Supported Structures," by Hao, H., July 1989, (PB91 229 161/AS)A08.
- UCB/EERC-89/07 "EADAP - Enhanced Arch Dam Analysis Program: Users's Manual," by Ghanaat, Y. and Clough, R.W., August 1989, (PB91 212 522)A06.
- UCB/EERC-89/08 "Seismic Performance of Steel Moment Frames Plastically Designed by Least Squares Stress Fields," by Ohi, K. and Mahin, S.A., August 1989, (PB91 212 597)A05.
- UCB/EERC-89/09 "Feasibility and Performance Studies on Improving the Earthquake Resistance of New and Existing Buildings Using the Friction Pendulum System," by Zayas, V., Low, S., Mahin, S.A. and Bozzo, L., July 1989, (PB92 143 064)A14.
- UCB/EERC-89/10 "Measurement and Elimination of Membrane Compliance Effects in Undrained Triaxial Testing," by Nicholson, P.G., Seed, R.B. and Anwar, H., September 1989, (PB92 139 641/AS)A13.
- UCB/EERC-89/11 "Static Tilt Behavior of Unanchored Cylindrical Tanks," by Lau, D.T. and Clough, R.W., September 1989, (PB92 143 049)A10.
- UCB/EERC-89/12 "ADAP-88: A Computer Program for Nonlinear Earthquake Analysis of Concrete Arch Dams," by Fenves, G.L., Mojtahedi, S. and Reimer, R.B., September 1989, (PB92 139 674/AS)A07.
- UCB/EERC-89/13 "Mechanics of Low Shape Factor Elastomeric Seismic Isolation Bearings," by Aiken, I.D., Kelly, J.M. and Tajirian, F.F., November 1989, (PB92 139 732/AS)A09.
- UCB/EERC-89/14 "Preliminary Report on the Seismological and Engineering Aspects of the October 17, 1989 Santa Cruz (Loma Prieta) Earthquake," by EERC, October 1989, (PB92 139 682/AS)A04.
- UCB/EERC-89/15 "Experimental Studies of a Single Story Steel Structure Tested with Fixed, Semi-Rigid and Flexible Connections," by Nader, M.N. and Astaneh-Asl, A., August 1989, (PB91 229 211/AS)A10.
- UCB/EERC-89/16 "Collapse of the Cypress Street Viaduct as a Result of the Loma Prieta Earthquake," by Nims, D.K., Miranda, E., Aiken, I.D., Whittaker, A.S. and Bertero, V.V., November 1989, (PB91 217 935/AS)A05.
- UCB/EERC-90/01 "Mechanics of High-Shape Factor Elastomeric Seismic Isolation Bearings," by Kelly, J.M., Aiken, I.D. and Tajirian, F.F., March 1990.
- UCB/EERC-90/02 "Javid's Paradox: The Influence of Preform on the Modes of Vibrating Beams," by Kelly, J.M., Sackman, J.L. and Javid, A., May 1990, (PB91 217 943/AS)A03.
- UCB/EERC-90/03 "Earthquake Simulator Testing and Analytical Studies of Two Energy-Absorbing Systems for Multistory Structures," by Aiken, I.D. and Kelly, J.M., October 1990, (PB92 192 988)A13.
- UCB/EERC-90/04 "Damage to the San Francisco-Oakland Bay Bridge During the October 17, 1989 Earthquake," by Astaneh-Asl, A., June 1990.
- UCB/EERC-90/05 "Preliminary Report on the Principal Geotechnical Aspects of the October 17, 1989 Loma Prieta Earthquake," by Seed, R.B., Dickenson, S.E., Riemer, M.F., Bray, J.D., Sitar, N., Mitchell, J.K., Idriss, I.M., Kayen, R.E., Kropp, A., Harder, L.F., Jr. and Power, M.S., April 1990, (PB 192 970)A08.
- UCB/EERC-90/06 "Models of Critical Regions in Reinforced Concrete Frames Under Seismic Excitations," by Zulfqar, N. and Filippou, F.C., May 1990.
- UCB/EERC-90/07 "A Unified Earthquake-Resistant Design Method for Steel Frames Using ARMA Models," by Takewaki, I., Conte, J.P., Mahin, S.A. and Pister, K.S., June 1990.
- UCB/EERC-90/08 "Soil Conditions and Earthquake Hazard Mitigation in the Marina District of San Francisco," by Mitchell, J.K., Masood, T., Kayen, R.E. and Seed, R.B., May 1990, (PB 193 267/AS)A04.
- UCB/EERC-90/09 "Influence of the Earthquake Ground Motion Process and Structural Properties on Response Characteristics of Simple Structures," by Conte, J.P., Pister, K.S. and Mahin, S.A., July 1990, (PB92 143 064)A15.

- UCB/EERC-90/10 "Experimental Testing of the Resilient-Friction Base Isolation System," by Clark, P.W. and Kelly, J.M., July 1990, (PB92 143 072)A08.
- UCB/EERC-90/11 "Seismic Hazard Analysis: Improved Models, Uncertainties and Sensitivities," by Araya, R. and Der Kiureghian, A., March 1988.
- UCB/EERC-90/12 "Effects of Torsion on the Linear and Nonlinear Seismic Response of Structures," by Sedarat, H. and Bertero, V.V., September 1989, (PB92 193 002/AS)A15.
- UCB/EERC-90/13 "The Effects of Tectonic Movements on Stresses and Deformations in Earth Embankments," by Bray, J. D., Seed, R. B. and Seed, H. B., September 1989.
- UCB/EERC-90/14 "Inelastic Seismic Response of One-Story, Asymmetric-Plan Systems," by Goel, R.K. and Chopra, A.K., October 1990, (PB93 114 767)A11.
- UCB/EERC-90/15 "Dynamic Crack Propagation: A Model for Near-Field Ground Motion.," by Seyyedian, H. and Kelly, J.M., 1990.
- UCB/EERC-90/16 "Sensitivity of Long-Period Response Spectra to System Initial Conditions," by Blasquez, R., Ventura, C. and Kelly, J.M., 1990.
- UCB/EERC-90/17 "Behavior of Peak Values and Spectral Ordinates of Near-Source Strong Ground-Motion over a Dense Array," by Niazi, M., June 1990, (PB93 114 833)A07.
- UCB/EERC-90/18 "Material Characterization of Elastomers used in Earthquake Base Isolation," by Papoulia, K.D. and Kelly, J.M., 1990.
- UCB/EERC-90/19 "Cyclic Behavior of Steel Top-and-Bottom Plate Moment Connections," by Harriott, J.D. and Astaneh-Asl, A., August 1990, (PB91 229 260/AS)A05.
- UCB/EERC-90/20 "Seismic Response Evaluation of an Instrumented Six Story Steel Building," by Shen, J.-H. and Astaneh-Asl, A., December 1990, (PB91 229 294/AS)A04.
- UCB/EERC-90/21 "Observations and Implications of Tests on the Cypress Street Viaduct Test Structure," by Bollo, M., Mahin, S.A., Moehle, J.P., Stephen, R.M. and Qi, X., December 1990, (PB93 114 775)A13.
- UCB/EERC-91/01 "Experimental Evaluation of Nitinol for Energy Dissipation in Structures," by Nims, D.K., Sasaki, K.K. and Kelly, J.M., 1991.
- UCB/EERC-91/02 "Displacement Design Approach for Reinforced Concrete Structures Subjected to Earthquakes," by Qi, X. and Moehle, J.P., January 1991, (PB93 114 569/AS)A09.
- UCB/EERC-91/03 "A Long-Period Isolation System Using Low-Modulus High-Damping Isolators for Nuclear Facilities at Soft-Soil Sites," by Kelly, J.M., March 1991, (PB93 114 577/AS)A10.
- UCB/EERC-91/04 "Dynamic and Failure Characteristics of Bridgestone Isolation Bearings," by Kelly, J.M., April 1991, (PB93 114 528)A05.
- UCB/EERC-91/05 "Base Sliding Response of Concrete Gravity Dams to Earthquakes," by Chopra, A.K. and Zhang, L., May 1991, (PB93 114 544/AS)A05.
- UCB/EERC-91/06 "Computation of Spatially Varying Ground Motion and Foundation-Rock Impedance Matrices for Seismic Analysis of Arch Dams," by Zhang, L. and Chopra, A.K., May 1991, (PB93 114 825)A07.
- UCB/EERC-91/07 "Estimation of Seismic Source Processes Using Strong Motion Array Data," by Chiou, S.-J., July 1991, (PB93 114 551/AS)A08.
- UCB/EERC-91/08 "A Response Spectrum Method for Multiple-Support Seismic Excitations," by Der Kiureghian, A. and Neuenhofer, A., August 1991, (PB93 114 536)A04.
- UCB/EERC-91/09 "A Preliminary Study on Energy Dissipating Cladding-to-Frame Connection," by Cohen, J.M. and Powell, G.H., September 1991, (PB93 114 510)A05.
- UCB/EERC-91/10 "Evaluation of Seismic Performance of a Ten-Story RC Building During the Whittier Narrows Earthquake," by Miranda,\* E. and Bertero, V.V., October 1991, (PB93 114 783)A06.
- UCB/EERC-91/11 "Seismic Performance of an Instrumented Six-Story Steel Building," by Anderson, J.C. and Bertero, V.V., November 1991, (PB93 114 809)A07.
- UCB/EERC-91/12 "Performance of Improved Ground During the Loma Prieta Earthquake," by Mitchell, J.K. and Wentz, Jr., F.J., October 1991, (PB93 114 791)A06.
- UCB/EERC-91/13 "Shaking Table - Structure Interaction," by Rinawi, A.M. and Clough, R.W., October 1991, (PB93 114 917)A13.
- UCB/EERC-91/14 "Cyclic Response of RC Beam-Column Knee Joints: Test and Retrofit," by Mazzoni, S., Moehle, J.P. and Thewalt, C.R., October 1991, (PB93 120 277)A03.
- UCB/EERC-91/15 "Design Guidelines for Ductility and Drift Limits: Review of State-of-the-Practice and State-of-the-Art in Ductility and Drift-Based Earthquake-Resistant Design of Buildings," by Bertero, V.V., Anderson, J.C., Krawinkler, H., Miranda, E. and The CUREe and The Kajima Research Teams, July 1991, (PB93 120 269)A08.
- UCB/EERC-91/16 "Evaluation of the Seismic Performance of a Thirty-Story RC Building," by Anderson, J.C., Miranda, E., Bertero, V.V. and The Kajima Project Research Team, July 1991, (PB93 114 841)A12.
- UCB/EERC-91/17 "A Fiber Beam-Column Element for Seismic Response Analysis of Reinforced Concrete Structures," by Taucer, F., Spacone, E. and Filippou, F.C., December 1991, (PB94 117 629AS)A07.

- UCB/EERC-91/18 "Investigation of the Seismic Response of a Lightly-Damped Torsionally-Coupled Building," by Boroschek, R. and Mahin, S.A., December 1991, (PB93 120 335)A13.
- UCB/EERC-92/01 "Studies of a 49-Story Instrumented Steel Structure Shaken During the Loma Prieta Earthquake," by Chen, C.-C., Bonowitz, D. and Astaneh-Asl, A., February 1992, (PB93 221 778)A08.
- UCB/EERC-92/02 "Response of the Dumbarton Bridge in the Loma Prieta Earthquake," by Fenves, G.L., Filippou, F.C. and Sze, D.T., January 1992, (PB93 120 319)A09.
- UCB/EERC-92/03 "Models for Nonlinear Earthquake Analysis of Brick Masonry Buildings," by Mengi, Y., McNiven, H.D. and Tanrikulu, A.K., March 1992, (PB93 120 293)A08.
- UCB/EERC-92/04 "Shear Strength and Deformability of RC Bridge Columns Subjected to Inelastic Cyclic Displacements," by Aschheim, M. and Moehle, J.P., March 1992, (PB93 120 327)A06.
- UCB/EERC-92/05 "Parameter Study of Joint Opening Effects on Earthquake Response of Arch Dams," by Fenves, G.L., Mojtahedi, S. and Reimer, R.B., April 1992, (PB93 120 301)A04.
- UCB/EERC-92/06 "Seismic Behavior and Design of Semi-Rigid Steel Frames," by Nader, M.N. and Astaneh-Asl, A., May 1992.
- UCB/EERC-92/07 "A Beam Element for Seismic Damage Analysis," by Spacone, E., Ciampi, V. and Filippou, F.C., August 1992.
- UCB/EERC-92/08 "Nonlinear Static and Dynamic Analysis of Reinforced Concrete Subassemblages," by Filippou, F.C., D'Ambrisi, A. and Issa, A., August 1992.
- UCB/EERC-92/09 "Evaluation of Code Accidental-Torsion Provisions Using Earthquake Records from Three Nominally Symmetric-Plan Buildings," by De la Llera, J.C. and Chopra, A.K., September 1992, (PB94 117 611)A08.
- UCB/EERC-92/10 "Slotted Bolted Connection Energy Dissipators," by Grigorian, C.E., Yang, T.-S. and Popov, E.P., July 1992, (PB92 120 285)A03.
- UCB/EERC-92/11 "Mechanical Characteristics of Neoprene Isolation Bearings," by Kelly, J.M. and Quiroz, E., August 1992, (PB93 221 729)A07.
- UCB/EERC-92/12 "Application of a Mass Damping System to Bridge Structures," by Hasegawa, K. and Kelly, J.M., August 1992, (PB93 221 786)A06.
- UCB/EERC-92/13 "Earthquake Engineering Research at Berkeley - 1992," by EERC, October 1992.
- UCB/EERC-92/14 "Earthquake Risk and Insurance," by Brillinger, D.R., October 1992, (PB93 223 352)A03.
- UCB/EERC-92/15 "A Friction Mass Damper for Vibration Control," by Inaudi, J.A. and Kelly, J.M., October 1992, (PB93 221 745)A04.
- UCB/EERC-92/16 "Tall Reinforced Concrete Buildings: Conceptual Earthquake-Resistant Design Methodology," by Bertero, R.D. and Bertero, V.V., December 1992, (PB93 221 695)A12.
- UCB/EERC-92/17 "Performance of Tall Buildings During the 1985 Mexico Earthquakes," by Terán-Gilmore, A. and Bertero, V.V., December 1992, (PB93 221 737)A11.
- UCB/EERC-92/18 "Dynamic Analysis of Nonlinear Structures using State-Space Formulation and Partitioned Integration Schemes," by Inaudi, J.A. and De la Llera, J.C., December 1992, (PB94 117 702/AS/A05).
- UCB/EERC-93/01 "Seismic Performance of an Instrumented Six-Story Reinforced-Concrete Building," by Anderson, J.C. and Bertero, V.V., 1993.
- UCB/EERC-93/02 "Evaluation of an Active Variable-Damping-Structure," by Polak, E., Meeker, G., Yamada, K. and Kurata, N., 1993, (PB93 221 711)A05.
- UCB/EERC-93/03 "An Experimental Study of Flat-Plate Structures under Vertical and Lateral Loads," by Hwang, S.-H. and Moehle, J.P., February 1993, (PB94 157 690/AS)A13.
- UCB/EERC-93/04 "Seismic Performance of a 30-Story Building Located on Soft Soil and Designed According to UBC 1991," by Terán-Gilmore, A. and Bertero, V.V., 1993, (PB93 221 703)A17.
- UCB/EERC-93/05 "Multiple-Support Response Spectrum Analysis of the Golden Gate Bridge," by Nakamura, Y., Der Kiureghian, A. and Liu, D., May 1993, (PB93 221 752)A05.
- UCB/EERC-93/06 "On the Analysis of Structures with Viscoelastic Dampers," by Inaudi, J.A., Zambrano, A. and Kelly, J.M., August 1993, PB94-165867.
- UCB/EERC-93/07 "Earthquake Analysis and Response of Concrete Gravity Dams Including Base Sliding," by Chávez, J.W. and Fenves, G.L., December 1993, (PB94 157 658/AS)A10.
- UCB/EERC-93/08 "Model for Anchored Reinforcing Bars under Seismic Excitations," by Monti, G., Spacone, E. and Filippou, F.C., December 1993.
- UCB/EERC-93/09 "A Methodology for Design of Viscoelastic Dampers in Earthquake-Resistant Structures," by Abbas, H. and Kelly, J.M., November 1993.
- UCB/EERC-93/10 "Tuned Mass Dampers Using Viscoelastic Dampers," by Inaudi, J.A., Lopez-Almansa, F. and Kelly, J.M., December 1993.
- UCB/EERC-93/11 "Nonlinear Homogeneous Dynamical Systems," by Inaudi, J.A. and Kelly, J.M., December 1993.
- UCB/EERC-93/12 "Synthesized Strong Ground Motions for the Seismic Condition Assessment of the Eastern Portion of the San Francisco Bay Bridge," by Bolt, B.A. and Gregor, N.J., December 1993, PB94-165842.

- UCB/EERC-93/13 "On the Analysis of Structures with Energy Dissipating Restraints," by Inaudi, J.A., Nims, D.K. and Kelly, J.M., December 1993.
- UCB/EERC-94/01 "Preliminary Report on the Seismological and Engineering Aspects of the January 17, 1994 Northridge Earthquake," by EERC, January 1994, (PB94 157 666/AS)A05.
- UCB/EERC-94/02 "Energy Dissipation with Slotted Bolted Connections," by Grigorian, C.E. and Popov, E.P., February 1994, PB94-164605.
- UCB/EERC-94/03 "The Influence of Plate Flexibility on the Buckling Load of Elastomeric Isolators," by Kelly, J.M., March 1994.
- UCB/EERC-94/04 "Insitu Test Results from Four Loma Prieta Earthquake Liquefaction Sites: SPT, CPT, DMT and Shear Wave Velocity," by Mitchell, J.K., Lodge, A.L., Coutinho, R.Q., Kayen, R.E., Seed, R.B., Nishio, S. and Stokoe II, K.H., April 1994.
- UCB/EERC-94/05 "Seismic Response of Steep Natural Slopes," by Sitar, N. and Ashford, S.A., May 1994.

**BC-TOP-9A**

**Revision 2**

**SEPTEMBER 1974**

**TOPICAL REPORT  
DESIGN OF STRUCTURES  
FOR MISSILE IMPACT**

**Bechtel Power Corporation  
San Francisco, California**



**TOPICAL REPORT**

**BC-TOP-9-A**

**Revision 2**

**DESIGN OF STRUCTURES FOR MISSILE IMPACT**

**PREPARED BY:**

**R. B. Linderman**

**J. V. Rotz**

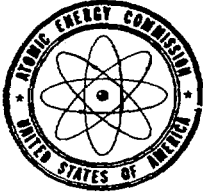
**G. C. K. Yeh**

**APPROVED BY:**

W. A. Brandes *W. A. Brandes*

H. W. Wahl *H. W. Wahl*

**CAVEAT: THIS REPORT HAS BEEN PREPARED BY AND FOR THE USE OF BECHTEL POWER CORPORATION AND ITS RELATED ENTITIES. ITS USE BY OTHERS IS PERMITTED ONLY ON THE UNDERSTANDING THAT THERE ARE NO REPRESENTATIVES OR WARRANTIES, EXPRESS OR IMPLIED, AS TO THE VALIDITY OF THE INFORMATION OR CONCLUSIONS CONTAINED HEREIN.**



UNITED STATES  
ATOMIC ENERGY COMMISSION  
WASHINGTON, D.C. 20545

Mr. John V. Morowski  
Vice President-Engineering  
Bechtel Power Corporation  
Fifty Beale Street  
San Francisco, California 94119

Dear Mr. Morowski:

The Regulatory staff has completed its review of Bechtel Power Corporation's Topical Report, BC-TOP-9, Revision 2, dated September 1974 and entitled "Design of Structures for Missile Impact". We conclude that the design criteria and procedures described by this report are acceptable to the Regulatory staff and that BC-TOP-9, Revision 2, is acceptable by reference in applications for construction permits and operating licenses. A summary of our evaluation is enclosed.

BC-TOP-9 does not provide all of the pertinent information required by the Regulatory staff in its review of specific applications. Therefore, the appropriate supplementary information identified in the Regulatory Position of the enclosed Topical Report Evaluation will have to be provided in individual Safety Analysis Reports.

The staff does not intend to repeat its review of BC-TOP-9, Revision 2, when it appears as a reference in a particular license application. Should Regulatory criteria or regulations change, such that our conclusions concerning BC-TOP-9, Revision 2, are invalidated, you will be notified and given the opportunity to revise and resubmit your topical report for review, should you so desire.

Mr. John V. Morowski

- 2 -

NOV 25 1974

We request that you reissue BC-TOP-9, Revision 2, dated September 1974 in accordance with the provisions of the "Elements of the Regulatory Staff Topical Report Review Program" which was forwarded to you on August 26, 1974. If you have any questions in this regard, please let us know.

Sincerely,



R. W. Klecker, Technical Coordinator  
for Light Water Reactors Group 1  
Directorate of Licensing

Enclosure:  
Topical Report Evaluation

## Topical Report Evaluation

Report: BC-TOP-9 Rev.2  
Report Title: Design of Structures for Missile Impact  
Report Date: September 1974  
Originating Organization: Bechtel Power Corporation  
Reviewed by: Structural Engineering Branch, November 1974

### Summary of Report

This report contains the current general procedures and criteria used by Bechtel Power Corporation for design of nuclear power plant structures and components against the effects of impact of missiles. The report covers the evaluation of local effects due to missiles impacting on both concrete and steel structural elements. It also covers the procedures used to evaluate the overall structural response to missile impact loads. Design guidelines related to use of dynamic capacity increase factors, allowable ductility ratio and allowable range of steel ratios used in concrete structural elements are also discussed in the report. Brief discussions of special problems related to (a) force-time history for automobile crash and (b) penetration of a missile through a liquid are included as a part of the report.

The formulae which can be used to predict the penetration resulting from missile impact are included in the report. The penetration and perforation formulae assume that the missile strikes the target normal to the surface, and the axis of the missile is assumed parallel to the line of flight. These assumptions result in a conservative estimate of local damage to the target. The formula used to predict the penetration is the Modified Petry equation, while that for perforation and spalling is the Ballistic Research Laboratory formula modified to allow its use for concrete strength other than 3000 psi by replacing the constant coefficient 7.8 by  $427/\sqrt{f'_c}$ . The wall thicknesses to prevent perforation and spalling are that calculated using the Ballistic Research Laboratory formula multiplied by factors of 1.25 and 2.5, respectively. The Ballistic Research Laboratory formula for steel is used to predict design thickness requirement

for steel targets. The thicknesses of steel targets to prevent perforation are obtained by multiplying 1.25 by the thicknesses for threshold perforation as determined by the BRL formula.

The report discusses both elastic and plastic modes of overall structural response of target subjected to a missile impact. Expressions for (a) velocities of missile and target after impact, (b) strain energy of a target required to stop a missile after impact, (c) target effective mass definition and (d) resistance functions for various target configurations are presented in the report. The overall structural response of a target is determined by equating the available target strain energy to the required strain energy to stop a missile. The resistance function for a structural element is determined using yield-line theory for concentrated loads impacting steel and reinforced concrete beam and slab. The allowable ductility ratios to be used for design are based on the available data from the literature accepted in the engineering practice. However the governing requirement for an overall structural response design consideration is that the maximum deflection of the target shall be limited so as not to impair the function of other safety related equipment. Due to the complexity of the impact phenomena, the target effective mass is conservatively derived based on the tests performed on concrete slabs and beams.

The report covers two types of special problems, i.e., determination of an empirical formula for force-time history of automobile crash and an evaluation of a missile velocity as it passes through a liquid. In deriving the force-time history of an automobile crash under front impact, the automobile is considered as a deformable missile and the structure a rigid target. The pertinent equations are based on theoretical considerations backed by experimental data.

The derivation of the velocity of a missile after it has penetrated through a liquid takes into consideration the buoyant force, which is variable during the process of immersion of the missile and constant after the entire missile is immersed in the liquid, and drag force which may be considered as constant for any particular set of conditions. The non-linear, second order, non homogeneous differential equation is transformed into a linear differential equation which is solved by applying pertinent boundary conditions.

For the postulated missiles and their properties as well as for structures, shields and barriers that are required to be designed against effects of missile impact, the report refers to the plant SAR.

Appendix A provides the cross reference between sections of the AEC's Standard SAR format and the sections of BC-TOP-9. Glossary of the report is given in Appendix B. A review of existing design formulas is given in Appendix C whereas Appendix D discusses theoretical derivation for force-time history associated with automobile crash and velocity of a missile penetrating through a liquid. Sample applications of the procedures presented in the report are shown in Appendix E with references and bibliography listed in Appendix F.

#### Summary of the Regulatory Evaluation

The Structural Engineering Branch of the Directorate of Licensing has reviewed the subject report and its appendices. The procedures covered by this report with the qualifications stated in the following Regulatory Position and augmentation of pertinent information that is referred to and to be provided in the plant SAR are judged to represent the present "state of the art" in the field of design of structures and components against missile impacts. If properly utilized in nuclear power plant structural design work, the procedures and criteria contained in the report should provide

conservative and acceptable bases for design of structural elements against missile impact effects.

#### Regulatory Position

The design criteria and procedures are acceptable to the Regulatory staff. The report may be referenced in future case applications provided that the following specific information reviewed and accepted by the Regulatory staff is included in individual SAR:

- a) Parameters that define the postulated missiles such as striking velocity, weight, missile configurations and impacting area, etc.
- b) Structures, shields and barriers that are required to be designed for missiles with their pertinent characteristics.
- c) If use of a ductility ratio greater than 10 (i.e.,  $\mu > 10$ ) is required to demonstrate design adequacy of structural elements against missile impact, such a usage should be identified in the plant SAR. Information justifying the use of this relatively high ductility value may become necessary for inclusion in the plant SAR. In such a case, the Regulatory staff will request the applicant to provide the information on a case by case basis.
- d) The evaluation of punching shear effect due to impact of unconventional missiles, is not included as a part of the overall structural response consideration in the report. The subject should be adequately addressed in individual plant SAR.

ABSTRACT

This report contains methods and procedures for evaluating the effects of missile impact on structures. A means to evaluate the change of velocity of a missile passing through a liquid is also included. Missile impact effects on structures are evaluated in terms of local damage (penetration, perforation, and spalling) and structural response. Empirical formulae are used to evaluate local effects. Structural dynamic principles are used to evaluate structural response.

ACKNOWLEDGMENT

This document is the result of a joint effort on the part of several contributors.

The following is a chronological account of major participants contributing to the development of this document:

Revision 0 (issued October, 1972) was prepared by M. Fakhari, B. Linderman, J. Rotz and M. Suarez and approved by A. J. Bingaman (Gaithersburg Office Chief Civil Engineer) and D. W. Halligan (Power and Industrial Division Chief Civil Engineer).

Revision 1 (issued July, 1973) was prepared by R. B. Linderman, M. Fakhari, J. V. Rotz, E. Thomas, G. A. Tuveson, and G. C. K. Yeh; and approved by W. A. Brandes (Los Angeles Power Division, Chief Civil Engineer) and L. G. Hinkelman (Thermal Power Organization, Chief Civil Engineer); Technical Consultant, N. M. Newmark.

Revision 2 (issued September, 1974) was prepared by R. B. Linderman, J. V. Rotz and G. C. K. Yeh; and approved by W. A. Brandes (Los Angeles Power Division, Chief Civil Engineer) and H. W. Wahl (Thermal Power Organization, Chief Civil Engineer); Technical Consultant, N. M. Newmark.

CONTENTS

<u>Section</u>	<u>Title</u>	<u>Page</u>
1.	INTRODUCTION	1-1
1.1	General	1-1
1.2	Approach	1-1
1.3	Missile Characteristics	1-2
1.4	Target Characteristics	1-2
2.	LOCAL EFFECTS	2-1
2.1	Reinforced Concrete Targets	2-1
2.1.1	Penetration	2-1
2.1.2	Perforation	2-2
2.1.3	Spalling	2-3
2.2	Steel Targets	2-3
2.3	Multiple Element Barriers	2-4
2.3.1	Reinforced Concrete Barrier	2-5
2.3.2	Steel Barrier	2-5
3.	STRUCTURAL RESPONSE TO MISSILE IMPACT LOAD	3-1
3.1	General	3-1
3.2	Velocity After Impact	3-1
3.3	Required Target Strain Energy Capacity	3-2
2   3.3.1	Elastic Impact	3-2
3.3.2	Plastic Impact	3-3
3.3.3	Force Time Function Known	3-3
3.4	Target Effective Mass	3-5
3.5	Structural Response by Energy Balance Method	3-7
3.5.1	General Procedures	3-7
3.5.2	Elastic Target Response	3-7
3.5.3	Elasto-Plastic Target Response	3-8
3.5.4	Non-Linear Target Responses	3-9
4.	DESIGN GUIDELINES	4-1
4.1	Allowable Stresses and Loadings	4-1
4.2	Design Parameters	4-1
4.3	Allowable Ductility Ratio	4-3

CONTENTS (Cont)

<u>Section</u>	<u>Title</u>	<u>Page</u>
5.	SPECIAL PROBLEMS	5-1
5.1	Force-Time History for Automobile Crash	5-1
5.2	Penetration of a Missile Through a Liquid	5-1
5.2.1	Liquid Depth is Less Than or Equal to Missile Length	5-2
5.2.2	Liquid Depth is Greater Than Missile Length ( $H > L$ )	5-2
5.2.3	Definitions of Notations	5-3

LIST OF APPENDICES

<u>Appendix</u>	<u>Title</u>	<u>Page</u>
APPENDIX A	Cross Reference Listing to AEC Standard SAR Format	A-1
APPENDIX B	Glossary	B-1
APPENDIX C	Review of Existing Formulas	C-1
APPENDIX D	Derivations	D-1
APPENDIX E	Sample Applications	E-1
APPENDIX F	References and Bibliography	F-1

LIST OF TABLES

<u>Table</u>	<u>Title</u>	<u>Page</u>
4-1	Dynamic Increase Factor (DIF)	4-4
4-2	Resistance-Yield Displacement Values for Beams	4-5
4-3	Resistance-Yield Displacement Values for Slabs	4-6
4-4	Ductility Ratios (From Reference 28)	4-7
5-1	Drag Coefficient for Variously Shaped Bodies in Incompressible Flow	5-4
C-1	Concrete Penetration, Perforation, and Spalling Formulas	C-5
C-2	Perforation in Steel Formulas	C-8

LIST OF ILLUSTRATIONS

<u>Figure</u>	<u>Title</u>	<u>Page</u>
2-1	Values of Penetration Coefficient ( $K_p$ ) for Reinforced Concrete	2-6
2-2	Penetration of Reinforced Concrete for Various Missiles (Modified Petry)	2-7
2-3	Perforation of Reinforced Concrete for Various Missiles (Ballistics Research Laboratory)	2-8
2   2-4	Penetration, Perforation, and Spalling of Reinforced Concrete Target by Postulated Tornado Missiles	2-9
3-1	Resistance-Displacement Functions With Associated Structural Response With and Without The Effects of Other Loads	3-12
3-2	Energy-Displacement Functions - Impact Loads Only	3-13
3-3	Energy-Displacement Functions - Impact Combined With Other Loads	3-14
2   4-1	Coefficients for Moment of Inertia of Cracked Sections	4-8
5-1	Penetration of a Missile in a Liquid	5-5
C-1	Typical Crater Profiles	C-9
2   C-2 thru C-22	Deleted	

## Section 1

### INTRODUCTION

#### 1.1 GENERAL

The design of nuclear power facilities includes the effects of missile impact on structures, systems, and equipment. External building surfaces, interior walls and floors, and special barriers (constructed of concrete and/or steel) that will resist or deflect missiles may be used to protect systems and equipment where necessary.

This report contains methods and preferred procedures to evaluate missile impact on structures and barriers. Missile effects are evaluated in terms of local damage (penetration, perforation, and spalling) and structural response.

Missiles may be generated by an event that is not related to plant operation, or by the failure of plant equipment. The primary sources of missiles, not related to plant operations are debris transported by tornado winds, and falling objects generated by activities near the plant site (such as commercial, industrial, or military activities). Missiles that may result from the failure of equipment generally result from the uncontrolled release of energy and forces from a pressurized system or rotating machinery. Missiles that may result from the failure of equipment are fittings, valve parts, various nuts and bolts, and parts of rotating machinery, etc.

#### 1.2 APPROACH

Determining the effect of missile impact is outlined in the following general steps. However, there are many interactive effects in each step that should be considered in the complete analysis.

- Determine missile characteristics.
- Define target, considering impact in combination with other loads and requirements (preliminary properties).
- Determine local effects of missile on target.
- Determine target characteristics for structural response and stability.
- Determine equivalent target mass during impact.
- Determine structural response.
- Evaluate structural integrity.
- Verify that the maximum deflection does not impair the function of other safety related systems.

### 1.3 MISSILE CHARACTERISTICS

Missile parameters required for missile impact analysis include trajectory, mass, velocity, geometry, and deformation characteristics. The geometry should include contact area, projected frontal area and variation of area with respect to length. Deformation characteristics include if the missile will deform or is rigid and if it is ductile or brittle. Missile geometry and deformation characteristics have a significant effect on penetration or perforation of a target. A pointed missile will penetrate deeper into a target than a blunt missile; it will also perforate a thicker target. Deformation of a missile during impact consumes energy, which results in diminished local damage.

Postulated missiles and their properties may vary with each plant and are defined in the Safety Analysis Report (SAR) for nuclear power plants.

### 1.4 TARGET CHARACTERISTICS

Structures or barriers (targets), providing missile protection, act as energy absorbers. The target absorbs the energy by local damage at the location of impact (i.e. penetration of the missile into the barrier) and by the structural response of the target.

Local damage depends on missile characteristics, target material properties, and structural response. Empirical methods are used to estimate local damage because of the complex phenomena associated with missile impact. The ability of a target to absorb energy by structural response depends on the dynamic properties of the target, support conditions and other imposed loads at the time of impact. Structural dynamic principles are used to estimate the structural response and determine if the target will remain stable during and after missile impact.

Structures, shields and barriers that are required to be designed for a missile are given in the Safety Analysis Reports.

Section 2

LOCAL EFFECTS

Predicting local damage in the impact area includes estimating depth of penetration, minimum thickness required to prevent perforation, and minimum thickness required to preclude spalling. The penetration and perforation formulae in this section assume that the missile strikes the target normal to the surface, and the axis of the missile is assumed parallel to the line of flight. These assumptions result in a conservative estimate of local damage to the target. Appendix C has information on the more common local effect formula and a discussion of the effects on the penetration for a missile striking a target at oblique angle.

2.1 REINFORCED CONCRETE TARGETS

2.1.1. PENETRATION

The depth to which a rigid missile will penetrate a reinforced concrete target of infinite thickness is estimated by the following formula

$$X = 12 K_p A_p \log_{10} \left( 1 + \frac{v_s^2}{215,000} \right) \quad (2-1)$$

where

X = Depth of missile penetration into concrete element of infinite thickness (inches)

Note: Usually this equation expresses the depth of penetration in feet; however, for this document it has been modified to express it in inches.

$K_p$  = Penetration coefficient for reinforced concrete (see Figure 2-1).

$A_p = \frac{W}{A} = \frac{\text{Missile weight}}{\text{Projected frontal area of missile}}$  (psf) | 2

$V_s$  = Striking velocity of missile (ft/sec). (Limit  $V_s \leq 1000$  ft/sec)

This formula is known as the Modified Petry formula:

When the element has a finite thickness the depth of penetration is:

$$X_1 = \left[ 1 + e^{-4 \left( \frac{t}{X} - 2 \right)} \right] X, \quad (t > 2X) \quad (2-2) \quad | 2$$

where

$X_1$  = Depth of penetration of missile into a concrete element of finite thickness (inches).

$e$  = Base of Napierian Logarithms

$t$  = Thickness of concrete element (inches)

2

Penetrations for various illustrative examples of missiles are shown in figures 2-2 and 2-4.

### 2.1.2 PERFORATION

The thickness of a concrete element that will just be perforated by a missile is given by:

$$T = \frac{427}{\sqrt{f'_c}} \frac{W}{D^{1.8}} \left( \frac{V_s}{1000} \right)^{1.33} \quad (2-3)$$

where

$T$  = Thickness of concrete element to be just perforated (inches)

$W$  = Weight of missiles (lb)

$D$  = Diameter of missiles (inches)

Note: For irregularly shaped missiles, an equivalent diameter is used. The equivalent diameter is taken as the diameter of a circle with an area equal to the circumscribed contact, or projected frontal area, of the non-cylindrical missile.

$V_s$  = Striking velocity of missile (ft/sec)

$f'_c$  = Compressive strength of concrete (psi)

This formula is known as the Ballistic Research Laboratory, BRL, formula.

The thickness,  $t_p$ , of a concrete element required to prevent perforation must be greater than  $T$ . It is recommended to increase  $T$  by 25 percent, but not more than 10 inches, to obtain the  $t_p$ , required to prevent perforation

$$t_p = 1.25T \leq T + 10 \text{ (in inches)} \quad (2-4)$$

The threshold of perforation, T, for various illustrative examples of missiles is shown in figures 2-3 and 2-4. | 2

### 2.1.3 SPALLING

Spalling of concrete from the side opposite the contact surface of the element may occur even if the missile will not perforate the element. For an estimate of the thickness that will just start spalling, it is recommended that the following equation be used:

$$T_s = 2T \quad (2-5)$$

where

$T_s$  = Concrete element thickness that will just start spalling (inches)

T = Concrete thickness to be just perforated (inches).  
See Equation (2-3)

The thickness,  $t_s$ , of a concrete element required to prevent spalling must be greater than  $T_s$ . It is recommended to increase  $T_s$  by 25 percent, but not more than 10 inches, to prevent spalling.

$$t_s = 1.25 T_s \leq T_s + 10 \text{ (in inches)} \quad (2-6)$$

### 2.2 STEEL TARGETS

Steel targets, such as pipes and mechanical equipment vessels, may be perforated by a missile. Sometimes, protruding elements of a missile may puncture a steel target when the entire missile does not perforate or pass through the target. The minimum contact area of a missile protrusion is used to calculate puncture thickness and the projected area of the entire missile is used to calculate perforation thickness.

The BRL Formula is shown below, modified by setting a material constant  $K = 1$  and solving directly for steel plate thickness, T, which will just be perforated by the missile,

$$T = \frac{\left(\frac{MV^2}{S}\right)^{2/3}}{672D} \quad (2-7)$$

where

T = Steel plate thickness to just perforate (inches).

M = Mass of the Missile (lb sec<sup>2</sup>/ft)

W = Weight of the Missile (lb)

V<sub>s</sub> = Striking Velocity of the Missile Normal to Target Surface (ft/sec)

D = Diameter of the Missile (in.)

Note: For irregularly shaped missiles the equivalent diameter is used. The equivalent diameter is taken as the diameter of a circle with an area equal to the circumscribed contact, or projected frontal area of the non-cylindrical missile.

The thickness, t<sub>p</sub>, of a steel barrier required to prevent perforation should exceed the thickness for threshold of perforations. It is recommended to increase the thickness, T, by 25 percent to prevent perforation.

$$t_p = 1.25T \quad (2-8)$$

### 2.3 MULTIPLE ELEMENT BARRIERS

It may be desirable to construct a missile barrier of several thinner elements, instead of one thick element. Analysis of missile barriers composed of several elements involves determining the residual velocity (V<sub>r</sub>) after perforation of one element and using this value for the striking velocity (V<sub>s</sub>) on the next element. The following formula is used to determine the residual velocity, V<sub>r</sub> (see Appendix C)

$$\begin{aligned} V_r &= \left( V_s^2 - V_p^2 \right)^{1/2} && \text{For } (V_p \leq V_s) \\ V_r &= 0 && \text{For } (V_p \geq V_s) \end{aligned} \quad (2-9)$$

where

2 | V<sub>r</sub> = residual velocity of missile after perforation of an element of thickness t. (fps)

V<sub>s</sub> = striking velocity of the missile normal to target surface (fps)

V<sub>p</sub> = velocity required to just perforate an element (fps)

### 2.3.1 REINFORCED CONCRETE BARRIER

Combining equations (2-3) and (2-9), the residual velocity of a missile perforating a concrete target is

$$V_r = \left[ V_s^2 - \left( \frac{\sqrt{f'_c} t D^{1.8}}{427W} \right)^{1.5} 10^6 \right]^{1/2} \quad (2-10)$$

where t = thickness of concrete element (inches)

### 2.3.2 STEEL BARRIER

Combining equations (2-7) and (2-9), the residual velocity of a missile perforating a steel target is

$$V_r = \left[ V_s^2 - \frac{1.12 \times 10^6 (Dt)^{1.5}}{W} \right]^{1/2} \quad (2-11)$$

where t = thickness of steel element (inches)

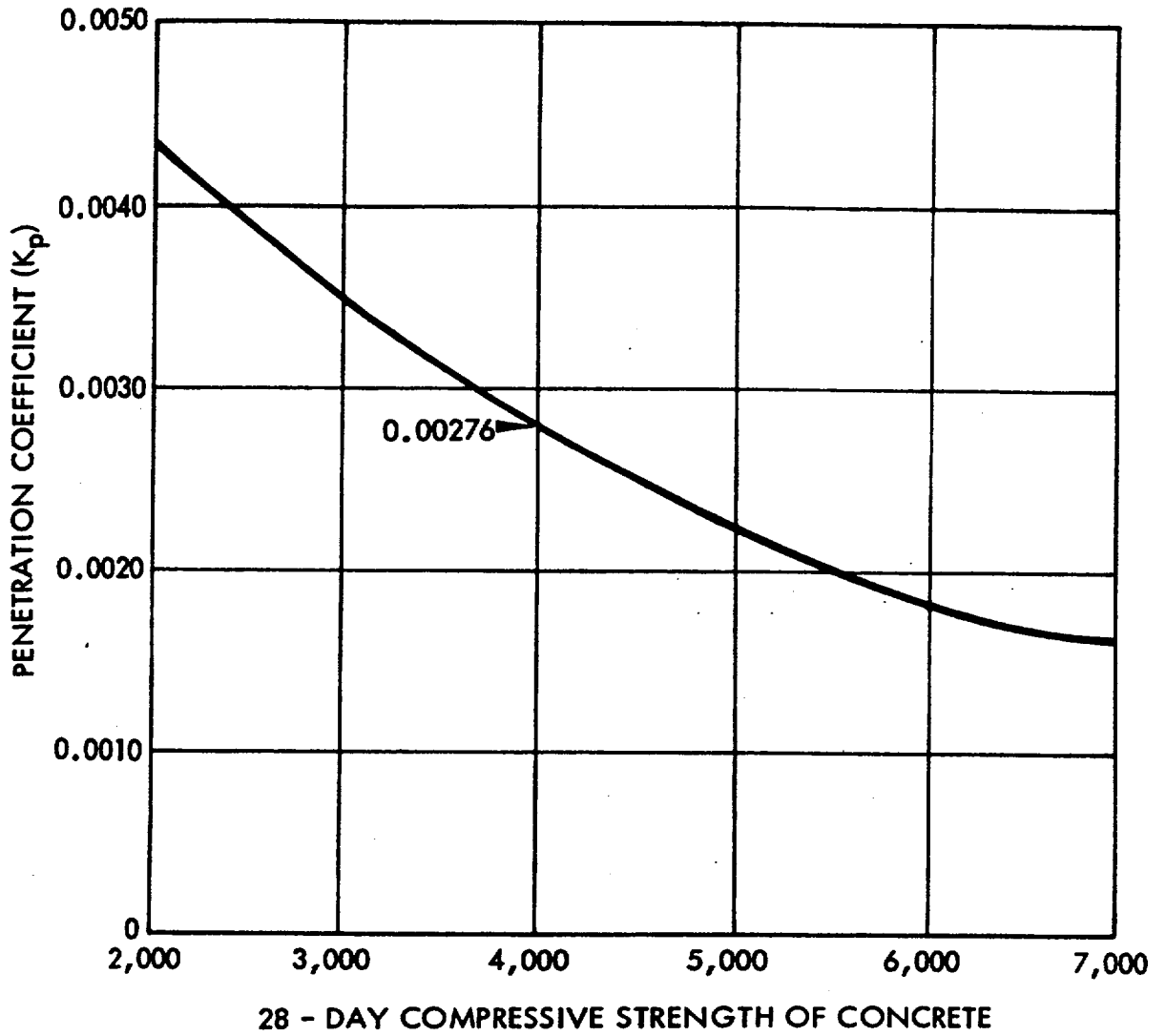


Figure 2-1

VALUES OF PENETRATION COEFFICIENT ( $K_p$ ) FOR REINFORCED CONCRETE  
(Reference 14)

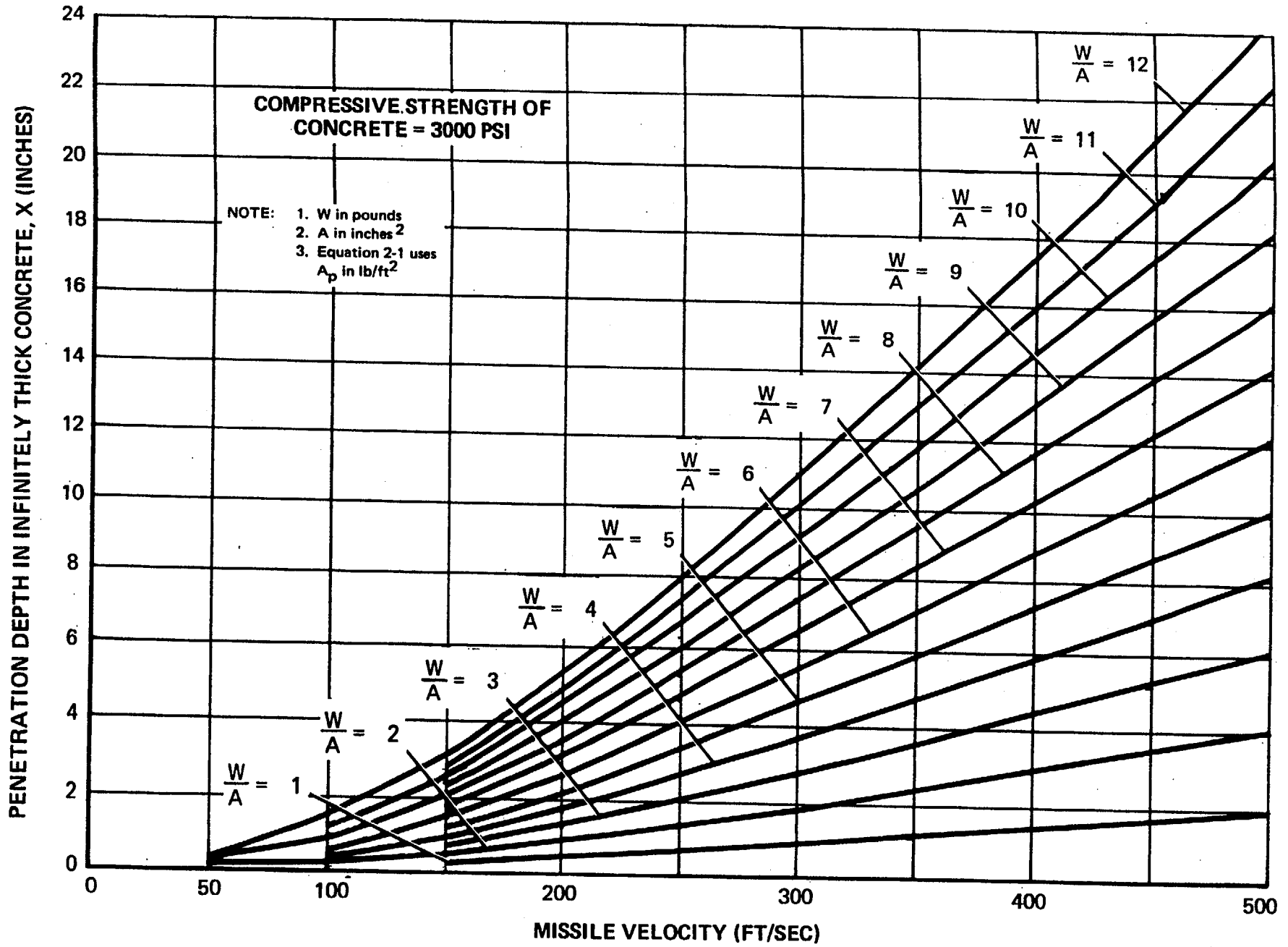


Figure 2-2

PENETRATION OF REINFORCED CONCRETE FOR VARIOUS MISSILES (MODIFIED PETRY)

CONCRETE THICKNESS TO BE JUST PERFORATED, T (INCHES)

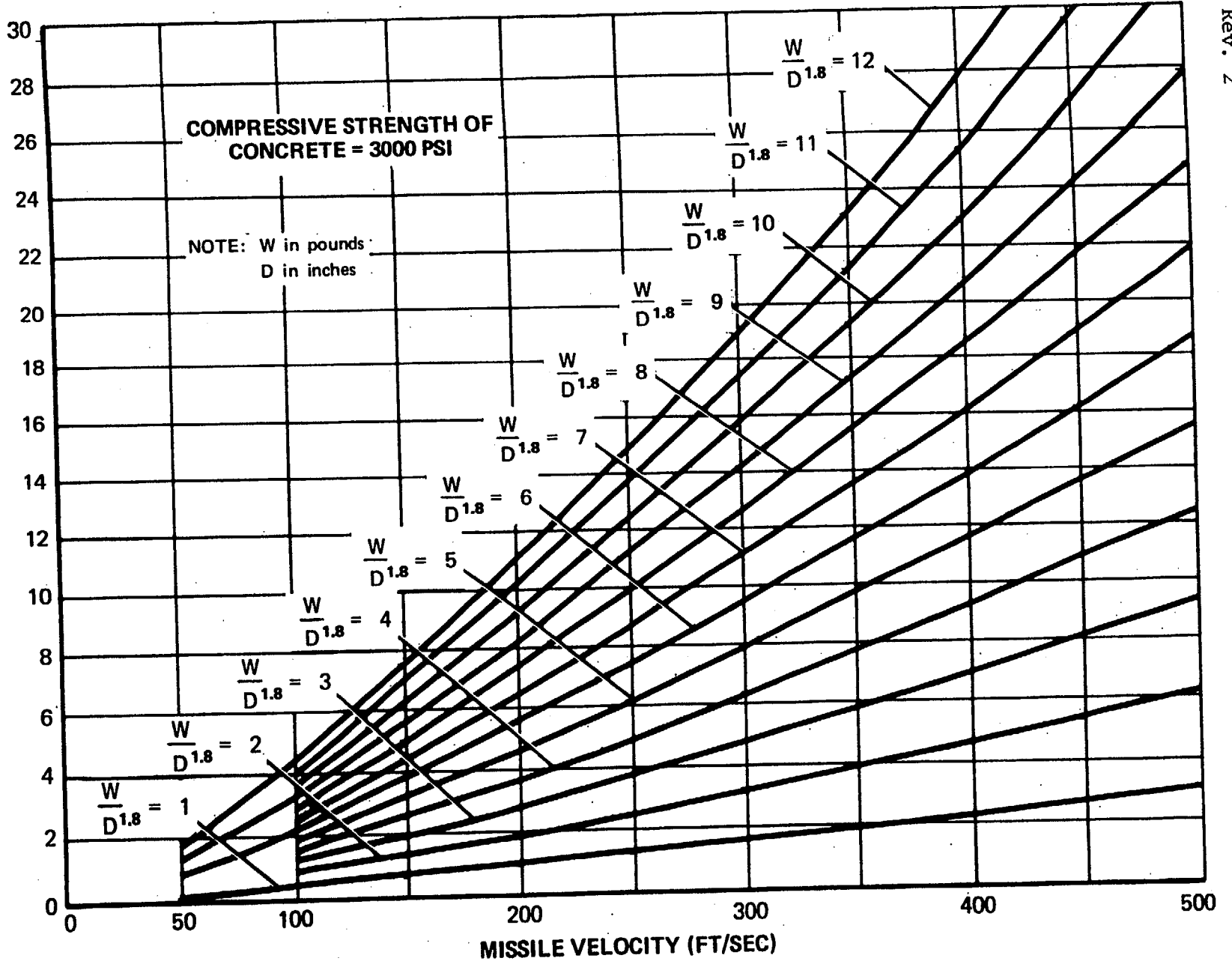


Figure 2-3

PERFORATION OF REINFORCED CONCRETE FOR

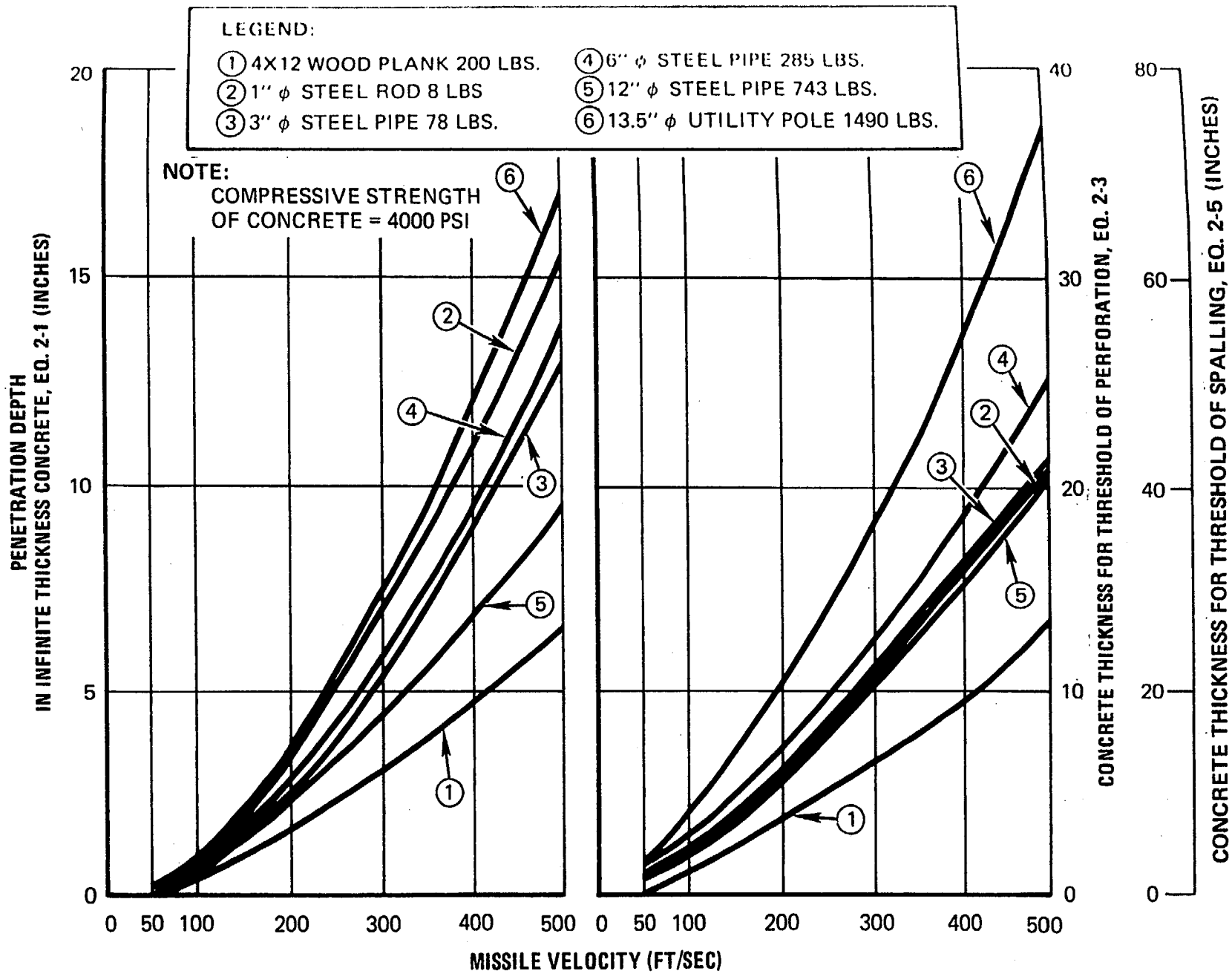


Figure 2-4

PENETRATION, PERFORATION, AND SPALLING OF REINFORCED CONCRETE TARGETS BY POSTULATED TORNADO MISSILES

### Section 3

#### STRUCTURAL RESPONSE TO MISSILE IMPACT LOAD

##### 3.1 GENERAL

When a missile strikes a target, large forces develop at the missile - target interface, which decelerate the missile and accelerate the target. If the interface forcing function is known, (experimentally determined), the target structure can be modeled mathematically and conventional numerical techniques can be used to predict structural response. For most cases, the forcing function is not known, and a rational method involving energy balance techniques is used to estimate structural response. This involves using the strain energy of the target at maximum response to balance the residual kinetic energy of the target (or target-missile combination) resulting from missile impact.

For investigation purposes, it is convenient to model the event as a missile of mass,  $M_m$ , and striking velocity,  $V_s$ , impacting a spring-backed target mass,  $M_e$ . The spring may be linear, bilinear, or non-linear, depending on the target structure resistance-displacement function. Since the actual coupled mass varies during impact, an estimated average effective target mass,  $M_e$  is used to evaluate inertia effects during impact.

The impact may be either elastic or plastic, depending on whether or not significant energy losses are sustained during impact. These losses are associated with inelastic deformations, local damage in the impact zone, etc.

Plastic impact is characterized by the missile remaining in contact with the target, subsequent to impact. In an elastic impact, the missile and target remain in contact for a very short period of time, and then disengage due to elastic interface restoring forces.

An elastic missile impact case is rarely encountered in nuclear plant design. For example, based on information available, a plastic collision can be considered for all postulated tornado-generated missiles.

##### 3.2 VELOCITY AFTER IMPACT

Since the duration of impact is very short, (usually less than a few milliseconds), the target mass displacement and the corresponding spring force are also very small. Neglecting the spring force effect during impact, (a slight conservatism), the velocities of the missile and target after impact are calculated from the following relationships:

$$V_m = \frac{V_s (M_m - eM_e)}{M_m + M_e} \quad (3-1)$$

$$V_T = \frac{V_s M_m (1+e)}{M_m + M_e} \quad (3-2)$$

$V_m$  = Missile velocity after impact

$V_T$  = Target velocity after impact

$V_s$  = Missile striking velocity

$M_m$  = Mass of missile

$M_e$  = Effective mass of target during impact

$e$  = Coefficient of restitution

### 3.3 REQUIRED TARGET STRAIN ENERGY CAPACITY

#### 3.3.1 ELASTIC IMPACT

Equations (3-1) and (3-2)<sup>(12)\*</sup> show that the velocity of the missile after impact is opposite to that of the target if  $M_m$  is less than  $eM_e$ . For this case, the strain energy,  $E_s$ , of the responding target spring required to diminish the target mass velocity to zero (maximum target response) is numerically equal to the kinetic energy of the target mass at the end of the impact duration.

$$E_s = \frac{M_e V_T^2}{2} \quad (3-3)$$

If the impact is determined to be elastic and the coefficient of restitution is not known, a conservative value of  $e$  equal to unity can be assumed. Making this substitution in equation (3-2), and substituting this value for  $V_T$  into equation 3-3, the required strain energy of the responding target is;

$$E_s = \frac{2M_m^2 M_e V_s^2}{(M_m + M_e)^2} \quad (3-4)$$

Referring again to equations (3-1) and (3-2), the velocity of the missile after impact is in the same direction as that of the target if  $M_m$  is greater than  $eM_e$ . In this case, the target spring decelerates the target mass, allowing the missile to overtake the target, which results in multiple impact.

If the impact is purely elastic ( $e = 1$ ), the target will eventually stop the missile through a series of impacts and absorb all the initial kinetic

\*References are in appendix F.

energy of the missile. The required strain energy of the responding target is then equal to the initial kinetic energy of the missile.

$$E_s = \frac{M V_s^2}{2} \quad (3-5)$$

### 3.3.2 PLASTIC IMPACT

For a plastic collision, the coefficient of restitution reduces to zero ( $e = 0$ ) and the missile and target masses attain the same velocity at the end of impact duration. If the impact is of short duration, the target displacement and corresponding spring force effect during impact are small, and can be conservatively neglected. The strain energy required to stop the target-missile combination is then the sum of the kinetic energy of the missile and the target masses at the end of the duration of impact.

$$E_s = \frac{M V_m^2}{2} + \frac{M_e V_T^2}{2} \quad (3-6)$$

From equations 3-1 and 3-2

$$V_m = V_T = \frac{M V_s}{M_m + M_e} \quad (3-7)$$

Substituting the value for  $V_m$  and  $V_T$  from equation (3-7) into equation (3-6), the required target strain energy is

$$E_s = \frac{M_m^2 V_s^2}{2 (M_m + M_e)} \quad (3-8)$$

### 3.3.3 FORCE TIME FUNCTION KNOWN

In some isolated cases, (such as for frontal impact of an automobile, see section 5.1), sufficient experimental data are available to enable definition of a force-time function,  $F(t)$ , at the interface between the missile and target. This enables direct solution of the equation of motion:

$$F(t) - R(x) = M_e \ddot{x} \quad (3-9)$$

$F(t)$  = Force-time function

$R(x)$  = Resisting spring force as a function of displacement,  $x$

$\ddot{x}$  = Acceleration of target mass

$M_e$  = Effective target mass

2 | Numerical methods are usually used for solution of equation 3-9 which is solved for the maximum value of displacement  $x_m$ . The target strain energy is then;

$$E_s = \int_0^{x_m} R(x) dx$$

An abbreviated conservative solution for required target strain energy can be obtained if  $R(x)$  during impact is small compared to  $F(t)$  and plastic or permanent deformation is dominant at the missile-target interface

The velocity of the target mass at time,  $t$ , is;

$$\dot{x}(t) = \int_0^t \ddot{x} dt = \int_0^t \frac{[F(t) - R(x)] dt}{M_e}$$

The kinetic energy of the target mass at time  $t$  is then

2 | 
$$E(t) = \frac{M_e [\dot{x}(t)]^2}{2}$$

or

$$E(t) = \frac{1}{2M_e} \left\{ \int_0^t [F(t) - R(x)] dt \right\}^2 \quad (3-10)$$

Equation (3-10) shows that deletion of the  $R(x)$  term will result in a conservative overestimate of  $E(t)$ . If  $R(x) \ll F(t)$  during impact,  $t$ , the inaccuracy is usually negligible. For this condition, the kinetic energy of the target mass at time  $t_1$  is conservatively estimated as;

$$E_{t_1} = \frac{\left[ \int_0^{t_1} F(t) dt \right]^2}{2M_e} \quad (3-11)$$

The applied impulse,  $I$ , is by definition, the area under the force-time curve.

$$I = \int_0^{t_1} F(t) dt$$

Making this substitution into equation (3-11);

$$E_{t_1} = \frac{I^2}{2M_e} = (1/2)M_e V_T^2 \quad (3-12)$$

If the elastic restoring forces at the missile-target interface are small, the velocity of the missile approaches that of the target at the end of time,  $t_1$ , equal to the duration of impact. The strain energy of the target required to stop the missile-target combination is then;

$$E_s = \frac{M_m V_m^2}{2} + \frac{I^2}{2M_e} \quad (3-13)$$

For a plastic collision,

$$V_m = V_T$$

From equation (3-12):

$$V_T^2 = \frac{I^2}{M_e^2}$$

and,

$$V_m^2 = \frac{I^2}{M_e^2}$$

Making this substitution into equation (3-13):

$$E_s = \frac{(M_m + M_e) I^2}{2M_e^2} \quad (3-14)$$

### 3.4 TARGET EFFECTIVE MASS

The effective target mass during impact varies from a low value at initial contact and generally increases to an upper limit during or at the end of the impact duration. Due to the complex phenomenology associated with missile impact, no general analytical solution is available to evaluate the effective coupled mass on a continuous time basis. The average effective mass can, however, be estimated, utilizing the results of impact tests on reinforced concrete beams<sup>(7)</sup> wherein the measured maximum structural response was used to back-calculate the average mass during impact.

Based on these data, the following formulae provide a lower limit estimate of  $M_e$  (which results in an upper limit estimate of kinetic energy after impact).

For concrete beams:

$$M_e = (D_x + 2T) \frac{B \gamma_c T}{g}, \quad \left[ \text{if } B \leq (D_y + 2T) \right]$$

$$M_e = (D_x + 2T)(D_y + 2T) \frac{\gamma_c T}{g}, \quad \left[ \text{if } B \geq (D_y + 2T) \right] \quad (3-15)$$

For concrete slabs:

$$M_e = (D_x + T)(D_y + T) \frac{\gamma_c T}{g} \quad (3-16)$$

For steel beams:

$$M_e = (D_x + 2d) M_x \quad (3-17)$$

For steel plates

$$M_e = D_x D_y \frac{\gamma_s t}{g} \quad (3-18)$$

$M_e$  = Average effective mass of target during impact

$M_x$  = Mass per unit length of steel beam

$D_x$  = Maximum missile contact dimension in the x direction (longitudinal axis for beams or slabs)

$D_y$  = Maximum missile contact dimension in the y direction (transverse to longitudinal axis for beams or slabs)

$T$  = Thickness or depth of concrete element

$t$  = Thickness of steel plate

$d$  = Depth of steel beam

$B$  = Width of concrete beam (not to exceed  $D_y + 2T$ )

$\gamma_c$  = Weight per unit volume of concrete

$\gamma_s$  = Weight per unit volume of steel

$g$  = Acceleration of gravity

### 3.5 STRUCTURAL RESPONSE BY ENERGY BALANCE METHOD

#### 3.5.1 GENERAL PROCEDURES

The strain energy,  $E_s$ , required to stop the target (or missile-target combination), is determined from the relationships in sections 3.2 and 3.3.

The resistance-displacement function,  $R(x)$ , for a concentrated load at the area of impact is determined from the target structure physical configuration and material properties.

The estimated maximum target response is determined by equating the available target strain energy to the required strain energy and solving for the maximum displacement  $x_m$ . (See Figure 3-1.)

#### 3.5.2 ELASTIC TARGET RESPONSE

For elastic response,

$$R(x) = kx$$

$k$  = Elastic spring constant

If no other loads are acting concurrently with the missile impact loading, the maximum response is

$$x_m = \left[ \frac{2 E_s}{k} \right]^{1/2} \quad (3-19)$$

If other loads are present on the target structure which will act concurrently with missile impact loads, the maximum combined displacement is determined as follows:

Then

$$x_m = x_o + x'$$

Since

$$x' = \left[ \frac{2 E_s}{k} \right]^{1/2}$$

Let

$x'$  = Displacement due to missile impact (See Figure 3-1)

$x_o$  = Displacement due to other loads

$x_m$  = Maximum combined displacement

2) it follows that

$$x_m = x_o + \left[ \frac{2 E_s}{k} \right]^{1/2} \quad (3-20)$$

### 3.5.3 ELASTO-PLASTIC TARGET RESPONSE

For elasto-plastic target response with no other concurrent loads acting:

$$R(x) = kx, \quad (0 < x \leq x_e)$$

$$R(x) = kx_e = R_m, \quad (x_e < x \leq x_m)$$

where

$$x_e = \text{Yield displacement}$$

$$R_m = \text{Plastic resistance.}$$

Then

$$E_s = R_m \left( x_m - \frac{x_e}{2} \right)$$

or

$$x_m = \frac{E_s}{R_m} + \frac{x_e}{2} \quad (3-21)$$

The required ductility ratio,  $\mu_r$ , is obtained from equation (3-21) by dividing both sides of the equation by  $x_e$ .

$$\mu_r = \frac{x_m}{x_e}$$

$$\mu_r = \frac{E_s}{x_e R_m} + \frac{1}{2} \quad (3-22)$$

If other loads are present on the target structure which will act concurrent with missile impact loads, the maximum combined displacement is determined as follows:

Let

$$x' = x_e - x_o \quad (\text{see figure 3-1})$$

$$x_o = \text{displacement due to other loads}$$

$x_e$  = yield displacement

$x_m$  = maximum combined displacement

$R_m$  = plastic resisting force

$k$  = elastic spring constant

Then

$$E_s = \frac{k(x')^2}{2} + kx'(x_m - x_e) \quad (\text{see figure 3-1})$$

or

$$x_m = \frac{E_s}{kx'} - \frac{x'}{2} + x_e$$

Substituting  $x' = x_e - x_o$  in the above equation gives

$$x_m = \frac{E_s}{k(x_e - x_o)} + \frac{x_e + x_o}{2} \quad (3-23)$$

The required ductility ratio,  $\mu_r$ , is obtained by dividing both sides of equation (3-23) by  $x_e$ .

$$\mu_r = \frac{E_s}{R_m(x_e - x_o)} + \frac{1 + x_o/x_e}{2} \quad (3-24)$$

The values of  $\mu_r$  should be less than the allowable ductility ratios  $\mu$  given in section 4.

#### 3.5.4 NON-LINEAR TARGET RESPONSES

If the resistance-displacement function is nonlinear (figure 3-1) the determination of structural response is facilitated by first defining the strain energy-displacement function, (see figure 3-2).

$$E_e = \int_0^x R(x) dx \quad (3-25)$$

$E_e$  = strain energy at displacement  $x$

$E_e$  = strain energy at displacement  $x$

When no other concurrent loads are acting, the maximum displacement occurs at the value of  $x$  where  $E_e$  is equal to  $E_s$ . The correct value of  $x_m$  is therefore the value of  $x$ , which will satisfy the following relationship:

$$E_s = \int_0^{x_m} R(x) dx \quad (3-26)$$

A typical graphical solution is shown in figure 3-2.

When other loads are acting concurrent with missile impact loading, the correct value of  $x_m$  will satisfy the following relationship:

$$E_s = \int_{x_0}^{x_m} R(x) dx - R_0(x_m - x_0) \quad (3-27)$$

$R_0$  = equivalent static resistance required for other loads  
(see figure 3-1)

$x_0$  = displacement associated with  $R_0$ .

A typical graphical solution for  $x_m$  is shown schematically in figure 3-3.

To provide an adequate margin of safety the values of  $E_s$  should satisfy the condition

$$E_s \leq F_s E_f \quad (3-28)$$

$E_f$  = impact strain energy capacity

$F_s$  = safety factor

$F_s = 0.5$  if  $R(x)$  is well defined from tests

$F_s = 0.25$  if  $R(x)$  is approximately determined (such as by failure analysis)

For impact only:

$$E_f = \int_0^{x_f} R(x) dx \quad (3-29)$$

$x_f$  = displacement at failure

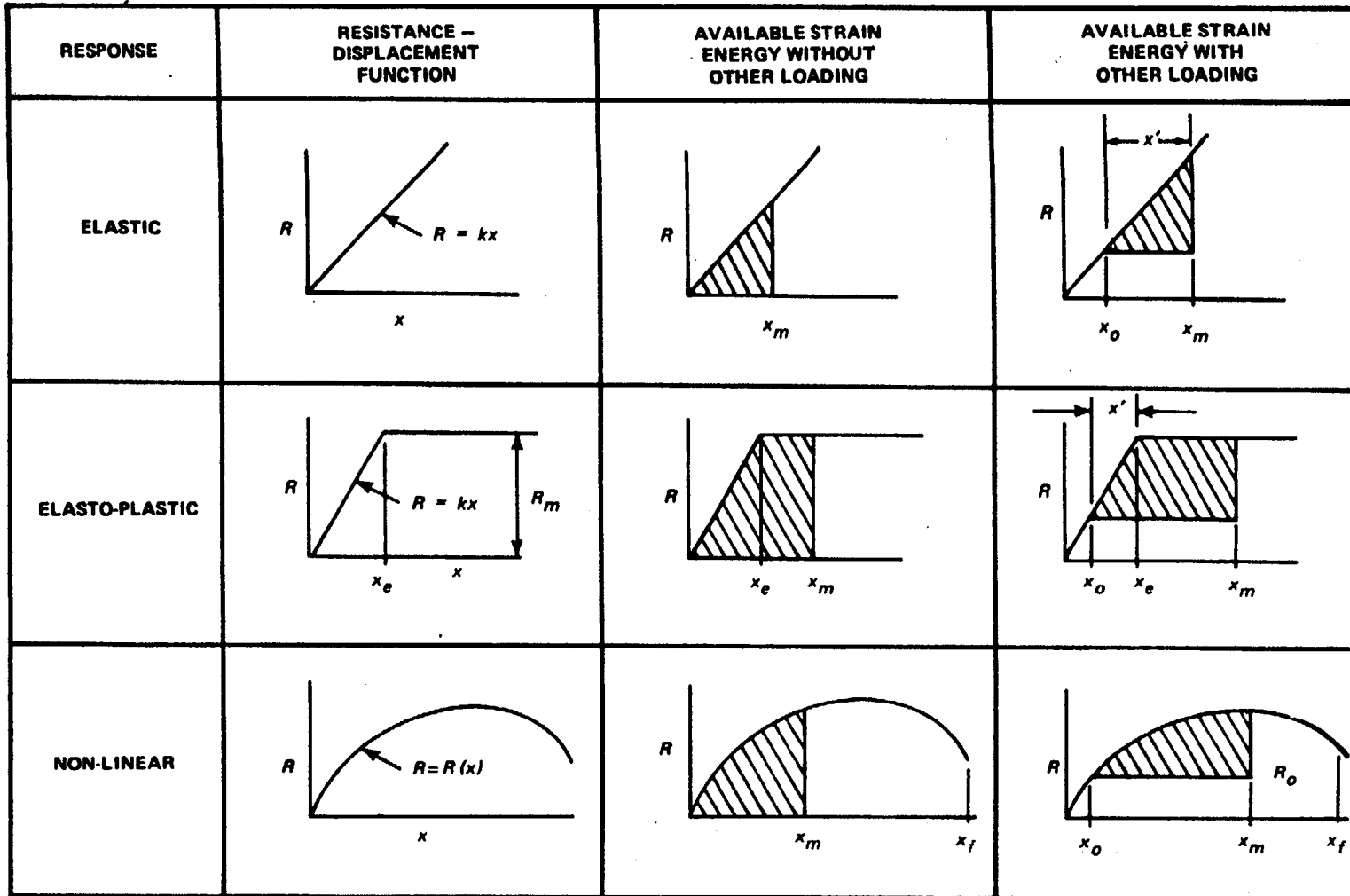
For impact combined with other loads:

$$E_f = \int_{x_0}^{x_f} R(x) dx - R_0 (x_f - x_0) \quad (3-30)$$

and

$$R_0 < R_f$$

$R_f$  = resistance at failure



SHADED AREA (STRAIN ENERGY) MUST EQUAL  $E_s$  (FROM SECTIONS 3.2 AND 3.3)

Figure 3-1

RESISTANCE-DISPLACEMENT FUNCTIONS WITH ASSOCIATED STRUCTURAL RESPONSE WITH AND WITHOUT THE EFFECT OF OTHER LOADS

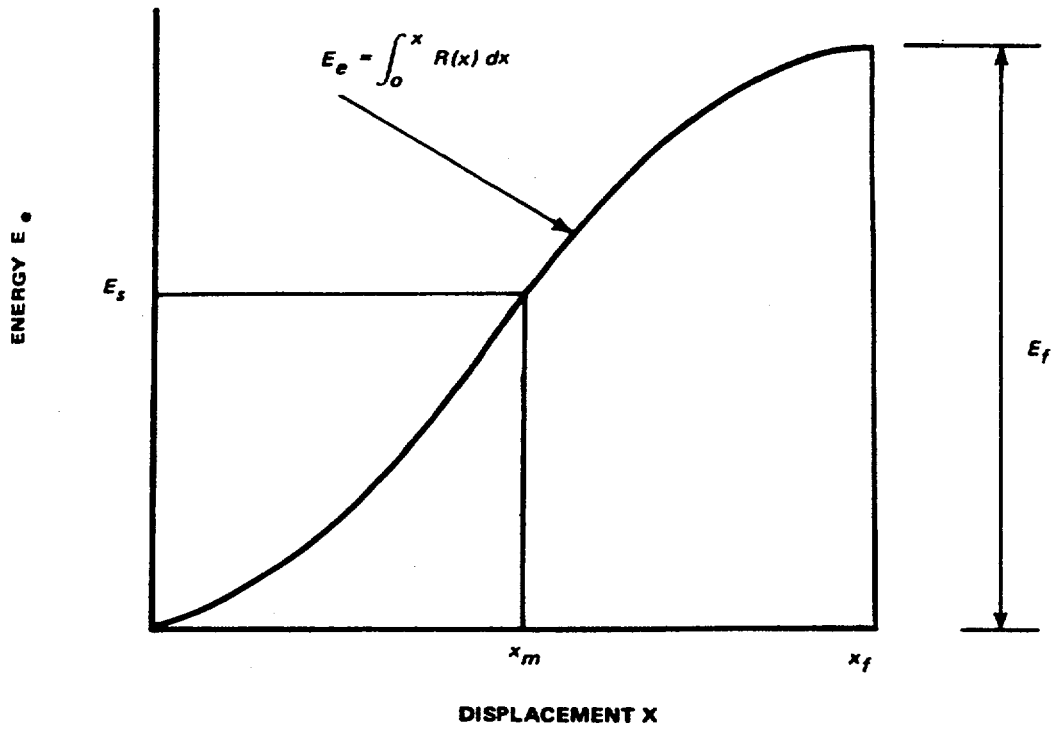


Figure 3-2  
ENERGY-DISPLACEMENT FUNCTIONS-  
IMPACT LOADS ONLY

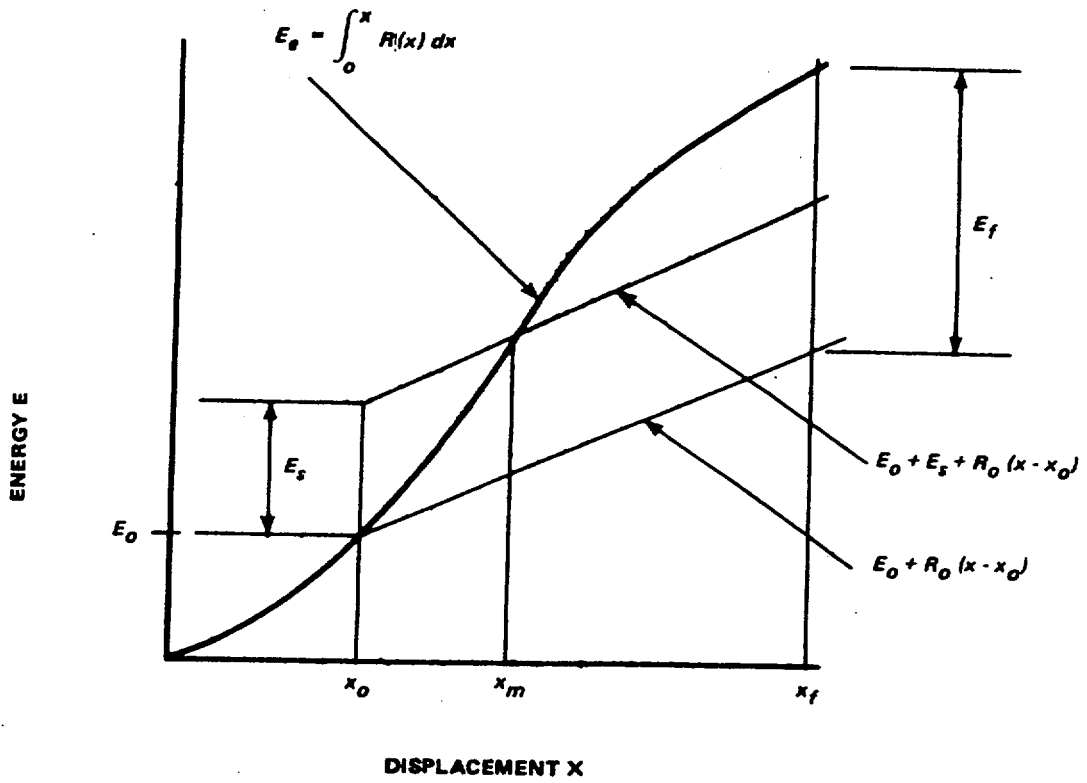


Figure 3-3

ENERGY-DISPLACEMENT FUNCTIONS -  
IMPACT COMBINED WITH OTHER LOADS

Section 4

DESIGN GUIDELINES

4.1 ALLOWABLE STRESSES AND LOADINGS

The combination of loadings, allowable stress and strain limits, and applicable codes used with the missile impact loading are given in the Safety Analysis Report. The resistance of a structural component must be based on its minimum strength, i.e., the minimum of its flexural or shearing capacity. The dynamic capacity of the structural elements must be based on material dynamic strength properties which are obtained by applying a dynamic increase factor (DIF) to the static strength value:

$$f_{\text{dyn}} = (\text{DIF}) f_{\text{stat}} \quad (4-1)$$

where

$f_{\text{dyn}}$  = allowable dynamic strength value

$f_{\text{stat}}$  = specified static strength value

DIF = dynamic increase factor

The dynamic increase factor for various materials are given in table 4-1.

4.2 DESIGN PARAMETERS

The resistance of typical structural elements, whose flexural strength defines the minimum capacity, and their yield displacement approximations are presented in tables 4-2 and 4-3. Similar equations can be developed for the load at other location on the structural element. It is preferable that the limiting capacity of an element be in the flexural mode not in shear. In evaluating the yield displacement with the usual elastic analysis, the moment of inertia must account for cracking of concrete sections. The empirical relation for this type of loading is an average moment of inertia  $I_a$  calculated as follows is:

$$I_a = \frac{1}{2} (I_g + I_c) = \frac{1}{2} \left( \frac{bt^3}{12} + Fbd^3 \right) \quad (4-2)$$

where

$I_g$  = moment of inertia of gross concrete cross section of thickness  $t$  about its centroid (neglecting steel areas)

$I_c$  = moment of inertia of the cracked concrete section

b = width of concrete section

F = coefficient for moment of inertia of cracked section with tension reinforcing only. (See figure 4-1.)

t = concrete thickness

d = distance from extreme compression fiber to centroid of tension reinforcing

The moment of inertia  $I_a$ , as calculated by equation (4-2), must be used in the displacement equation in tables 4-2 and 4-3 for all reinforced concrete members. The ultimate moment capacity of a concrete section shall be considered as the moment strength

$$M_u = 0.9 A_s f_{dy} (d - a/2) \quad (4-3)$$

where

$A_s$  = area of tensile reinforcing steel

$f_{dy}$  = allowable dynamic yield stress for reinforcing steel

d = distance from extreme compression fiber to centroid of tension reinforcing

a = depth of equivalent rectangular stress block

If the element has compression steel, it should be considered and the appropriate equation used.

The amount of reinforcing steel in a concrete members must satisfy the following criteria:

For members with tension steel only:

$$\frac{1.4 \sqrt{f'_c}}{f_y} \left(\frac{t}{d}\right)^2 \leq \frac{A_s}{bd} \leq \frac{0.25 f'_c}{f_y} \quad (4-4)$$

For members with tension and compression steel:

$$\frac{1.4 \sqrt{f'_c}}{f_y} \left(\frac{t}{d}\right)^2 \leq \frac{A_s}{bd} \quad (4-4a)$$

$$\frac{A_s - A'_s}{bd} \left(\frac{t}{d}\right)^2 \leq \frac{0.25 f'_c}{f_y}$$

where

$f'_c$  = compression strength of concrete

$A'_s$  = area of compressive reinforcement of concrete

#### 4.3 ALLOWABLE DUCTILITY RATIO

The maximum allowable ductility ratios for concrete and steel members are presented in Table 4-4. However, the maximum deflection shall be limited so as not to impair the function of other safety related equipment.

2

Table 4-1  
DYNAMIC INCREASE FACTOR  
(DIF)  
(From Ref. 19)

I. <u>Reinforced or Prestressed Concrete</u>	
<u>Concrete</u>	DIF
Compression	1.25
Diagonal Tension & Direct Shear (Punch Out)	1.0
Bond	1.0
<u>Reinforcing Steel</u>	
2   Tension & Compression For 40ksi yield strength steel	1.2
	60ksi yield strength steel
Diagonal Tension & Direct Shear (Stirrups)	1.0
II. Structural Steel	
2   Flexure, Tension, & Compression for 40ksi yield strength steel	1.2
	60ksi yield strength steel
Shear	1.0

Table 4-2  
RESISTANCE-YIELD DISPLACEMENT  
VALUES FOR BEAMS

DESCRIPTION	RESISTANCE	YIELD DISPLACEMENT
(1) CANTILEVER	$R = \frac{M_u}{L}$	$X_e = \frac{RL^3}{3EI}$   2
(2) SIMPLY SUPPORTED	$R = \frac{4M_u}{L}$	$X_e = \frac{RL^3}{48EI}$   2
(3) FIXED SUPPORTS	$R = \frac{4(M_u^+ + M_u^-)}{L}$	$X_e = \frac{RL^3}{192EI}$   2
(4) MULTI-SPAN	$R = \frac{4(M_u^+ + M_u^-)}{L}$	$X_e = \frac{0.011RL^3}{EI}$   2

Where  $M_u^+$  = ULTIMATE POSITIVE MOMENT CAPACITY  
 $M_u^-$  = ULTIMATE NEGATIVE MOMENT CAPACITY  
 $I$  = MOMENT OF INERTIA (in<sup>4</sup>)  
 FOR REINFORCED CONCRETE  $I = I_a$ ,  
 SEE EQUATION 4-2.



Table 4-4

DUCTILITY RATIOS  
(From Reference 28)

Max. Allowable Value of  $\mu$

2

Reinforced Concrete

Flexure

Beams

$$\frac{0.10}{p-p'} \leq 10$$

Slabs

$$\frac{0.10}{p-p'} \leq 30$$

Compression

Walls & Columns

1.3

where

$p$  is the ratio of tensile reinforcement

$$= \frac{A_s}{bd}$$

$p'$  is the ratio of compressive reinforcement

$$= \frac{A'_s}{bd'}$$

Steel Elements

Members proportioned to preclude lateral and local buckling

Flexure, compression and shear

20

Steel Columns

Proportioned to preclude elastic buckling

1.3

Members stressed in tension only

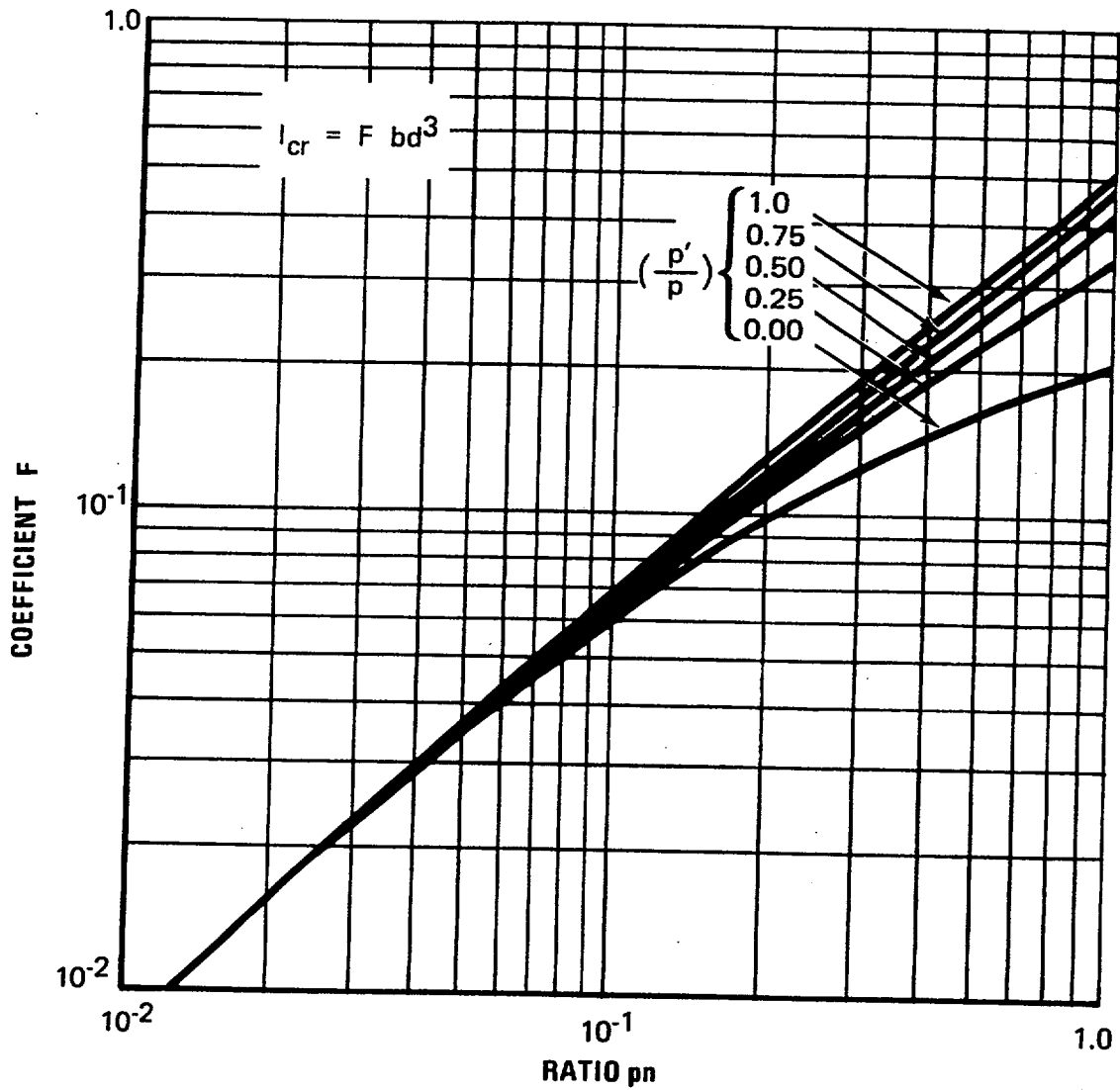
$$0.5 \frac{e_u}{e_y}$$

$e_u$  = ultimate strain

$e_y$  = yield strain

2

2



$$p = \frac{A_s}{bd}, \quad p' = \frac{A'_s}{bd}, \quad n = \frac{E_s}{E_c}$$

$$F = \frac{K^3}{3} + pn(1-K)^2 + \left(\frac{2n-1}{n}\right) (pn) \frac{p'}{p} \left(K - \frac{d'}{d}\right)^2$$

$$\frac{2n-1}{n} \cong 1.9, \quad \frac{d'}{d} \cong 0.10, \quad K = -m + (m^2 + 2q)^{1/2}$$

$$m = pn \left(1 + 1.9 \frac{p'}{p}\right), \quad q = pn \left(1 + 0.19 \frac{p'}{p}\right)$$

Figure 4-1  
COEFFICIENTS FOR MOMENT OF INERTIA  
OF CRACKED SECTIONS

SECTION 5

SPECIAL PROBLEMS

Two special problems are the determination of an empirical formula for force-time history of automobile crash, and the evaluation of a missile's velocity as it passes through a liquid.

5.1 FORCE-TIME HISTORY FOR AUTOMOBILE CRASH

In deriving the force-time history of an automobile crash under frontal impact, the automobile is considered as a deformable missile and the structure as a rigid target. According to Appendix D, Paragraph D.1, which is based on a theoretical consideration and considerable experimental data, the force-time history under such a condition is approximately as follows:

$$F(t) = 0.625 V_s W_m \sin 20t, \quad (0 \leq t \leq 0.0785 \text{ sec}) \quad (5-1)$$

$$F(t) = 0 \quad (t > 0.0785 \text{ sec})$$

where

$t$  = time from the instant of initial contact (sec)

$F(t)$  = time-dependent force on target (lb)

$V_s$  = striking velocity of the automobile (ft/sec)

$W_m$  = weight of automobile (lb)

References on derivations of more elaborate force-time histories for automobile crashes are given in reference 11.

5.2 PENETRATION OF A MISSILE THROUGH A LIQUID

To evaluate the effect of a missile on a target that is submerged in a liquid, determine the striking velocity of the missile,  $V$ , after it has penetrated through a depth,  $H$ , of liquid covering the target (figure 5-1). This involves evaluating the velocity change due to missile weight, the buoyant force, and the drag force.

The penetration of a missile as it enters a liquid depends on the geometric shape of the missile. For the vertical entry of a missile with uniform horizontal cross-sectional area  $A_0$ , and length  $L$ , the depth of penetration and the velocity at a depth,  $x$ , are in terms of two functions of  $x$ . (The functions are evaluated at  $x = H$  or  $L$ .)

$$Z_1(x) = g/a + bA_0(1-2ax)/2a^2 + e^{-2ax}(v_0^2 - g/a - bA_0/2a^2), \quad (0 \leq x \leq L) \quad (5-1)$$

$$Z_2(x) = v_2^2 + e^{-2ax} \left\{ bA_0 \left[ e^{2aL}(1-2aL) - 1 \right] / 2a^2 + v_0^2 + g(e^{2aL} \gamma/\gamma_m - 1)/a \right\},$$

(x ≥ L) (5-2)

Notations used above are defined at the end of this section. Missile penetration in a liquid can be categorized by the following cases:

5.2.1 LIQUID DEPTH IS LESS THAN OR EQUAL TO MISSILE LENGTH ( $H \leq L$ )

5.2.1.1 If  $Z_1(x)$  is Negative or Zero at Depth  $x = H$  ( $Z_1(H) \leq 0$ )

The missile will not strike the target. It will penetrate a depth  $H_1 \leq H$  such that  $Z_1(H_1) = 0$ , and then float to the liquid surface.

5.2.1.2 If  $Z_1(x)$  is Positive at Depth  $x = H$  ( $Z_1(H) > 0$ )

The striking velocity at depth H is

$$v = [Z_1(H)]^{1/2} \quad (5-3)$$

5.2.2 LIQUID DEPTH IS GREATER THAN MISSILE LENGTH ( $H > L$ )

5.2.2.1 If  $Z_2(x)$  is Negative or Zero at Depth  $x = L$  ( $Z_2(L) \leq 0$ )

The missile will not strike the target. It will penetrate a depth  $H_1 \leq L$  such that  $Z_2(H_1) = 0$ , and then float to the liquid surface.

5.2.2.2 If  $Z_2(x)$  is Positive at Depth  $x = L$  ( $Z_2(L) > 0$ )

The missile will penetrate the liquid deeper than L. There are two possibilities:

A. If  $Z_2(x)$  is Negative or Zero at Depth  $x = H$  ( $Z_2(H) \leq 0$ )

The missile will not strike the target. It will penetrate a depth  $H_2$  ( $L < H_2 \leq H$ ) such that  $Z_2(H_2) = 0$ , and then float to the liquid surface.

B. If  $Z_2(x)$  is Positive at Depth  $x = H$  ( $Z_2(H) > 0$ )

The striking velocity at depth H is

$$v = [Z_2(H)]^{1/2} \quad (5-4)$$

In case the missile shape does not have a uniform cross-sectional area, refer to equations (D-23) and (D-36) in Appendix D.2 for more general solutions.

### 5.2.3 DEFINITIONS OF NOTATIONS

$$a = \gamma A_0 C_D / 2W \quad (5-5)$$

$$b = \gamma g / W \quad (5-6)$$

$g$  = gravitational acceleration  
( $g = 32.17 \text{ ft/sec}^2$  at sea level)

$W$  = weight of missile

$\gamma$  = weight density of liquid  
( $\gamma = 62.4 \text{ lb/ft}^3$  for water at  $80^\circ\text{F}$ )

$\gamma_m$  = weight density of the missile

$x$  = depth of missile c.g. below the initial c.g. as shown in figure 5-1.

$A_0$  = horizontal cross-sectional area of the missile (constant over Length  $L$ )

$C_D$  = drag coefficient (given in table 5-1 or other references on fluid mechanics) which is a function of  $L/d$ ,  $R$  and shape of the missile.

$L$  = vertical length of the missile

$d$  = characteristic dimension of the missile as shown in table 5-1.

$$R = \text{Reynolds number} = \frac{V_0 d}{\nu} \quad (5-7)$$

$\nu$  = kinematic viscosity of the liquid  
( $\nu = 0.95 \times 10^{-5} \text{ ft}^2/\text{sec}$  for water at  $80^\circ\text{F}$ )

$V_0$  = initial velocity of the missile at  $x = 0$  (See figure 5-1)

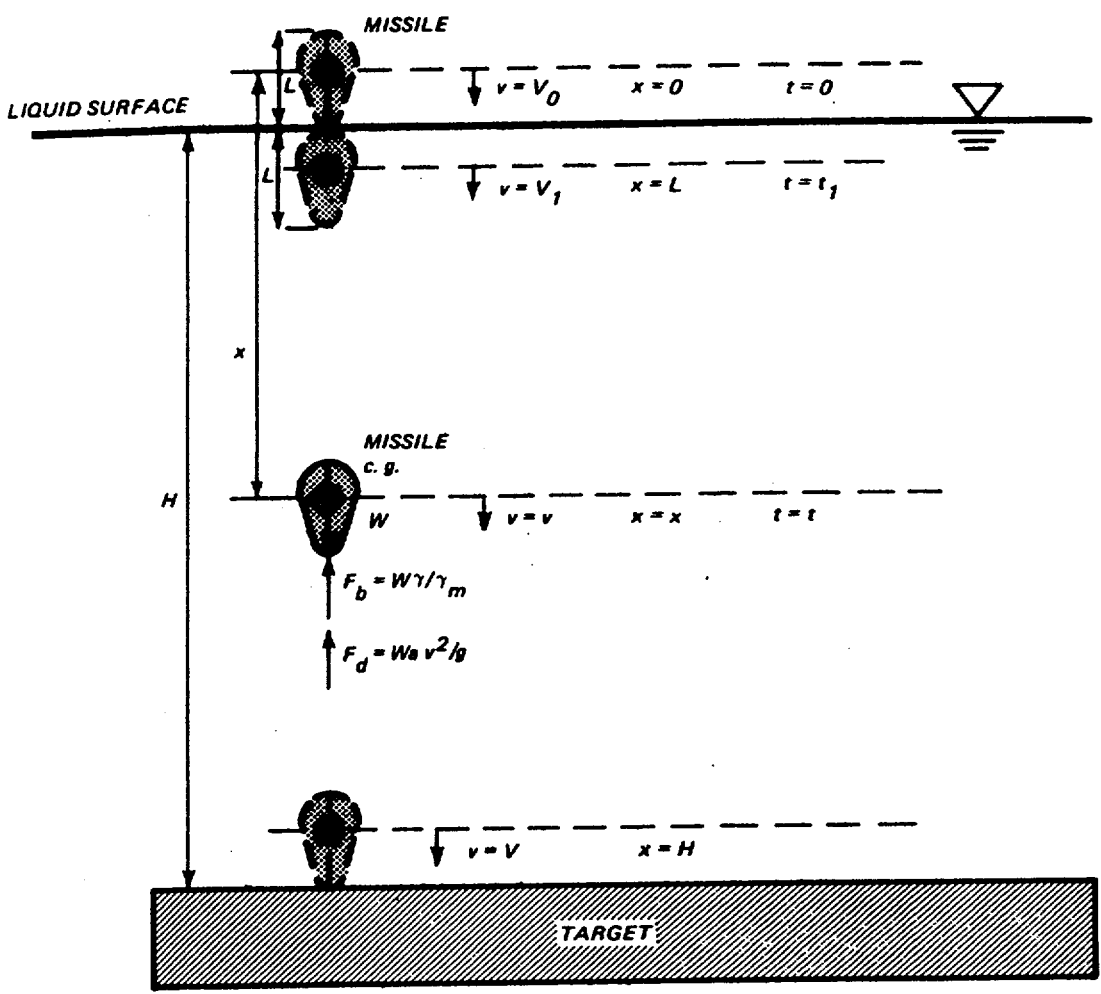
$V$  = striking velocity of the missile at  $x = H$  (See figure 5-1)

$$V_2 = \text{terminal velocity} = \left[ g(1 - \gamma/\gamma_m)/a \right]^{1/2} \quad (5-8)$$

Table 5-1

DRAG COEFFICIENT FOR VARIOUSLY SHAPED BODIES IN INCOMPRESSIBLE FLOW<sup>(25)</sup>

Form of Body	L/d	R	C <sub>D</sub>
Circular disk		$>10^3$	1.12
Tandem disks, L = spacing d = diameter	0 1 2 3	$>10^3$	1.12 0.93 1.04 1.54
Rectangular plate, L = length d = width	1 5 20 $\infty$	$>10^3$	1.16 1.20 1.50 1.95
Circular cylinder (axis    to flow) L = length d = diameter	0 1 2 4 7	$>10^3$	1.12 0.91 0.85 0.87 0.99
Circular cylinder (axis $\perp$ to flow) L = length d = diameter	1 5 20 $\infty$	$10^5$	0.63 0.74 0.90 1.20
	5 $\infty$	$>5 \times 10^5$	0.35 0.33
Streamlined foil (1 : 3 airplane strut) L = span d = chord	$\infty$	$>4 \times 10^4$	0.07
Hemisphere: Hollow upstream Hollow downstream		$>10^3$	1.33 0.34
Sphere		$10^5$	0.5
		$>3 \times 10^5$	0.20
Ellipsoid (1 : 2, major axis    to flow)		$>2 \times 10^5$	0.07
Airship hull (model)		$>2 \times 10^5$	0.05



NOTE: SEE APPENDIX D, PARAGRAPH D.2 FOR AN ANALYSIS OF THIS CASE.

Figure 5-1  
PENETRATION OF A MISSILE IN A LIQUID

APPENDIX A

CROSS REFERENCE LISTING TO AEC STANDARD SAR FORMAT

This appendix shows the cross reference between sections of AEC's Standard SAR format and the sections of this topical report.

AEC SAR Format

3.5.4

BC-TOP-9

2.0, 3.0, 4.0

APPENDIX B

GLOSSARY

B.1 PENETRATION

Penetration is the displacement of the missile into the target. It is a measure of the depth of the crater formed at the zone of impact.

B.2 PERFORATION

Perforation is "full Penetration" or where the missile passes through the target with or without exit velocity (of missile).

B.3 SPALLING OF CONCRETE

Spalling is the peeling off of the back face of the target opposite to the face of impact.

B.4 DUCTILITY RATIO

The ductility ratio is the ratio of the maximum deflection to the deflection at the "effective yield point."

B.5 EFFECTIVE YIELD POINT

That point on an idealized bilinear resistance function separating the elastic and perfectly plastic portion of the function. The effective yield point is based on the strength of the structure by ultimate (or plastic) design methods.

B.6 ELASTIC IMPACT

An elastic collision is characterized by elastic deformations at the missile-target interface.

B.7 PLASTIC IMPACT

A plastic collision is characterized by inelastic deformation and local damage of the missile and/or target in the impact zone. For a purely plastic collision, elastic restoring forces at the missile-target interface and associated elastic rebound energy release converge to zero.

## APPENDIX C

### REVIEW OF EXISTING FORMULAS

#### C.1 PENETRATION AND PERFORATION

The most common formulas used in determining the local effects of a missile on a target, such as penetration, perforation, and spalling for missiles striking either a concrete or steel target, are given in tables C-1 and C-2. These tables include equations C-1 through C-11. These are the current state-of-the-art formulas on impact analysis, which consists primarily of empirical methods based on experiments conducted for specific and limited applications. Generally, the experiments were conducted for the Government using missiles, such as bombs and bullets, and having velocities above 1000 ft/sec. Current impact analysis assumes that the missile impinges the target normal to the surface. The effects of the oblique angle of striking at various velocities are illustrated in figure C-1. It can be seen that assuming normal striking of the target is conservative, since a small deviation from a normal impact decreases the depth of penetration considerably.

The Army Corps of Engineers and National Defense Research Committee equations (table C-1) for penetration, perforation, and spalling have a term, which depends only on the diameter of the missile. However, this term provides overly conservative results when a low velocity and large diameter missile is considered. For example: as  $V_s \rightarrow 0$  the penetration approaches  $0.5D$ ; perforation approaches  $(1.8)D$ ; and spalling approaches  $(2.8)D$ , which is not realistic.

Experimental data with velocities below 500 ft/sec are just beginning to develop, with the emphasis on the effect of impact on the target. Some experiments have been completed with missile velocities in the range of interest. However, the tests were not necessarily conducted for target information. (21) Therefore, available pertinent data are limited.

The modified Petry formula has had the widest application for determining the penetration of a missile into concrete targets and is adopted for use at the present time. It was developed by the Poncelet theory, provides estimate of penetration, and has functioned best in the velocity range of interest. Also, conservatism is built into this approach because of the following:

- A. The angle of striking the target has a large effect if the angle is greater than  $20^\circ$ . A normal angle of strike is assumed.

- B. The probability of a missile being oriented in a manner that would produce the greatest penetration is remote. In addition, any rotational effect tends to increase the area of impact.
- C. Conservative estimates for weight, velocity, area of impact, and target strength provide conservatism.

Even though the modified Petry formula was developed in 1910, the material coefficient for penetration,  $K_p$ , has been revised by experiments and is reported by Amirikian (14) and shown in figure 2-1.

The BRL formula for perforation of concrete targets is used. It is selected instead of the modified Petry formula of  $T = 2X$  because the BRL formula was developed for perforation and not as an approximation from a penetration.

The BRL equation, given in equation (2-3), has been modified to account for concrete strength other than 3000 psi by replacing the constant coefficient 7.8 by  $427/\sqrt{f'_c}$  in equation (C-7). (3)

Two steel perforation formulas are available, the Ballistic Research Laboratories (BRL) formula (2) (3) and the Stanford Research Institute formula, known as the Stanford Equation. (20) The Stanford Equation is based on experimental data, using missile velocities within the range of interest. However, its limits of applicability are very restrictive because most missiles encountered fall outside the range of the Stanford Equation.

The Ballistic Research formula, table C-2, is used with an assigned value of  $K$  equal to unity. Rearranging terms and solving directly for  $T$  leads to the formula for calculating the threshold of perforation.

$$T = \frac{\left(\frac{MV^2}{2}\right)^{2/3}}{672D} \quad (C-12)$$

The Stanford Equation (table C-2) has the following defined limits of applicability:

$$0.1 < T/D < 0.8,$$

$$0.002 < T/L < 0.05,$$

$$10 < L/D < 50,$$

$$5 < W/D < 8,$$

$$8 < W/T < 100,$$

$$70 < V_s < 400,$$

L = length of cylindrical missile

$V_s$  = striking missile velocity normal to the target surface for the threshold of perforation (ft/sec)

Solving equation (C-11) directly for plate thickness gives,

$$T = \sqrt{0.045 \frac{W_m V_s^2}{DS} + 0.0022 \left(\frac{W}{W_s}\right)^2} - 0.047 \frac{W}{W_s} \quad (C-13) \quad | \quad 2$$

where,

$$E = \frac{W_m V_s^2}{2g}$$

$W_m$  = weight of missiles (pounds)

A parametric study comparing the BRL formula and the Stanford Equation, within the limits of applicability of the Stanford Equation, showed the BRL and SRI formula are generally in good agreement for the shorter spans. But, for longer spans the SRI formula is less conservative. Considering this and the narrow band of limits for the SRI equation the BRL equation is used for design. | 2

## C.2 MULTIPLE ELEMENT BARRIER EQUATION

Equation (2-9) assumed the residual kinetic energy of the missile after perforation ( $E_r$ ) is the difference between the kinetic energy of the missile before impact ( $E_k$ ) and the energy required to perforate the steel ( $E_p$ )

$$E_r = E_k - E_p = \frac{MV_r^2}{2} = \frac{MV_s^2}{2} - \frac{MP}{2} \quad (C-14)$$

where

M = mass of the missile  $\left(\frac{\text{lb-sec}^2}{\text{ft}}\right)$

Solving for  $V_r$

$$V_r = \left( V_s^2 - V_p^2 \right)^{1/2}$$

This equation<sup>(27)</sup> neglects the mass of the plug which may be punched out of the target, which would be very small for a steel target; for a concrete target, the concrete would fracture and not act in conjunction with the missile mass.

$V_p$  can be obtained from equations (2-3) and (2-7) by solving for  $V_s$ , which will be the velocity to just perforate,  $V_p$ , when a given thickness of target,  $t$ , is used.

Table C-1

## CONCRETE PENETRATION, PERFORATION, AND SPALLING FORMULAS (Sheet 1 of 3)

Identification	Formula	Remarks	Equation No.
<b>A. Penetration into Reinforced Concrete</b>			
Modified Petry (Refs. 13, 14, 15)	$X = 12K \frac{A}{p p} \log_{10} \left( 1 + \frac{v_s^2}{215,000} \right)$	For infinitely thick slab	C-1
	$X_1 = \left[ 1 + e^{-4 \left( \frac{t}{X} - 2 \right)} \right] X$	Depth of penetration for slabs with Finite thickness. $X_1 \rightarrow X$ when $t \rightarrow 3X$	
Army Corps of Engineers and National Defense Research Committee (Refs. 13, 16, 17)	$X = \frac{282}{\sqrt{f'_c}} \frac{W D^{0.215}}{D^2} \left( \frac{v_s}{1000} \right)^{1.5} + 0.5D$		C-2
Ammann & Whitney (Refs. 18, 19).	$X = \frac{282 N W D^{0.2}}{\sqrt{f'_c} D^2} \left( \frac{v_s}{1000} \right)^{1.8}$		C-3
<b>B. Concrete Thickness to be Just Perforated</b>			
Modified Petry (Refs. 13, 14, 15)	$T = 2X$	X is obtained from Equation (C-1)	C-4

C-5

2

BC-TOP-9-A  
Rev. 2

Table C-1

CONCRETE PENETRATION, PERFORATION, AND SPALLING FORMULAS (Sheet 2 of 3)

Identification	Formula	Remarks	Equation No.
<b>B. Concrete Thickness to be Just Perforated (Con't)</b>			
Army Corps of Engineers (Refs. 13, 16)	$T = 1.35D + 1.24X$	X is obtained from Equation (C-2)	C-5
National Defense Research Committee (Refs. 13, 17)	$T = 1.23D + 1.07X$	X is obtained from Equation (C-2)	C-6
Ballistic Research Laboratories (Modified) (Ref. 13)	$T = 7.8 \frac{W}{D} \left( \frac{V_s}{1000} \right)^{1.33}$	For $f'_c = 3000$ psi	C-7
	$T = \frac{427}{\sqrt{f'_c}} \frac{W}{D} \left( \frac{V_s}{1000} \right)^{1.33}$	For any value $f'_c$ Ref. 3	
<b>C. Concrete Thickness to be Just Spalled</b>			
2   Army Corps of Engineers (Refs. 13, 16)	$T_s = 2.2D + 1.35X$	X is obtained from Equation (C-2)	C-8
2   National Defense Research Committee (Refs. 13, 17)	$T_s = 2.28D + 1.13X$	X is obtained from Equation (C-2)	C-9

C-6

Table C-1

CONCRETE PENETRATION, PERFORATION, AND SPALLING FORMULAS (Sheet 3 of 3)

W = Weight of Missile (lb.)

$V_s$  = Striking Velocity of Missile (ft/sec.)

D = Diameter of Missile (in.)

$A_p$  =  $\frac{\text{Missile Weight}}{\text{Projected Frontal Area of Missile}}$  (psf)

X = Depth of Penetration into Slab of Infinite Thick Concrete (in.)

$X_1$  = Depth of Penetration into a Finite Thickness Slab of Concrete (in.)

t = Thickness of the Slab (in.)

$f'_c$  = Compressive Strength of Concrete (psi)

$K_p$  = Experimentally Obtained Material Coefficient for Penetration (See Figure 2-1)

N = Nose Factor =  $0.72 + 0.25 (n - 0.25)^{1/2}$

n =  $\frac{\text{radius of nose section}}{\text{diameter of missile}}$

T = Thickness To Be Just Perforated (in.)

$T_s$  = Thickness To Be Just Spalled (in.)

NOTE: Some of the equations have been rewritten to reflect consistent units and terminology.

C-7

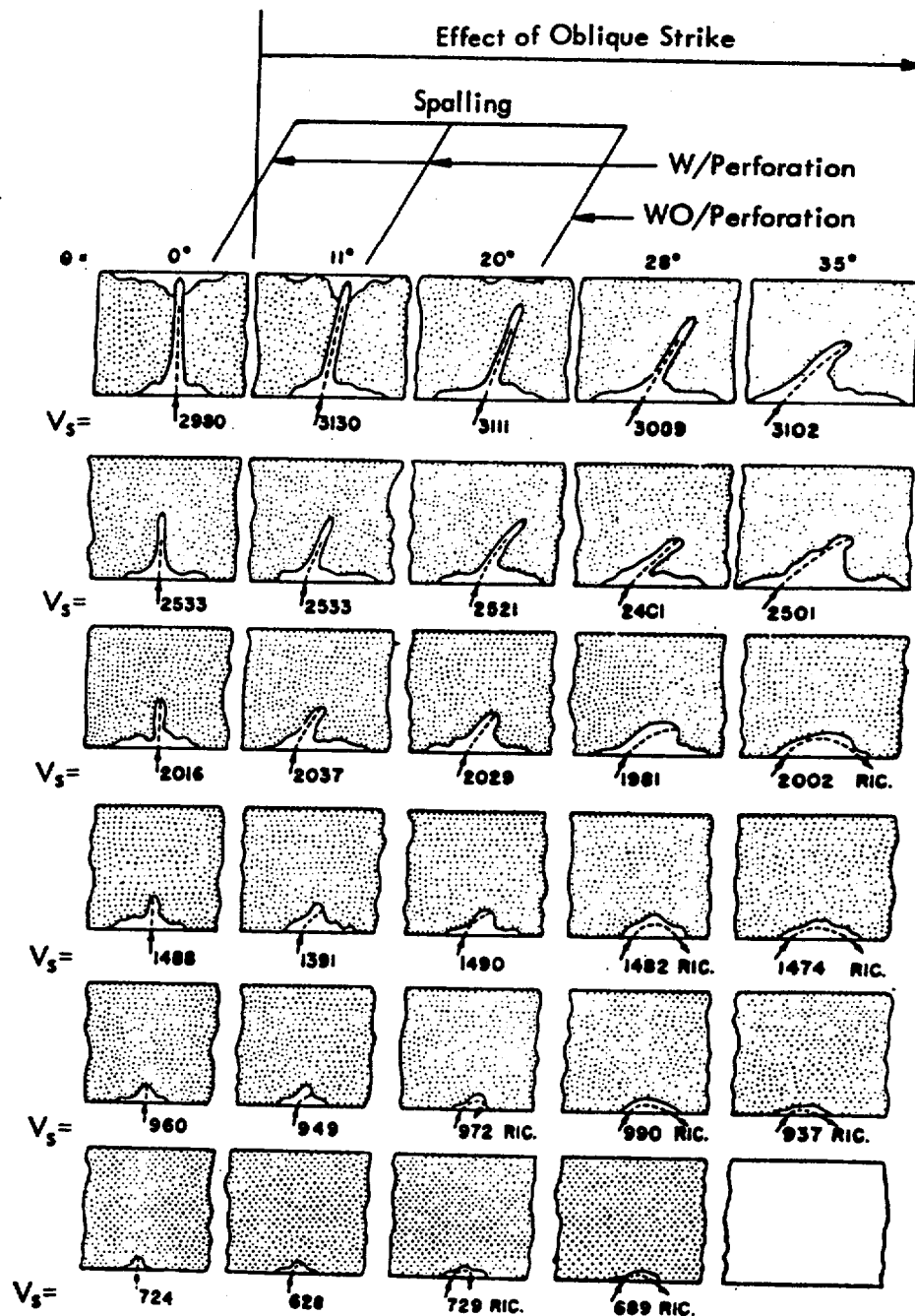
Table C-2

## PERFORATION IN STEEL FORMULAS

BC-TOP-9-A  
Rev. 2

Identification	Formula	Remarks	Equation No.
Ballistic Research Lab (Refs. 2, 3, 13)	$T^{3/2} = \frac{0.5 M V_s^2}{17,400 K^2 D^{3/2}}$		C-10
Stanford Research Institute (Ref. 20)	$\frac{E}{D} = \frac{S}{46,500} \left( 16,000 T^2 + 1,500 \frac{W}{W_s} T \right)$	See Limits page C-3	C-11

- T = steel thickness to be just perforated (in.)
- M = mass of the missile (lb-sec<sup>2</sup>/ft),
- V<sub>s</sub> = striking velocity of the missile normal to target surface (ft/sec),
- K = constant depending on the grade of the steel, (K is usually = 1,)
- D = diameter of the missile (in.)
- E = critical kinetic energy required for perforation (ft-lb),
- S = ultimate tensile strength of the target minus the tensile stress in the steel (psi)
- W = length of a square side between rigid supports (in.),
- W<sub>s</sub> = length of a standard width (4 in.). (See Ref. 20)



37 MM. M80 Projectile  
 Concrete Thickness = 22". Compressive strength = 5700 lbs/in.<sup>2</sup>  
 Striking velocity ( $V_s$ ) and angle of obliquity ( $\theta$ ) shown.  
 Stuck projectiles and path of ricochet projectiles shown.

Figure C-1

TYPICAL CRATER PROFILES

APPENDIX D  
DERIVATIONS

D.1 DERIVATION OF FORCE-TIME HISTORY FOR AUTOMOBILE CRASH, EQUATION (5-1)

An approximate relationship has been observed in experiments on automobile crashes. (22) The deceleration per unit deformation associated with the crushing force was observed to be approximately the same for a wide variety of standard-size U.S. automobile makes and models. The deceleration during a frontal impact is as follows:

$$-\ddot{x} = 12.5g x \quad (D-1)$$

where

$-\ddot{x}$  = deceleration (ft/sec<sup>2</sup>)

$x$  = distance automobile crushes into target (ft)

$g$  = gravitational acceleration (ft/sec<sup>2</sup>)

Newton's law of motion and equation (D-1) give the relation

$$F = -\frac{W}{g} \ddot{x} = 12.5 \frac{W}{g} x \quad (D-2)$$

where

$W_m$  = weight of automobile (lb)

Equation (D-1) is the motion for an undamped linear oscillator with a unit mass and a spring constant equal to 12.5g. Its solution with initial zero deformation is

$$x = C \sin (12.5g)^{1/2} t \quad (D-3)$$

To determine the constant, C, consider the balance of the input kinetic energy,  $E_m$ , by the striking automobile with work done by the impact force plus energy lost,  $E_L$ , by other phenomena such as target response

$$E_m = \frac{1}{2} \frac{W}{g} v_s^2 = \frac{1}{2} F_{\max} x_{\max} + E_L \quad (D-4)$$

where

$v_s$  = striking velocity of the automobile (ft/sec).

In the conservative case of  $E_L = 0$  the constant C can be determined by substituting equations (D-2) and (D-3) into equation (D-4)

$$C = \left( \frac{1}{12.5g} \right)^{1/2} V_s \quad (D-5)$$

Finally substituting equations (D-3) and (D-5) into equation (D-2) gives the force-time history

$$\begin{aligned} F &= 12.5 W_m \left( \frac{1}{12.5g} \right)^{1/2} V_s \sin (12.5g)^{1/2} t \\ &= 0.625 V_s W_m \sin 20 t \end{aligned} \quad (D-6)$$

2 | This is a sine wave of frequency  $\omega = 20$  rad/sec and period  $T = 2\pi/\omega = 0.314$  sec. The maximum force occurs at  $t = T/4 = 0.0785$  sec when the velocity of the striking automobile is zero relative to the rigid surface and then rapidly reducing to zero. Thus under the condition of plastic collision (i.e., missile and target acquire same velocity after impact) the duration of the impact force is from  $t = 0$  to  $t = T/4 = 0.0785$  sec. At 2 |  $t = 0.0785$  sec., the force diminishes from a maximum value to zero.

As an example of using the resulting expressions, consider the experimental data in reference 23. Test No. 505-IW for a 1963 Plymouth automobile striking a rigid wall yielded the following data.

$$\begin{aligned} W_m &= 3270 \text{ lb} \\ V_s &= 53.3 \text{ mph} = 78.17 \text{ ft/sec} \\ x_{\max} &= 3.82 \text{ ft} \\ gF_{\text{ave}}/W_m &= 25g \\ &(\text{average over distance}) \end{aligned}$$

From equations (D-3) and (D-5) and the above data the stopping distance is

$$x_{\max} = \left( \frac{1}{12.5g} \right)^{1/2} (78.17) = 3.91 \text{ ft}$$

2 | According to the forcing function equation (D-6) the average deceleration (average over distance, not over time) for Test No. 505-IW is

$$gF_{\text{ave}}/W_m = gF_{\max}/2W_m = (0.625)(78.17)g/2 = 24.42g$$

which agrees with the test result (25g) quite closely.

D.2 DERIVATION OF THE VELOCITY OF A MISSILE AFTER IT HAS PENETRATED THROUGH A LIQUID

Consider the motion of a missile, length  $L$ , entering a liquid medium and striking a target at depth  $H$  from the liquid surface, as shown in figure 5-1. When the missile first hits the liquid, a compressive shock wave may be generated in the liquid with a resulting loss of missile velocity. This is called the "compression phase" of liquid entry in reference 24, (page 18). As the missile displaces the liquid it experiences a hydrodynamic force with variable impact drag coefficient  $C_p$ . This "liquid-displacement phase" further reduces the velocity. After the maximum missile cross-sectional area is immersed, the "cavity drag phase" is initiated in which the drag coefficient  $C_D$  may be considered constant. In this appendix the velocity of the missile during liquid entry is analyzed on the assumptions that the velocity loss in the "compression phase" is negligible and that the impact drag coefficient  $C_p$  in the "liquid-displacement phase" is equal to the drag coefficient  $C_D$  in the "cavity drag phase." Since  $C_p$  is always smaller than  $C_D$  (see reference 24, page 30 and figure 2-7) these assumptions give more conservative (high) results for the missile velocity. Only the case of vertical entry (normal to the horizontal liquid surface) is considered.

Under these assumptions, the equation of missile motion is

$$\frac{W}{g} \ddot{x} = W - F_b - F_d \quad (D-7)$$

where

$W$  = Weight of missile

$g$  = gravitational acceleration

$x$  = depth of missile c.g. below the initial c.g. as shown in figure 5-1

$t$  = time after initial contact of missile with liquid

$F_b$  = buoyant force

$F_d$  = drag force

and a dot denotes differentiation with respect to  $t$ .

Between  $x = 0$  and  $x = L$  the buoyant force varies with  $x$

$$F_b = \gamma \int_0^x A(x_1) dx_1 = \gamma f(x), \quad (0 \leq x \leq L) \quad (D-8)$$

where

$\gamma$  = weight density of the liquid

$A(x_1)$  = horizontal cross-sectional area of the missile at vertical distance  $x_1$  from the tip

When  $x > L$  the buoyant force is a constant

$$F_b = W\gamma/\gamma_m, (x > L) \quad (D-9)$$

where

$\gamma_m$  = weight density of missile

The drag force is given by the expression

$$F_d = \gamma A_m C_D v^2 / 2g \quad (D-10)$$

where

$A_m$  = maximum horizontal cross-sectional area of missile

$v = \dot{x}$  = velocity of missile at depth  $x$

If the liquid is assumed to be incompressible, the drag coefficient,  $C_D$ , in equation (D-10) is a function of the missile shape and the Reynolds number  $R$ , defined as

$$R = \frac{V_0 d}{\nu} \quad (D-11)$$

where

$d$  = characteristic dimension of missile as shown in table 5-1

$V_0$  = initial velocity (at  $t=0$  and  $x=0$ ) of missile

$\nu$  = kinematic viscosity of liquid

Table 5-1 from reference 25 lists some typical values of  $C_D$  for variously shaped bodies in incompressible fluid flow. Reference 24 (page 35) presents some  $C_D$  values for a family of nose shapes. Other references on fluid mechanics can also be consulted.

Substituting equations (D-8), (D-9) and (D-10) into equation (D-7) results in the following two forms of the equation of motion and solutions:

A. For  $0 \leq x \leq L$

$$\ddot{x} + ax^2 + bf(x) - g = 0, \quad (0 \leq x \leq L) \quad (D-12)$$

where

$$a = \gamma A_m C_D / 2W \quad (D-13)$$

$$b = \gamma g / W \quad (D-14)$$

and  $f(x)$  is given in equation (D-8).

This is a nonlinear, second order, nonhomogeneous, ordinary differential equation for  $x(t)$ .

According to reference 26 (page 551) it can be solved as follows:

Let

$$y(x) = \dot{x}^2 = v^2 \quad (D-15)$$

Then if a prime denotes differentiation with respect to  $x$ ,

$$y'(x) = 2\dot{x}(\dot{x})' = 2\dot{x} \ddot{x} / \dot{x} = 2 \ddot{x} \quad (D-16)$$

Equation (D-12) becomes

$$y'(x) + 2ay(x) = 2g - 2bf(x) \quad (D-17)$$

which is a linear, first order, nonhomogeneous, ordinary differential equation for  $y(x)$ , and has the solution

$$y(x) = \left\{ 2 \int \mu(x) [g - bf(x)] dx + c \right\} / \mu(x) \quad (D-18)$$

where  $c$  is the integration constant and

$$\mu(x) = e^{\int 2adx} = e^{2ax} \quad (D-19)$$

Substituting equation (D-19) into equation (D-18) gives

$$\begin{aligned}
 y(x) &= v^2 = e^{-2ax} \left[ 2g \int e^{2ax} dx - 2b \int e^{2ax} f(x) dx + c \right] \\
 &= g/a - 2be^{-2ax} G(x) + c e^{-2ax}, \quad (0 \leq x \leq L)
 \end{aligned}
 \tag{D-20}$$

where

$$G(x) = \int e^{2ax} f(x) dx = \int e^{2ax} \left[ \int_0^x A(x_1) dx_1 \right] dx \tag{D-21}$$

in which equation (D-8) has been used.

At the initial position (See figure 5-1)  $x = 0$ ,  $v = v_0$ , and equation (D-20) gives

$$c = v_0^2 - g/a + 2bG(0) \tag{D-22}$$

Then equation (D-20) becomes

$$\begin{aligned}
 y(x) = v^2 &= g/a + e^{-2ax} \left\{ v_0^2 - g/a \right. \\
 &\quad \left. + 2b [G(0) - G(x)] \right\}, \quad (0 \leq x \leq L)
 \end{aligned}
 \tag{D-23}$$

At  $x = L$  equation (D-21) gives

$$G(L) = \left\{ \int e^{2ax} \left[ \int_0^x A(x_1) dx_1 \right] dx \right\}_{x=L} \tag{D-24}$$

and equation (D-23) gives

$$\begin{aligned}
 y(L) = v_1^2 &= v_2^2 + g/\gamma_m a + e^{-2aL} \left\{ v_0^2 - g/a \right. \\
 &\quad \left. + 2b [G(0) - G(L)] \right\}
 \end{aligned}
 \tag{D-25}$$

where  $V_1$  is the missile velocity at  $x = L$  (See figure 5-1) and

$$V_2^2 = \frac{g}{a} \left( 1 - \gamma/\gamma_m \right) \quad (D-26)$$

Consider the special case of a missile with uniform horizontal cross-sectional area  $A_0$ . Then  $A(x_1) = A_0$ . Equation (D-21) gives

$$\begin{aligned} G(x) &= \int_0^x e^{2ax} \left( \int_0^x A_0 dx_1 \right) dx = A_0 \int_0^x x e^{2ax} dx \\ &= A_0 e^{2ax} (2ax-1)/4a^2, \quad (0 \leq x \leq L) \end{aligned} \quad (D-27)$$

from which

$$G(0) = -A_0/4a^2 \quad (D-28)$$

and

$$G(L) = A_0 e^{2aL} (2aL-1)/4a^2 \quad (D-29)$$

Equation (D-23) becomes

$$\begin{aligned} v^2 &= g/a + bA_0 (1 - 2ax)/2a^2 + e^{-2ax} \left( v_0^2 - g/a \right. \\ &\quad \left. - bA_0/2a^2 \right), \quad (0 \leq x \leq L) \end{aligned} \quad (D-30)$$

Formulas for other missile shapes can be derived similarly.

B. For  $x \geq L$

$$\ddot{x} + ax^2 + g\gamma/\gamma_m - g = 0, \quad (x \geq L) \quad (D-31)$$

This is a special case of equation (D-12) with

$$f(x) = g\gamma/\gamma_m b, \quad (x \geq L) \quad (D-32)$$

which, when substituted into equation (D-20), gives

$$v^2 = V_2^2 + ke^{-2ax}, \quad (x \geq L) \quad (D-33)$$

The integration constant  $k$  can be determined by the condition that at  $x = L$ ,  $v = V_1$  obtained in equation (D-25)

$$k = (V_1^2 - V_2^2) e^{2aL} \quad (D-34)$$

Hence the missile velocity at  $x \geq L$  is given by

$$v = \left[ V_2^2 + (V_1^2 - V_2^2) e^{-2a(x-L)} \right]^{1/2}, \quad (x \geq L) \quad (D-35)$$

Substituting  $V_1$  from equation (D-25) into equation (D-35) gives

$$v = \left\{ V_2^2 + e^{-2ax} \left[ 2b (G(0) - G(L)) + V_0^2 + g \left( e^{2aL} \frac{\gamma}{\gamma_m - 1} \right) / a \right] \right\}^{1/2}, \quad (x \geq L) \quad (D-36)$$

In the special case of a missile with uniform horizontal cross-sectional area  $A_0$  equations (D-28) and (D-29) are substituted into equation (D-36) to give

$$v = \left\{ V_2^2 + e^{-2ax} \left[ bA_0 \left( e^{2aL} (1 - 2aL) - 1 \right) / 2a^2 + V_0^2 + g \left( e^{2aL} \frac{\gamma}{\gamma_m - 1} \right) / a \right] \right\}^{1/2}, \quad (x \geq L) \quad (D-37)$$

At  $x = H$ , when the missile strikes the target (See figure 5-1) the velocity  $V$  is given by equation (D-36) or equation (D-37) with  $x$  replaced by  $H$ .

APPENDIX E

SAMPLE APPLICATIONS

E.1 CONCRETE (PENETRATION, PERFORATION AND SPALLING)

A 4-inch x 12-inch wooden plank, weighing 108 pounds, strikes at 300 mph (440 fps) in a normal head-on collision with a reinforced concrete ( $f'_c = 3000$  psi) wall. The plank has a 48 square inch cross-sectional area with the equivalent diameter of 7.8 inches.

E.1.1 PENETRATION

Penetration is given by equation (2-1):

$$X = 12 K_p A_p \text{Log}_{10} \left( 1 + \frac{v_s^2}{215000} \right)$$

For 3000 psi concrete  $K_p = 0.00348$  (figure 2-1)

and

$$A_p = \frac{108}{48/144} = 324 \text{ psf}$$

Then

$$X = 12 \times 0.00348 \times 324 \times \text{Log}_{10} \left( 1 + \frac{440^2}{215000} \right) = 3.77 \text{ in.}$$

When the thickness of a wall is less than  $3 \times 3.77 = 11.3$  in., the depth of penetration is given by equation (2-2):

$$X_1 = \left[ 1 + e^{-4\left(\frac{t}{X} - 2\right)} \right] X$$

For example, for a wall with thickness  $t = 8$  in., we get:

$$X_1 = \left[ 1 + e^{-4\left(\frac{8}{3.77} - 2\right)} \right] \times 3.77 = 6.08 \text{ in.}$$

### E.1.2 PERFORATION

The thickness of a wall to be just perforated is given by formula 2-3:

$$T = \frac{427}{\sqrt{f'_c}} \frac{W}{D^{1.8}} \left( \frac{V_s}{1000} \right)^{1.33}$$

For  $f'_c = 3000$  psi,

$$T = \frac{427}{\sqrt{3000}} \frac{108}{7.8^{1.8}} \left( \frac{440}{1000} \right)^{1.33} = 7.01 \text{ in.}$$

Therefore, the concrete thickness required to prevent perforation according to equation 2-4 is:

$$t_p = 1.25 \times 7.01 = 8.76 \text{ in.}$$

### E.1.3 SPALL

The thickness of a wall to be just spalled is given by equation (2-5).

$$T_s = 2 T = 2 \times 7.01 = 14.02 \text{ in.}$$

Therefore, the concrete thickness required to prevent spalling according to equation (2-6) is:

$$t_s = 1.25 \times 14.02 = 17.53 \text{ in.}$$

## E.2 STEEL TARGETS

Given: A ten pound missile one inch in diameter impacts a target at 200 ft/sec.

Question: Find the thickness of steel plate,  $T$ , to just perforate and the thickness  $t_p$  required to prevent perforation.

Solution: Use equation (2-7) and (2-8)

Then

$$T = \frac{\left[ \frac{10}{2 \times 32.2} (200)^2 \right]^{2/3}}{672(1)} = 0.5 \text{ inches}$$

and  $t_p = 1.25 \times 0.5 = 0.625$  inches.

### E.3 STRUCTURAL RESPONSE

Consider a 10 lb solid metal missile of 1-inch diameter striking with 200 ft/sec velocity at the mid-span of a simply-supported steel I-beam of 10 ft span and AISC designation W6x12<sup>(8)</sup> with static yield strength  $f_y = 50,000$  psi. It is required to evaluate the structural response of the beam according to Section 3 under the condition of plastic impact.

According to equation (3-17) the effective mass of the steel beam may be conservatively estimated as the mass of a 13-inch length of the beam (since the depth of beam  $d = 6''$  and  $D_x = 1''$ , the missile diameter) which is for W6x12 beam<sup>(8)</sup>,

$$M_e = \frac{(12)(13)}{12g} = 13/g$$

According to equation (3-8) for plastic impact, the required target strain energy to absorb the impact energy is

$$E_s = \frac{M_m^2 v_s^2}{2(M_m + M_e)} = \frac{\left(\frac{10}{g}\right)^2 (200 \times 12)^2}{2\left(\frac{10}{g} + \frac{13}{g}\right)} = 32,440 \text{ in.-lb}$$

The resistance-displacement function of a simply-supported beam under central loading can be idealized as a bilinear function (figure 3-1 and table 4-2) with

$$R_m = \frac{4M_u}{L} = \frac{8If_d y}{Ld} = \frac{8(21.7)(50,000)(1.2)}{(10 \times 12)(6)} = 14,467 \text{ lb}$$

and

$$x_e = \frac{R_m L^3}{48EI} = \frac{(14,467)(10 \times 12)^3}{48(30 \times 10^6)(21.7)} = 0.80 \text{ in.}$$

where the value of the moment of inertia,  $I$ , for the beam cross-section is taken from reference 8, and modulus of elasticity  $E = 30 \times 10^6$  and dynamic increase factor  $DIF = 1.2$  (table 4-1) have been used.

According to figure 3-1 the maximum strain energy for purely elastic structural response is

$$E_e = \frac{1}{2} R_m x_e = \frac{1}{2} (14,467)(0.80) = 5,787 \text{ in.-lb}$$

which is less than  $E_s = 32,440$  in.-lb, so the structural response is elasto-plastic. Then according to equation (3-22) the required ductility ratio is

$$\mu_r = \frac{E_s}{x R_e m} + \frac{1}{2} = \frac{32,440}{(0.80)(14,467)} + 0.5 = 3.30$$

2 | Since, according to table 4-4 the allowable ductility ratio for a steel  
2 | beam under lateral loads is 20, this beam can withstand the postulated  
missile impact if no other loads are acting simultaneously. In case other  
loads are present as missile impacts and remain in effect throughout the  
structural response the required ductility ratio should be evaluated by  
equation (3-24) instead of equation (3-22).

#### E.4 MISSILE PENETRATION THROUGH WATER

Consider the postulated accident condition of a fuel shipping cask (the missile) falling from an overhead crane and possibly damaging the spent fuel pool floor slab (the target) underneath. The cask is a cylinder with length  $L = 17$  ft, diameter  $d = 7$  ft, and weight  $W = 2 \times 10^5$  lb. [The spent fuel pool contains water of depth  $H = 37$  ft. If the cask is to drop  $h = 11$  ft to just hit the water surface the initial velocity is

$$v_0 = (2 gh)^{1/2} = [2(32.17)(11)]^{1/2} = 26.6 \text{ ft/sec.}$$

The Reynolds number is, according to equation (5-7),

$$R = \frac{v_0 d}{\nu} = \frac{(26.6)(7)}{0.93 \times 10^{-5}} = 2.0 \times 10^7.$$

Since  $L/d = 17/7 = 2.43$  the drag coefficient is, according to table 5-1 for the case of circular cylinder with axis parallel to flow and with  $R > 10^3$ ,

$$C_D = 0.854$$

The horizontal cross-sectional area is

$$A_0 = \pi d^2/4 = \pi(7)^2/4 = 38.5 \text{ ft}^2.$$

Then equation (5-5) gives

$$a = \frac{\gamma C_D A_0}{2W} = \frac{(62.4)(0.854)(38.5)}{2(2 \times 10^5)} = 0.0051 \text{ ft}^{-1},$$

and equation (5-6) gives

$$b = \frac{\gamma g}{W} = \frac{(62.4)(32.17)}{2 \times 10^5} = 0.010 \text{ ft}^{-1} \text{ sec}^{-1}.$$

The weight density of the cask is

$$\gamma_m = \frac{W}{A_0 L} = \frac{2 \times 10^5}{(38.5)(17)} = 305.6 \text{ lb/ft}^3.$$

According to equation (5-8) the terminal velocity is

$$\begin{aligned} v_2 &= \left[ g \left( 1 - \gamma/\gamma_m \right) / a \right]^{1/2} \\ &= \left[ (32.17) \left( 1 - 62.4/305.6 \right) / 0.0051 \right]^{1/2} = 70.9 \text{ ft/sec.} \end{aligned}$$

Since  $H > L$ , and according to equation (5-2)

$$\begin{aligned} z_2(L) &= v_2^2 + e^{-2aL} \left\{ \frac{bA_0}{2a^2} \left[ e^{2aL} (1 - 2aL) - 1 \right] \right. \\ &\quad \left. + v_0^2 + \frac{g}{a} \left( e^{2aL} \gamma/\gamma_m - 1 \right) \right\} = \\ &= (70.9)^2 + e^{-2(0.0051)(17)} \left\{ \frac{(0.01)(38.5)}{2(0.005)^2} \left[ e^{0.1734} (1 - 0.1734) \right. \right. \\ &\quad \left. \left. - 1 \right] + (26.6)^2 + \frac{(32.17)}{0.0051} \left( e^{0.1734} 62.4/305.6 - 1 \right) \right\} = \\ &= 5027 + (0.8408) \left[ -4193 \right] = 1502 > 0, \end{aligned}$$

the value of  $Z_2(H)$  should be calculated:

$$Z_2(H) = v_2^2 + e^{-2aH} \left\{ bA_0 \left[ e^{2aL} (1 - 2aL) - 1 \right] / 2a^2 + v_0^2 + g \left( e^{2aL} \gamma / \gamma_m - 1 \right) / a \right\} = (70.9)^2 + e^{-2(0.0051)(37)} (-4193) =$$

$$5027 + (0.6856)(-4193) = 2152 > 0$$

Finally the striking velocity of the cask on the spent fuel pool floor slab is, according to equation (5-4).

$$v = \left[ Z_2(H) \right]^{1/2} = (2152)^{1/2} = 46.4 \text{ ft/sec}$$

It is interesting to note that if the spent fuel pool is dry the striking velocity would be

$$v = \left[ 2g (h + H) \right]^{1/2} = \left[ 2 (32.17) (11 + 37) \right]^{1/2} = 55.6 \text{ ft/sec}$$

For missiles of lighter weights, the reduction of striking velocity due to the presence of a liquid would be more pronounced.

## APPENDIX F

## REFERENCES AND BIBLIOGRAPHY

F.1 REFERENCES

1. Rotz, J. V., Yeh, G. C. K., Bertwell, W., Tornado and Extreme Wind Design Criteria for Nuclear Power Plants, Topical Report, BC-TOP-3, Revision 3, Bechtel Power Corporation, August 1974. | 2
2. Russell, C. R., Reactor Safeguards, MacMillan, New York, 1962.
3. Fundamentals of Protective Design, TM 5-855-1, Headquarters, Department of the Army, Washington, D.C., July 1965.
4. Norris, C. H., et al., Structural Design for Dynamic Loads, McGraw-Hill Book Company, Inc., New York, New York, 1959.
5. Goldsmith, W., Impact, Edward Arnold, Ltd., London, 1960.
6. John M. Biggs, Introduction to Structural Dynamics, McGraw-Hill 1964, pp. 202-244.
7. Newmark, N. M., and Richart, F. E., Impact Tests of Reinforced Concrete Beams, NDRC Report No. A-125, A-213, and A-304, 1941-1946.
8. A.I.S.C. Steel Construction Manual, 7th Edition, American Institute of Steel Construction, N. Y., N. Y., 1970.
9. Building Code Requirements for Reinforced Concrete, ACI Standard 318-71, American Concrete Institute, Detroit, Michigan, 1971. | 2
10. N. H. Burns, C. P. Siess, Plastic Hinging in Reinforced Concrete, ASCE Proc. V92 (J. Struct. Div.) n ST 5 Oct. 1966.
11. Vail, C. F., "Dynamic Modeling of Automobile Structures from Test Data," System Identification of Vibrating Structures - Mathematical Models from Test Data, The American Society of Mechanical Engineers, N. Y. (1972) pp. 149-177.
12. Harris, C. M., and Crede, C. E., Shock and Vibration Handbook, McGraw-Hill Book Company, N. Y., 1961.
13. Gwaltney, R. C., Missile Generation and Protection in Light-Water-Cooled Power Reactor Plants, ORNL NSIC-22, Oak Ridge National Laboratory, Oak Ridge, Tennessee, for the U. S. Atomic Energy Commission, September 1968.
14. A. Amirikian, Design of Protective Structures, Report NP-3726, Bureau of Yards and Docks, Department of the Navy, August 1950. | 2

15. Samuely, F. J., and Hamann, C. W., Civil Protection, The Architectural Press, London, 1939.
16. Fundamentals of Protective Design, Report ATI207821, Army Corps of Engineers, Office of the Chief of Engineers, 1946.
17. National Defense Research Committee, Effects of Impact and Explosion, Summary Technical Report of Division 2, Volume 1, Washington, D.C.
18. Industrial Engineering Study to Establish Safety Design Criteria for Use in Engineering of Explosive Facilities and Operations Wall Response, a Report Submitted to Process Engineering Branch, A.P.M.E.D. Picatinny Arsenal, Dover, N. J., April 1963.
19. Structures to Resist the Effects of Accidental Explosions, TM 5-1300, Department of the Army, Washington, D.C., July 1965.
20. White, R. W., and Botsford, N. B., Containment of Fragments from a Runaway Reactor, Report SRIA-113, Stanford Research Institute, September 15, 1963.
21. Hardrock Silo Debris Impact Program, Phase I Testing, Test Report, Physics International Co./Bechtel Corp., (unpublished).
22. Emori, R. I., Analytical Approach to Automobile Collisions, Paper No. 680016, Automotive Engineering Congress, Detroit, Michigan (1968).
23. Ivey, D. L., Ruth, E., and Hirsch, T. J., Feasibility of Lightweight Cellular Concrete for Vehicle Crash Cushions, Paper presented at the Annual Meeting of the Highway Research Board, Washington, D.C. (1970).
24. Kornhauser, M., Structural Effects of Impact, Spartan, Baltimore, Maryland, 1960.
25. Rouse, H., and Howe, J. W., Basic Mechanics of Fluids, John Wiley and Son Inc., New York (1953).
26. Kamke, E., Differentialgleichungen Lösungsmethoden und Lösungen, Vol. I. Gewöhnliche Differentialgleichungen (1942), Akademische Verlagsgesellschaft, Becker & Erler Kom.-Ges., Leipzig.
27. Recht, R. F., and Ipson, T. W., Ballistic Perforation Dynamics, J. of Appl. Mechanics, ASME, Sept. 1963.
28. Newmark, N. M., and Haltiwanger, J. D., Air Force Design Manual, AFSWC-TDR-62-138, prepared by the University of Illinois for Air Force Special Weapons Center, Kirtland Air Force Base, N. M., 1962.

29. Johansen, K. W., Yield-Line Formulae For Slabs, Cement & Concrete Association, London (Translation by Paulin M. Katborg).
30. Ferguson, P. M., Reinforced Concrete Fundamentals, 3rd Edition, John Wiley 1973.
31. Hognestad, E., Yield-Line Theory For the Ultimate Flexural Strength of Reinforced Concrete Slabs, ACF Journal 24 No. 7 March 1953.
32. Wood, R. H. Plastic and Elastic Design of Slabs and Plates, Ronald Press Co., 1961.
33. Timoshenko, S. and Woinowsky-Kriegers, S., Theory of Plates and Shells, Mc-Graw-Hill, 1959.
34. Cowell, W. L., Dynamic Tests of Concrete Reinforcing Steels, Technical Report R394, U.S. Naval Civil Engineering Laboratory, 1965.
35. Watstein, D., Effect of Straining Rate on the Compressive Strength and Elastic Properties of Concrete, Journal of the American Concrete Institute, Vol. 24, No. 8, 1953.
36. McHenry, D., Shideler, J. J., Review of Data on Effect of Speed in Mechanical Testing of Concrete, Bulletin D9, Portland Cement Association Research and Development Laboratories, (also reprint, Special Technical Publication No. 185, by ASTM, 1956).
37. Rao, N. R. N., Lohrmann, M., Tall, L., Effect of Strain Rate On The Yield Stress Of Structural Steels, Fritz Laboratory Reprint No. 293, Lehigh University Institute of Research, (also Journal of Materials, Vol. 1, No. 1, American Society for Testing and Materials, March 1966).
38. Gaston, J. R., Siess, C. P., and Newmark, N. M., An Investigation of the Load-Deformation Characteristics of Reinforced Concrete Beams Up to the Point of Failure, University of Illinois, December 1952, Reprint July 1959.
39. Denton, D. R., A Dynamic Ultimate Strength Study of Simply Supported Two-Way Reinforced Concrete Slabs, TR 1-789, U.S. Army Engineers Waterways Experiment Station, Corps of Engineers, Vicksburg, Mississippi, July 1967.
40. Albritton, G. E., Response of Deep Reinforced and Unreinforced Concrete Slabs to Static and Dynamic Loading, ASCE National Meeting on Structural Engineering, September 30 - October 04, 1968.
41. Untrauer, R. E., Behavior and Design of Deep Structural Members, Part 4, Dynamic Tests of Reinforced Concrete Deep Beams, University of Illinois, May 1960.
42. Corley, W. G., Rotational Capacity of R/C Beams, ASCE Proceedings, Journal of Structural Division, October 1966.

2

43. Feldman, A., Siess, C. P., Investigation of Resistance and Behavior of Reinforced Concrete Beams Subjected to Dynamic Loading, University of Illinois, September 1956.
44. Chelapati, Kennedy E. Wall Probabilistic Assessment of Aircraft Hazard for Nuclear Power Plants, First International Conference on Structural Mechanics in Reactor Technology Berlin 20-24 September 1971.

F.2 BIBLIOGRAPHY

1. A.I.S.C. Plastic Design in Steel, American Institute of Steel Construction, N.Y., N.Y., 1959.
2. Beedle, Lynn S., Plastic Design of Steel Frames, John Wiley & Sons, Inc., 1958.
3. Commentary of Plastic Design in Steel, A.S.C.E. Manual of Engineering Practice, No. 41, 1961.
4. Design for Pipe Break Effects, BN-TOP-2, Bechtel Corp., August 1972.
5. Design of Structures to Resist the Effects of Atomic Weapons, The, EM 1110-345-414 to 421, Massachusetts Institute of Technology for the Office of Chief of Engineers, U.S. Army, Washington, D.C., 1957.
6. Horger, O. J., Metals Engineering Design. American Society of Mechanical Engineers Handbook, McGraw-Hill, New York, 1953.
7. Johansen, K. W., "Pladeformler Formelsamling", Polyteknish Forening, Copenhagen, 2nd Edition, 1954.
8. Johansen, K. W., "Pladeformler", Polyteknish Forening, Copenhagen, 2nd Edition, 1949.
9. Lorenz, Hanz, Gilbert Associates, Inc., Aircraft Impact Design, Power Engineering, Nov. 1970.
10. Newmark, N. M., et al. Notes on Blast Resistant Design, Bechtel Associates Symposium, New York, 1968 (unpublished).
11. Rinder, R., Saffian, L. W., Wachtell, S., Cohen, E., Dobbs, N., Manual for Design of Protective Structures Used in Exposive Processing and Storage Facilities TR3808, Picatinny Arsenal, Dover, New Jersey/Amman and Whitney, New York, New York, November 1968.
12. Wilkins, M. L., Calculation of Elastic-Plastic Flow, UCRL-7322, Lawrence Radiation Laboratory, Livermore, California, January 24, 1969, Rev 1.

12